

REPORT DOCUMENTATION PAGE

Form Approved
OMB No. 0704-0188

Public reporting burden for this collection of information is estimated to average 1 hour per response, including the time for reviewing instructions, searching existing data sources, gathering and maintaining the data needed, and completing and reviewing the collection of information. Send comments regarding this burden estimate or any other aspect of this collection of information, including suggestions for reducing this burden, to Washington Headquarters Services, Directorate for Information Operations and Reports, 1215 Jefferson Davis Highway, Suite 1204, Arlington, VA 22202-4302, and to the Office of Management and Budget, Paperwork Reduction Project (0704-0188), Washington, DC 20503.

1. AGENCY USE ONLY (Leave Blank)	2. REPORT DATE 31 August, 2004	3. REPORT TYPE AND DATES COVERED Final Progress Report 01 June 01 - 31 May 04	
4. TITLE AND SUBTITLE Modeling the Dynamics of Gully and Arroyo Development: Fort Carson and Pinon Canyon Maneuver Site, Colorado		5. FUNDING NUMBERS DAAD19-01-1-0615	
6. AUTHORS Dr. Gregory E. Tucker		8. PERFORMING ORGANIZATION REPORT NUMBER	
7. PERFORMING ORGANIZATION NAME(S) AND ADDRESS(ES) Oxford University School of Geography and the Environment Mansfield Road, Oxford OX1 3TB United Kingdom			
9. SPONSORING / MONITORING AGENCY NAME(S) AND ADDRESS(ES) U. S. Army Research Office P.O. Box 12211 Research Triangle Park, NC 27709-2211		10. SPONSORING / MONITORING AGENCY REPORT NUMBER 41586.6 - EV	
11. SUPPLEMENTARY NOTES The views, opinions and/or findings contained in this report are those of the author(s) and should not be construed as an official Department of the Army position, policy or decision, unless so designated by other documentation.			
12a. DISTRIBUTION / AVAILABILITY STATEMENT Approved for public release; distribution unlimited.		12b. DISTRIBUTION CODE	
13. ABSTRACT (Maximum 200 words) This report summarizes the findings and accomplishments of the study. It covers publications and degrees, technical advancement (software), and scientific findings. Copies of published journal articles and unpublished reports are included as appendices.			
14. SUBJECT TERMS		15. NUMBER OF PAGES	
		16. PRICE CODE	
17. SECURITY CLASSIFICATION OF REPORT	18. SECURITY CLASSIFICATION OF THIS PAGE	19. SECURITY CLASSIFICATION OF ABSTRACT	20. LIMITATION OF ABSTRACT

NSN 7540-01-280-5500

Standard Form 298 (Rev. 2-89)
Prescribed by ANSI Std. Z39-1
298-102

BEST AVAILABLE COPY

20041102 061

REPORT DOCUMENTATION PAGE (SF298)

(Continuation Sheet)

Page 1 of 34 (excluding appendices)

**MODELING THE DYNAMICS OF GULLY AND ARROYO FORMATION,
FORT CARSON AND PINON CANYON MANEUVER SITE, COLORADO**

Proposal # 41586-EV

Agreement number DAAD19-01-1-0615

FINAL REPORT

Reporting Period 1 June, 2001 to 31 May, 2004

Prepared by Gregory E. Tucker

Current address:

Department of Geological Sciences

CIRES

University of Colorado

2200 Colorado Avenue

Boulder, CO 80309-0399

email: gtucker@cires.colorado.edu

August, 2004

DISTRIBUTION STATEMENT A
Approved for Public Release
Distribution Unlimited

(1) Publications during reporting period

(a) Manuscripts submitted but not yet published:

- (1) Solyom, P., and Tucker, G.E., The effect of limited storm duration on landscape evolution, drainage basin geometry and hydrograph shapes: *Journal of Geophysical Research ES*, in press 2004.
- (2) Istanbuluoglu, E., Bras, R.L., Flores, H., and Tucker, G.E., Implications of Bank Failures and Fluvial Erosion for Gully Development: Field Observations and Modeling. Submitted to *Journal of Geophysical Research - Earth Surface*, March, 2004.

(b) Papers published in peer-reviewed journals or books

- (1) Bogaart, P.W., Tucker, G.E., and de Vries, J.J. (2003) Channel network morphology and sediment dynamics under alternating periglacial and temperate regimes: A numerical simulation study: *Geomorphology*, vol. 54, no. 3/4, p. 257-277.
- (2) Collins, D., Bras, R., and Tucker, G.E. (2004) Modeling the effects of vegetation-erosion coupling on landscape evolution: *Journal of Geophysical Research - Earth Surface*, v. 109, no. F3, F03004, doi:10.1029/2003JF000028.

- (3) Gasparini, N.M., Tucker, G.E., and Bras, R.L. (2004) Network-scale dynamics of grain-size sorting: Implications for downstream fining, stream-profile concavity, and drainage basin morphology: *Earth Surface Processes and Landforms*, 29(4), 401-422.
- (4) Tucker, G.E. (2004) Drainage basin sensitivity to tectonic and climatic forcing: implications of a stochastic model for the role of entrainment and erosion thresholds. *Earth Surface Processes and Landforms*, 29, 185-205.
- (5) Snyder, N.P., Whipple, K.X., Tucker, G.E., and Merritts, D.J. (2003) The importance of a stochastic distribution of floods and erosion thresholds in the bedrock river incision problem: *Journal of Geophysical Research*, vol. 108, no. B2, doi:10.1029/2001JB001655.
- (6) Bras, R.L., Tucker, G.E., and Teles, V.T. (2003) Six myths about mathematical modeling in geomorphology: in *Prediction in Geomorphology*, edited by P. Wilcock and R. Iverson, American Geophysical Union, pp. 63-79.
- (7) Baldwin, J.A., Whipple, K.X., and Tucker, G.E. (2003) Implications of the shear-stress river incision model for the timescale of post-orogenic decay of topography: *Journal of Geophysical Research*. Vol. 108, No. B3, doi: 10.1029/2001JB000550.
- (8) Snyder, N.P., Whipple, K.X., Tucker, G.E., and Merritts, D.J. (2003) Channel response to tectonic forcing: field analysis of stream morphology and hydrology in the Mendocino triple junction region, northern California: *Geomorphology*, Vol. 53, pp. 97-127.
- (9) Arnold, L.J., Stokes, S., Bailey, R., Fattahi, M., Colls, A.E., and Tucker, G. (2002) Optical dating of potassium feldspar using far-red (>665nm) IRSL emissions: A comparative study using fluvial sediments from the Loire River, France. *Quaternary Science Reviews*, 22, 1093-1098.
- (10) Tucker, G.E., and Whipple, K.X. (2002) Topographic outcomes predicted by stream erosion models: Sensitivity analysis and intermodel comparison, *Journal of Geophysical Research*, v. 107, no. B9, 2179, doi:10.1029/2001JB000162.
- (11) Whipple, K.X., and Tucker, G.E. (2002) Implications of sediment-flux dependent river incision models for landscape evolution: *Journal of Geophysical Research*, v. 107, no. B2, DOI 10.1029/2000JB000044.
- (12) Tucker, G.E., Lancaster, S.T., Gasparini, N.M., and Bras, R.L. (2001) The Channel-Hillslope Integrated Landscape Development (CHILD) Model, in *Landscape Erosion and Evolution Modeling*, edited by R.S. Harmon and W.W. Doe III, Kluwer Academic/Plenum Publishers, pp. 349-388.
- (13) Tucker, G.E., Lancaster, S.T., Gasparini, N.M., Bras, R.L., and Rybarczyk, S.M. (2001) An Object-Oriented Framework for Hydrologic and Geomorphic Modeling Using Triangulated Irregular Networks. *Computers and Geosciences*, 27(8), pp. 959-973.
- (14) Niemann, J.D., Gasparini, N.M., Tucker, G.E., and Bras, R.L. (2001) A quantitative evaluation of Playfair's Law and its use in testing long-term stream erosion models, *Earth Surface Processes and Landforms*, 26, pp. 1317-1332.

(c) Conference papers (not published in proceedings):

- (1) Solyom, P.B., and Tucker, G.E. (2003) Hypothesis for a channel head stability criterion on the basis of the full continuity equation for sediment transport: paper presented at AGU Fall Meeting, December 2003.
- (2) Tucker, G.E., Clevis, Q., Lock, G., Lancaster, S.T., and Desitter, A. (2003) Modeling the stratigraphy and preservation potential of meandering stream deposits: paper presented at AGU Fall Meeting.
- (3) Tucker, G.E. (2003) Nonlinearity and stochastic effects in long-term stream erosion: Invited paper presented at Geological Society of America Penrose Conference on Tectonics, Climate and Landscape Evolution, Taroko National Park, Taiwan, January, 2003.

- (4) Solyom, P., and Tucker, G.E. (2003) The effect of limited storm duration on landscape evolution, drainage basin geometry and hydrograph shapes: Paper presented at AGU-EGS-EUG joint conference, Nice, France, April, 2003.
- (5) Gasparini, N.M., Bras, R.L., and Tucker, G.E. (2003) Network-scale dynamics of sediment mixtures: how do tectonics affect surface bed texture and channel slope? Paper presented at AGU-EGS-EUG joint conference, Nice, France, April, 2003.
- (6) Tucker, G.E. (2003) Topographic sensitivity to tectonic and climatic forcing: implications of a stochastic model for the role of entrainment and erosion thresholds. Paper presented at British Geomorphological Research Group Annual Conference, September, 2003.
- (7) Robinson, R., and Tucker, G.E. (2003) Channel geometry adjustment in long-term river basin evolution: plausible alternatives to regime theory? Paper presented at British Geomorphological Research Group Annual Conference, September, 2003.
- (8) Solyom, P., and Tucker, G.E. (2003) The effect of catchment geometry on non-steady state runoff production, landscape evolution and channel network optimality. Paper presented at British Geomorphological Research Group Annual Conference, September, 2003.
- (9) Tucker, G.E. (2003) Topographic sensitivity to tectonic and climatic forcing: implications of a stochastic model for the role of entrainment and erosion thresholds. Paper presented at British Geomorphological Research Group Annual Conference, September, 2003.
- (10) Istanbuluoglu, E., Flores, H., Bras, R.L., and Tucker, G.E. (2003) Implications of fluvial erosion and bank failures on gully development and growth. Paper presented at AGU Fall Meeting.
- (11) Gasparini, N.M., Bras, R.L., and Tucker, G.E. (2003) Erosion and Sedimentation in Response to Climate Change: a Numerical Study Using a Multiple Grain-size Sediment Transport Model. Paper presented at AGU Fall Meeting.
- (12) Solyom, P., and Tucker, G.E. (2003) Hypothesis for a Channel Head Stability Criterion on the Basis of the Full Continuity Equation for Sediment Transport. Paper presented at AGU Fall Meeting.
- (13) Tucker, G.E., Clevis, Q., Lock, G., Lancaster, S.T., and Desitter, A. (2003) Modeling the stratigraphy and preservation potential of meandering stream deposits. Paper presented at AGU Fall Meeting.
- (14) Collins, D.B., Bras, R.L., and Tucker, G.E. (2002) Ecogeomorphic modeling of biodiversity and disturbance: Paper presented at American Geophysical Union fall meeting, San Francisco, December 2002.
- (15) Tucker, G.E. (2002) Community sediment models: lessons from landscape evolution modeling. Paper presented at *Workshop on Community Sediment Models*, Boulder, February 2002.
- (16) Tucker, G.E., Arnold, L., Solyom, P., Stokes, S., Bras, R., Collins, D., Flores, H., and Gasparini, N. (2002) Gully initiation by extreme rainfall events: case study from the Colorado High Plains, USA. Paper presented at *Dryland Rivers: Process and Product*, Aberdeen, Scotland, August 8-9, 2002.
- (17) Tucker, G.E., Solyom, P., Arnold, L., Stokes, S., Collins, D., and Bras, R. (2002) Gully initiation by extreme events: theory and case study from the Colorado High Plains, USA. Paper presented at *British Geomorphological Research Group annual conference*, Leeds, England, September 12-14, 2002.
- (18) Tucker, G.E., Solyom, P., Arnold, L., and Stokes, S. (2002) Gully and arroyo erosion. Presentation at *Workshop on Arroyos*, Oxford Centre for Industrial and Applied Mathematics, November, 2002.

- (19) Solyom, P., and Tucker, G.E. (2002) Modelling the effect of storm duration change on runoff production and landscape evolution. Paper presented at British Geomorphological Research Group (BGRG) Postgraduate Symposium, Leeds, UK, April, 2002.
- (20) Collins, D.B., Bras, R.L., and Tucker, G.E. (2001) Modeling the influence of vegetation dynamics on landscape evolution. Paper presented at American Geophysical Union spring meeting, Boston.
- (21) Tucker, G.E., Collins, D.B., and Bras, R.L. (2001) A stochastic model of vegetation-erosion interaction and its influence on denudation time series. Paper presented at *Earth System Processes – Global Meeting*, Edinburgh, Scotland, June 24-28, 2001.
- (22) Collins, D.B., Bras, R.L., and Tucker, G.E. (2001) Meta-stable vegetation cover and erosion cycles. Paper presented at American Geophysical Union fall meeting, San Francisco.
- (23) Snyder, N.P., Whipple, K.X., Tucker, G.E., and Merritts, D.J. (2001) Modeling stochastic floods and erosion thresholds in bedrock rivers: field data from northern California. Paper presented at American Geophysical Union fall meeting, San Francisco.
- (24) Whipple, K.X., and Tucker, G.E. (2001) The role of sediment flux in bedrock channel incision and landscape evolution: model predictions and data needs. Paper presented at American Geophysical Union fall meeting, San Francisco.

2. Scientific personnel and honors/awards/degrees

Personnel (includes only Oxford-affiliated personnel; MIT-affiliated personnel are reported separately):

- Dr. Gregory E. Tucker, PI
- Mr. Peter Solyom, D.Phil. student
- Mr. Lee Arnold, D.Phil. student
- Mr. Tumbikanani Mtika, MSc awarded 2001
- Dr. Stephen Stokes (OSL geochronology; co-supervisor of Arnold)
- Dr. Vanessa Winchester (Dendrogeomorphology)
- Mr. Arnaud Desitter (Software engineering)

3. Report of inventions

None.

4. Scientific progress and accomplishments

- Improved cross-platform compatibility, including resolution of floating-point handling differences among compilers and chipsets. Recent versions of CHILD have been compiled for Linux, MacOS, Sun, and Intel platforms.
- Random number generator enhancements, including read/write of current random generator state (which allows runs to be interrupted and re-started from exactly the same state), and independent random-number sequences for different modules.
- Run-time (rather than compile-time) selection of erosion/transport formulas.

Other new capabilities include the following:

- Module to simulate channel sidewall erosion/sedimentation by slab failure (Istanbulluoglu et al., in review).¹
- Time Series handling module that provides a general input-file format and parsing capability to handle time-varying parameters, such as mean storm intensity or infiltration capacity.
- Module simulating plunge-pool erosion (Flores, 2004).¹
- Option for computing peak storm discharge based on catchment geometry and storm duration (Solyom and Tucker, in press).
- Addition of new alternative erosion and sediment transport algorithms, including the Bridge-Dominic formula and a modified form of the Meyer-Peter-Mueller formula (Tucker, 2004).
- In connection with a related project on alluvial valley evolution, a module has been developed to record depositional stratigraphy at high space-time resolution, and bugs in the stream-meander module that caused the model to crash under conditions of rapid sedimentation have been fixed.

4.3 Origins and Controls on Arroyo Networks: Results from Paleohydrology and Aerial Photograph Analysis

Introduction

Understanding erosion and sediment transport in rangeland landscapes is important for a variety of reasons. From the perspective of land management, effective erosion control requires an understanding of the nature, frequency and magnitude of the climatic, hydrologic, biotic, and geomorphic drivers. From the perspective of long-term landscape evolution, a quantitative understanding of the "rules of the landscape" is needed in order to answer questions such as: What are the frequency and magnitude properties of sediment movement, and how do these change with scale? How sensitive are rates of sediment movement and topographic change to climatic, tectonic, or human forcing? What interpretations of the Quaternary landscape-change record are consistent with the mechanics and chemistry of the driving processes? In addition, in the particular case of the central Rocky Mountains piedmont, which we investigate here, quantitative models of rangeland dynamics are needed to test the plausibility of the hypothesis that climatic oscillation has driven accelerated denudation along the margins of the Rocky Mountains (e.g., Zhang et al., 2001).

¹ Implemented in MIT version; merger with CU-Oxford code base pending.

and discuss, we have opted for inclusiveness. As a result, some of the publications included as appendices deal with rather general issues (such as the role of erosion thresholds in the mechanics of channel evolution) with implications that extend beyond the immediate question of gully physics. Likewise, because of the collaborative nature of this project, we have not tried to separate explicitly the work performed by the Oxford and MIT teams, though this report does emphasize the Oxford team's activities.

The project has involved contributions from many people. In particular, the project has benefited greatly from the work of graduate students and postdoctoral researchers at MIT and the University of Oxford, who are the lead authors of many of the appendices in this report. They include: Lee Arnold (OSL dating and stochastic modeling), Daniel Collins (vegetation modeling), Homero Flores (plunge-pool erosion modeling, soils analysis), Dr. Erkan Istanbuluoglu (slab-failure measurement and modeling), Tumbikanani Mtika (channel head analysis), and Peter Solyom (erosion-hydrology modeling, catchment-shape controls). In addition, Dr. Stephen Stokes and Dr. Vanessa Winchester of the University of Oxford generously contributed time and expertise, as well as the use of their laboratories. Arnaud Desitter made vast improvements to the performance, efficiency, and capabilities of the CHILD code. Quintijn Clevis made significant contributions to CHILD's floodplain and stratigraphy modules, and Patrick Bogaart developed the original TimeSeries module in CHILD. We are also grateful for field assistance from Bill Bennett, Domenico Capolongo, Nicole Gasparini, Salvatore Grimaldi, Quintijn Clevis, and Vanessa Teles. John Kuzmiak of the U.S.G.S. Pueblo Office kindly provided access to high-resolution rainfall and discharge records. Finally, the support of the Fort Carson Directorate of Environmental Compliance and Management (DECAM) has been invaluable to the project. It would not have been possible without their help. In particular, we would like to thank Brian Goss, James Kulbeth, Jeff Linn, Bruce Miller, Linda Moeder, and Dan Sharps.

4.2 CHILD Model Development and Capabilities

One of the main aims of the project was to add new capabilities to the CHILD model. Here, these capabilities are summarized. Applications and results from sensitivity analyses appear in various sections below.

Improvements to mesh-generation algorithms, low-level routines, and utility functions include the following:

- Implementation and testing of the fast Tipper algorithm for Delaunay triangulation. This resulted in a mesh-generation speed improvement on the order of 10^2 .
- General performance tuning and removal of memory leaks.
- Improved input-file handling, with fast random (rather than sequential) access of input data files.
- Implementation of a network-accessible source code management, update and retrieval system using the open-source Concurrent Version System (CVS). The system allows for file modification by multiple, concurrent developers, for retrieval of past file versions, and provides many other developer features.
- Creation of a browser-accessible auto-documentation system for the source code using the Doxygen document generator.

based definition, terrain with low to moderate relief in which either present-day or glacial maximum climate supported a climax vegetation of predominantly low-

growing species such as shrubs and grasses. This definition includes much of the piedmont landscapes of the North American west, much of southern Africa, large areas of Australian lowlands, Mediterranean regions, South American pampas, and similar regions.

The geomorphology of rangelands is commonly characterized by ephemeral or intermittent stream channels and unchanneled valleys. Dry channels, variously called "gullies," "arroyos," "wadis" or other regional terms, are common. Whatever the name, ephemeral channels in rangelands are often incised into valley-floor alluvium or occasionally bedrock (e.g., Cooke and Reeves, 1976; Graf, 1983; Bull, 1997; Prosser and Slade, 1994; Boardman et al., 2003). Here the term arroyo is used to refer to incised, ephemeral channels with steep sidewalls and a rectilinear to U-shaped cross section. (Note that by including incised ephemeral channels of all sizes we depart from the definition of Graf (1988), who preferred the term "gully" for smaller channels. However, "gully" is commonly used to refer to any small, incised channel regardless of morphology, and is therefore too general for our purposes).

Arroyos networks are zones of concentrated geomorphic activity, and an understanding of sediment budgets and landscape sensitivity therefore requires a quantitative understanding of their governing mechanisms. A great deal has been written on arroyo networks, particularly those in the U.S. west. The bulk of the literature, however, has concentrated on understanding the trigger factors (e.g., grazing, subtle climate change, or other causes) for widespread arroyo incision near the close of the 19th century (e.g., Cooke and Reeves, 1976; Graf, 1983; Antevs, 1952). Although "ultimate causes" have proven difficult to untangle, it is clear that (a) there usually is a strong correlation between the advent of intensive grazing and widespread channel incision (e.g., Graf, 1988), but equally, in some parts of the world, ancient filled channels indicate that incision has occurred repeatedly during the late Quaternary, indicating that European-scale livestock grazing is not the only possible trigger.

A number of studies have focused on documenting patterns of channel change in drylands, using repeat channel surveys, space-time substitution and other methods. These studies have yielded a valuable database of observations and led to the development of conceptual models to describe a typical "arroyo cycle". Schumm (1977) argued that arroyos commonly undergo a phase of rapid incision, followed by widening and subsequent aggradation as stream power decreases and sediment supply from sidewalls increases. This view was modified by Elliott et al. (1999) to include the possibility of subsequent phases of incision. Leopold (1951) showed that arroyo trenching in the U.S. southwest was correlated with a period of increased rainfall intensity and decreased mean rainfall, and argued that this subtle climate change was sufficient to drive widespread incision. This view was challenged by Schumm and Parker (1973) and Patton and Schumm (1975), who argued on the basis of field observations and laboratory experiments that repeated episodes of incision and infilling can occur due to internal dynamics within a drainage network and do not require external forcing. If correct, this means that past episodes of incision or infilling will not necessarily provide any information about environmental change. (It would not imply that channel incision is unpredictable, but that the driving factors are predominantly internal (e.g., patterns of channel width, gradient, stream power, etc) rather than external.) Bull (1997) developed a conceptual model for discontinuous ephemeral streams in which deposition of a fan-like deposit below a discontinuous channel leads to a gradual increase in gradient, until stream power is sufficient to drive incision.

Despite these advances, we still lack a quantitative, process-based theory for arroyo formation and development, though recent models have begun to address this issue (Howard, 1999; Bull et al., 2000; Kirkby and Bull, 2000; Istanbuloglu et al., in review) and related problems such as the role of vegetation dynamics in ephemeral channel networks (Collins et al., in press). To develop and test such a theory, quantitative observations are needed on arroyo hydrology, kinematics (rates of morphologic change), vegetation patterns, and erosion and sedimentation rates. Here we report on observations collected from gullied drainage basins in central and southern Colorado, USA. These observations, together with inferences drawn from numerical modeling, point toward (a) a highly episodic pattern of arroyo initiation and growth, (b) the importance of intense, convective storms in driving channel incision and advance, and (c) the central role of rangeland vegetation as an erosion mediator.

Field setting

The primary field settings are Fort Carson, Colorado, and its satellite training facility, Pinon Canyon Maneuver Site. Our primary study sites within these installations are shown in Figures 1 and 2.

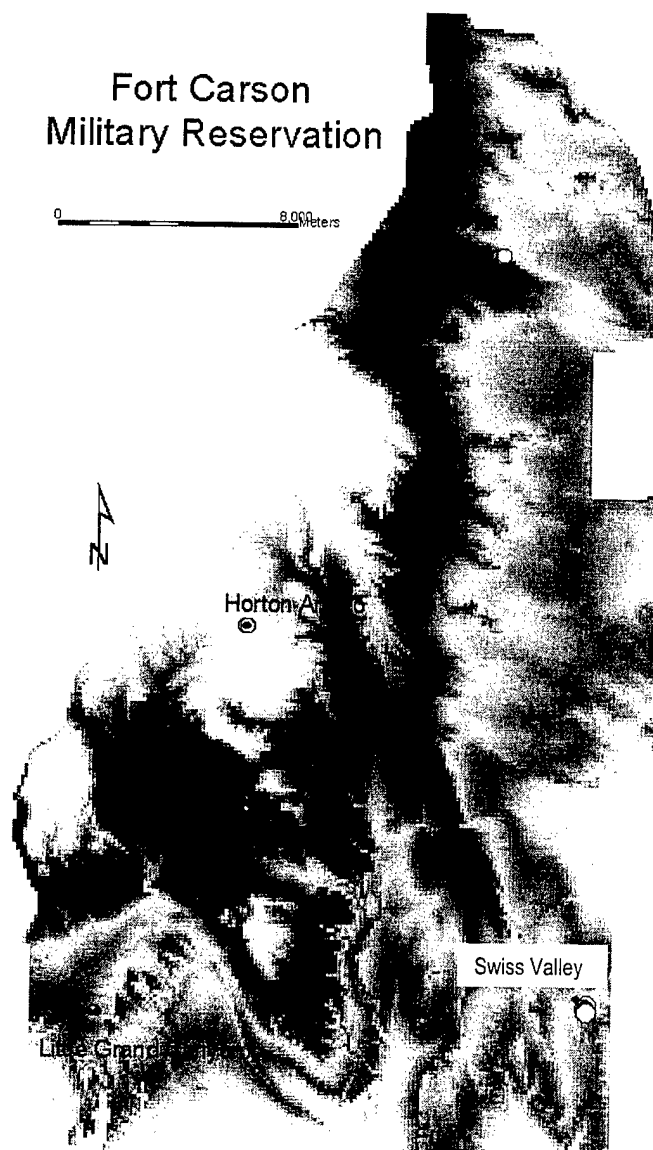


Figure 1: Location of study areas within Fort Carson.

Site FC-1: Little Grand Canyon

This is a several hundred meter long and deeply incised arroyo in Training Area 42 (Figure 3). It is incised into a combination of Quaternary alluvium and interbedded shales and fine sands of the Cretaceous Carlile shale and Greenhorn limestone formations. The head of the arroyo has multiple branches. The

northernmost of these is the deepest (10 to 15m just below the main headscarp); below this, the channel gradually shallows until the channel floor intersects the valley floor about half a kilometer below the largest headscarp. A portion of the northern branch trends almost perpendicular to the valley axis. Within the wall of this branch are three prominent filled paleochannels; the base of the largest of these is on the order of 10m below the valley floor. The alluvial infill exposed within these channels is also exposed throughout the sidewalls of the main channel. The eastern side of the basin contains cliff-forming outcrops of the Fort Hays limestone member of the Niobrara formation. Examination of 1937 aerial photographs reveals that the gully was present in 1937. Between 1937 and 1999 the headcut in its main active branch extended about 30 meters, at an average rate of about 50cm/yr. Since 1937, a shallower channel formed upstream of the main headcut. As of 1999 this upper channel was about 80 meters long; its minimum average extension rate is 1.3 meters per year.

Three large filled paleochannels are exposed along a section of the deep main channel (Figure 4). Three preliminary OSL dates of fill near the base of one of these yields an estimated ages in the early-mid Holocene. It is interesting to note that these dates correspond with the Altithermal period, a time of heightened aridity throughout the southwest.

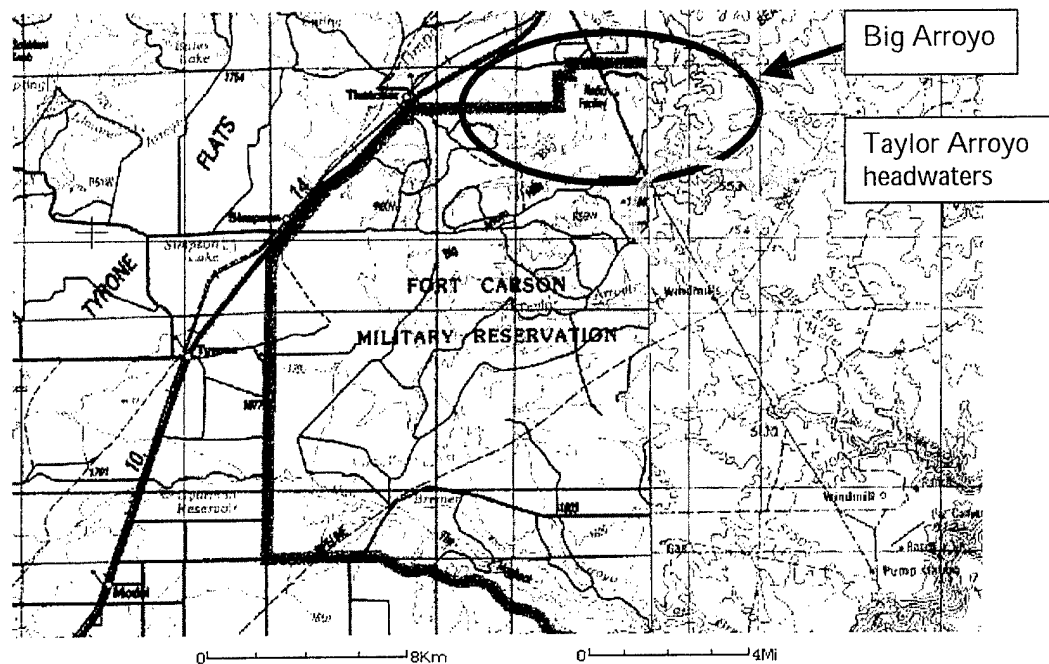


Figure 2: Location of main study areas at PCMS.

Site FC-2: Swiss Valley (also known as "Big Valley")

This site is an east-southeast oriented drainage basin along the eastern base perimeter in the south of Fort Carson (Figure 1, 5). It contains a branching arroyo network whose channels extend nearly to Route 1. The main channel is interrupted by

two large check dams, one near the perimeter fence and one upstream. The catchment is underlain predominantly by sub-horizontal shales and interbedded limestone-shale sequences belonging to the Smoky Hill shale member of the Niobrara formation. Capping this along the basin-margin ridges is an unconsolidated deposit of gravelly alluvium (Quaternary Nussbaum alluvium) sourced from red granites within the Front Range. The presence of this unit implies that the basin rim is a remnant of one of the lower pediment surfaces that occur along much of the Front Range. Within the central part of the valley is a clay-rich (shale-derived) alluvial infill. To the north of the main channel and beginning just below the upper check dam, this clay-rich alluvium is incised by a series of narrow, north-south oriented channels. These channels contain abundant evidence of active piping, including sinkholes and arches. Other piping-associated features, such as pillars and subterranean plunge-pools (?) are present along the walls of the main channel.

The main channel below the upper check dam locally cuts into bedrock, but more commonly is incised into valley-floor alluvium. Multiple, inset filled paleochannels outcrop along the channel walls (Figure 6). The fill within these channels is variable, ranging from stratified granite-derived sands and gravels to massive to stratified platy shales and fine sandstones (?).

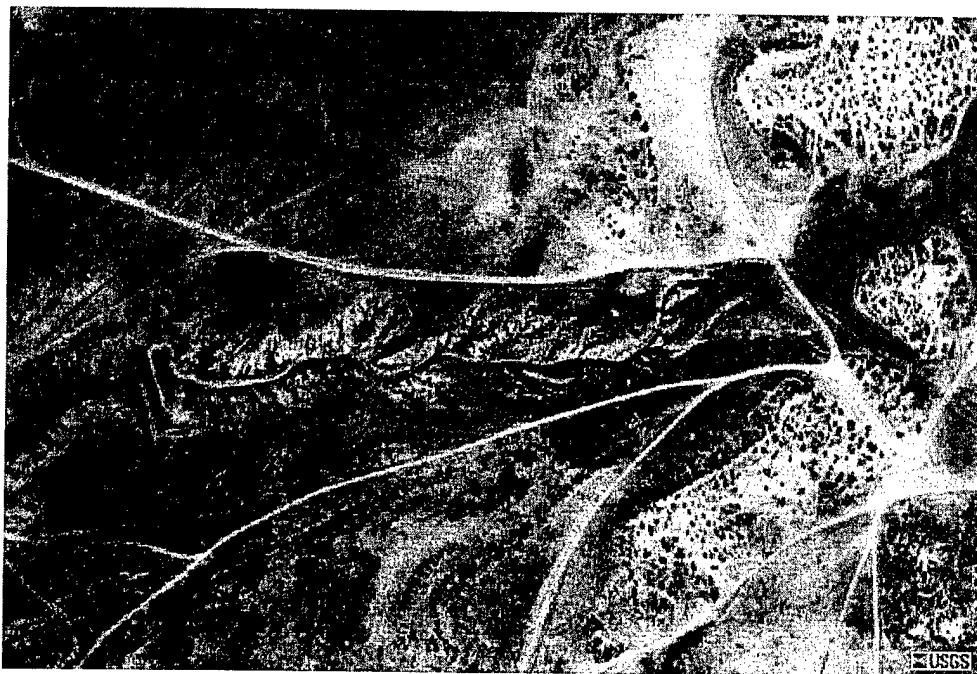


Figure 3A: Little Grand Canyon in a 1999 USGS aerial photograph. Length from head to EC dam is about 800m.

REPORT DOCUMENTATION PAGE (SF298)
(Continuation Sheet)
Page 1 of 34 (excluding appendices)

**MODELING THE DYNAMICS OF GULLY AND ARROYO FORMATION,
FORT CARSON AND PINON CANYON MANEUVER SITE, COLORADO**

Proposal # 41586-EV

Agreement number DAAD19-01-1-0615

FINAL REPORT
Reporting Period 1 June, 2001 to 31 May, 2004

Prepared by Gregory E. Tucker

Current address:
Department of Geological Sciences
CIRES
University of Colorado
2200 Colorado Avenue
Boulder, CO 80309-0399
email: gtucker@cires.colorado.edu

August, 2004

(1) Publications during reporting period

(a) Manuscripts submitted but not yet published:

- (1) Solyom, P., and Tucker, G.E., The effect of limited storm duration on landscape evolution, drainage basin geometry and hydrograph shapes: *Journal of Geophysical Research ES*, in press 2004.
- (2) Istanbuluoglu, E., Bras, R.L., Flores, H., and Tucker, G.E., Implications of Bank Failures and Fluvial Erosion for Gully Development: Field Observations and Modeling. Submitted to *Journal of Geophysical Research - Earth Surface*, March, 2004.

(b) Papers published in peer-reviewed journals or books

- (1) Bogaart, P.W., Tucker, G.E., and de Vries, J.J. (2003) Channel network morphology and sediment dynamics under alternating periglacial and temperate regimes: A numerical simulation study: *Geomorphology*, vol. 54, no. 3/4, p. 257-277.
- (2) Collins, D., Bras, R., and Tucker, G.E. (2004) Modeling the effects of vegetation-erosion coupling on landscape evolution: *Journal of Geophysical Research - Earth Surface*, v. 109, no. F3, F03004, doi:10.1029/2003JF000028.

- (3) Gasparini, N.M., Tucker, G.E., and Bras, R.L. (2004) Network-scale dynamics of grain-size sorting: Implications for downstream fining, stream-profile concavity, and drainage basin morphology: *Earth Surface Processes and Landforms*, 29(4), 401-422.
- (4) Tucker, G.E. (2004) Drainage basin sensitivity to tectonic and climatic forcing: implications of a stochastic model for the role of entrainment and erosion thresholds. *Earth Surface Processes and Landforms*, 29, 185-205.
- (5) Snyder, N.P., Whipple, K.X., Tucker, G.E., and Merritts, D.J. (2003) The importance of a stochastic distribution of floods and erosion thresholds in the bedrock river incision problem: *Journal of Geophysical Research*, vol. 108, no. B2, doi:10.1029/2001JB001655.
- (6) Bras, R.L., Tucker, G.E., and Teles, V.T. (2003) Six myths about mathematical modeling in geomorphology: in *Prediction in Geomorphology*, edited by P. Wilcock and R. Iverson, American Geophysical Union, pp. 63-79.
- (7) Baldwin, J.A., Whipple, K.X., and Tucker, G.E. (2003) Implications of the shear-stress river incision model for the timescale of post-orogenic decay of topography: *Journal of Geophysical Research*, Vol. 108, No. B3, doi: 10.1029/2001JB000550.
- (8) Snyder, N.P., Whipple, K.X., Tucker, G.E., and Merritts, D.J. (2003) Channel response to tectonic forcing: field analysis of stream morphology and hydrology in the Mendocino triple junction region, northern California: *Geomorphology*, Vol. 53, pp. 97-127.
- (9) Arnold, L.J., Stokes, S., Bailey, R., Fattahi, M., Colls, A.E., and Tucker, G. (2002) Optical dating of potassium feldspar using far-red (>665nm) IRSL emissions: A comparative study using fluvial sediments from the Loire River, France. *Quaternary Science Reviews*, 22, 1093-1098.
- (10) Tucker, G.E., and Whipple, K.X. (2002) Topographic outcomes predicted by stream erosion models: Sensitivity analysis and intermodel comparison, *Journal of Geophysical Research*, v. 107, no. B9, 2179, doi:10.1029/2001JB000162.
- (11) Whipple, K.X., and Tucker, G.E. (2002) Implications of sediment-flux dependent river incision models for landscape evolution: *Journal of Geophysical Research*, v. 107, no. B2, DOI 10.1029/2000JB000044.
- (12) Tucker, G.E., Lancaster, S.T., Gasparini, N.M., and Bras, R.L. (2001) The Channel-Hillslope Integrated Landscape Development (CHILD) Model, in *Landscape Erosion and Evolution Modeling*, edited by R.S. Harmon and W.W. Doe III, Kluwer Academic/Plenum Publishers, pp. 349-388.
- (13) Tucker, G.E., Lancaster, S.T., Gasparini, N.M., Bras, R.L., and Rybaczky, S.M. (2001) An Object-Oriented Framework for Hydrologic and Geomorphic Modeling Using Triangulated Irregular Networks. *Computers and Geosciences*, 27(8), pp. 959-973.
- (14) Niemann, J.D., Gasparini, N.M., Tucker, G.E., and Bras, R.L. (2001) A quantitative evaluation of Playfair's Law and its use in testing long-term stream erosion models, *Earth Surface Processes and Landforms*, 26, pp. 1317-1332.

(c) Conference papers (not published in proceedings):

- (1) Solyom, P.B., and Tucker, G.E. (2003) Hypothesis for a channel head stability criterion on the basis of the full continuity equation for sediment transport: paper presented at AGU Fall Meeting, December 2003.
- (2) Tucker, G.E., Clevis, Q., Lock, G., Lancaster, S.T., and Desitter, A. (2003) Modeling the stratigraphy and preservation potential of meandering stream deposits: paper presented at AGU Fall Meeting.
- (3) Tucker, G.E. (2003) Nonlinearity and stochastic effects in long-term stream erosion: Invited paper presented at Geological Society of America Penrose Conference on Tectonics, Climate and Landscape Evolution, Taroko National Park, Taiwan, January, 2003.

- (4) Solyom, P., and Tucker, G.E. (2003) The effect of limited storm duration on landscape evolution, drainage basin geometry and hydrograph shapes: Paper presented at AGU-EGS-EUG joint conference, Nice, France, April, 2003.
- (5) Gasparini, N.M., Bras, R.L., and Tucker, G.E. (2003) Network-scale dynamics of sediment mixtures: how do tectonics affect surface bed texture and channel slope? Paper presented at AGU-EGS-EUG joint conference, Nice, France, April, 2003.
- (6) Tucker, G.E. (2003) Topographic sensitivity to tectonic and climatic forcing: implications of a stochastic model for the role of entrainment and erosion thresholds. Paper presented at British Geomorphological Research Group Annual Conference, September, 2003.
- (7) Robinson, R., and Tucker, G.E. (2003) Channel geometry adjustment in long-term river basin evolution: plausible alternatives to regime theory? Paper presented at British Geomorphological Research Group Annual Conference, September, 2003.
- (8) Solyom, P., and Tucker, G.E. (2003) The effect of catchment geometry on non-steady state runoff production, landscape evolution and channel network optimality. Paper presented at British Geomorphological Research Group Annual Conference, September, 2003.
- (9) Tucker, G.E. (2003) Topographic sensitivity to tectonic and climatic forcing: implications of a stochastic model for the role of entrainment and erosion thresholds. Paper presented at British Geomorphological Research Group Annual Conference, September, 2003.
- (10) Istanbuluoglu, E., Flores, H., Bras, R.L., and Tucker, G.E. (2003) Implications of fluvial erosion and bank failures on gully development and growth. Paper presented at AGU Fall Meeting.
- (11) Gasparini, N.M., Bras, R.L., and Tucker, G.E. (2003) Erosion and Sedimentation in Response to Climate Change: a Numerical Study Using a Multiple Grain-size Sediment Transport Model. Paper presented at AGU Fall Meeting.
- (12) Solyom, P., and Tucker, G.E. (2003) Hypothesis for a Channel Head Stability Criterion on the Basis of the Full Continuity Equation for Sediment Transport. Paper presented at AGU Fall Meeting.
- (13) Tucker, G.E., Clevis, Q., Lock, G., Lancaster, S.T., and Desitter, A. (2003) Modeling the stratigraphy and preservation potential of meandering stream deposits. Paper presented at AGU Fall Meeting.
- (14) Collins, D.B., Bras, R.L., and Tucker, G.E. (2002) Ecogeomorphic modeling of biodiversity and disturbance: Paper presented at American Geophysical Union fall meeting, San Francisco, December 2002.
- (15) Tucker, G.E. (2002) Community sediment models: lessons from landscape evolution modeling. Paper presented at *Workshop on Community Sediment Models*, Boulder, February 2002.
- (16) Tucker, G.E., Arnold, L., Solyom, P., Stokes, S., Bras, R., Collins, D., Flores, H., and Gasparini, N. (2002) Gully initiation by extreme rainfall events: case study from the Colorado High Plains, USA. Paper presented at *Dryland Rivers: Process and Product*, Aberdeen, Scotland, August 8-9, 2002.
- (17) Tucker, G.E., Solyom, P., Arnold, L., Stokes, S., Collins, D., and Bras, R. (2002) Gully initiation by extreme events: theory and case study from the Colorado High Plains, USA. Paper presented at *British Geomorphological Research Group annual conference*, Leeds, England, September 12-14, 2002.
- (18) Tucker, G.E., Solyom, P., Arnold, L., and Stokes, S. (2002) Gully and arroyo erosion. Presentation at *Workshop on Arroyos*, Oxford Centre for Industrial and Applied Mathematics, November, 2002.

- (19) Solyom, P., and Tucker, G.E. (2002) Modelling the effect of storm duration change on runoff production and landscape evolution. Paper presented at British Geomorphological Research Group (BGRG) Postgraduate Symposium, Leeds, UK, April, 2002.
- (20) Collins, D.B., Bras, R.L., and Tucker, G.E. (2001) Modeling the influence of vegetation dynamics on landscape evolution. Paper presented at American Geophysical Union spring meeting, Boston.
- (21) Tucker, G.E., Collins, D.B., and Bras, R.L. (2001) A stochastic model of vegetation-erosion interaction and its influence on denudation time series. Paper presented at *Earth System Processes - Global Meeting*, Edinburgh, Scotland, June 24-28, 2001.
- (22) Collins, D.B., Bras, R.L., and Tucker, G.E. (2001) Meta-stable vegetation cover and erosion cycles. Paper presented at American Geophysical Union fall meeting, San Francisco.
- (23) Snyder, N.P., Whipple, K.X., Tucker, G.E., and Merritts, D.J. (2001) Modeling stochastic floods and erosion thresholds in bedrock rivers: field data from northern California. Paper presented at American Geophysical Union fall meeting, San Francisco.
- (24) Whipple, K.X., and Tucker, G.E. (2001) The role of sediment flux in bedrock channel incision and landscape evolution: model predictions and data needs. Paper presented at American Geophysical Union fall meeting, San Francisco.

2. Scientific personnel and honors/awards/degrees

Personnel (includes only Oxford-affiliated personnel; MIT-affiliated personnel are reported separately):

- Dr. Gregory E. Tucker, PI
- Mr. Peter Solyom, D.Phil. student
- Mr. Lee Arnold, D.Phil. student
- Mr. Tumbikanani Mtika, MSc awarded 2001
- Dr. Stephen Stokes (OSL geochronology; co-supervisor of Arnold)
- Dr. Vanessa Winchester (Dendrogeomorphology)
- Mr. Arnaud Desitter (Software engineering)

3. Report of inventions

None.

4. Scientific progress and accomplishments

4.1 Introduction

Gully erosion is one of the most dramatic outcomes of environmental change, whether that change is of natural or anthropogenic origin. The initiation and growth of gully systems can lead to significant land degradation. The resulting sediment loads can lead to significant downstream impacts, including water quality degradation, reservoir and waterway sedimentation, and disturbance of aquatic ecosystems. In some cases, gully growth may halt or reverse following a period of landscape recovery; in others, the initiation of gully systems may trigger a self-enhancing feedback effect in which gullies continue to propagate long after the initial disturbance is removed.

In order to develop a better understanding of gully networks and their physics, this project has brought together a complementary suite of techniques: mathematical and numerical modeling, field survey, repeat aerial photograph analysis, paleohydrology, optically stimulated luminescence (OSL) dating, and dendrogeomorphology. The most general aim is to develop a better quantitative understanding of the dynamics of gully initiation and growth. More specifically, we have sought to achieve the following objectives:

- Develop an improved landscape evolution model capable of simulating the key processes involved in rangeland gully formation and evolution;
- Test this model by discovering necessary and sufficient conditions (e.g., processes, parameters, and boundary conditions) required to explain key features of semi-arid gully/arroyo systems;
- Discover testable implications of key contributing factors, such as sediment-entrainment thresholds, grassland vegetation dynamics, and convective-storm hydrology, by conducting sensitivity experiments in which process parameters can be varied independently;
- Test the hypothesis of autocyclicality (i.e., no independent trigger necessary) in observed alternating erosion-deposition cycles, by determining whether autocyclicality can be reproduced numerically;
- Document the tempo of gully erosion on three different time scales: annual (via repeat field survey), multi-decadal (via analysis of historic and modern aerial photographs), and late Quaternary (via OSL dating);
- Test the potential for dendrogeomorphic methods to contribute useful quantitative data on channel evolution and dynamics;
- Assess the potential for turning the research-grade numerical model into practical decision-support tools for land management, and the data and computational ingredients required.

This report discusses progress made toward each of these objectives, and the methods employed.

This report is organized as a series of sections dealing with one or more aspects of the project. In many cases, these refer to reprints of published papers, which are included as appendices. In several areas, the objectives of this project have overlapped with those of related research activities, leading to publications that combine elements of two or more projects. In choosing which publications to include

and discuss, we have opted for inclusiveness. As a result, some of the publications included as appendices deal with rather general issues (such as the role of erosion thresholds in the mechanics of channel evolution) with implications that extend beyond the immediate question of gully physics. Likewise, because of the collaborative nature of this project, we have not tried to separate explicitly the work performed by the Oxford and MIT teams, though this report does emphasize the Oxford team's activities.

The project has involved contributions from many people. In particular, the project has benefited greatly from the work of graduate students and postdoctoral researchers at MIT and the University of Oxford, who are the lead authors of many of the appendices in this report. They include: Lee Arnold (OSL dating and stochastic modeling), Daniel Collins (vegetation modeling), Homero Flores (plunge-pool erosion modeling, soils analysis), Dr. Erkan Istanbuluoglu (slab-failure measurement and modeling), Tumbikanani Mtika (channel head analysis), and Peter Solyom (erosion-hydrology modeling, catchment-shape controls). In addition, Dr. Stephen Stokes and Dr. Vanessa Winchester of the University of Oxford generously contributed time and expertise, as well as the use of their laboratories. Arnaud Desitter made vast improvements to the performance, efficiency, and capabilities of the CHILD code. Quintijn Clevis made significant contributions to CHILD's floodplain and stratigraphy modules, and Patrick Bogaart developed the original TimeSeries module in CHILD. We are also grateful for field assistance from Bill Bennett, Domenico Capolongo, Nicole Gasparini, Salvatore Grimaldi, Quintijn Clevis, and Vanessa Teles. John Kuzmiak of the U.S.G.S. Pueblo Office kindly provided access to high-resolution rainfall and discharge records. Finally, the support of the Fort Carson Directorate of Environmental Compliance and Management (DECAM) has been invaluable to the project. It would not have been possible without their help. In particular, we would like to thank Brian Goss, James Kulbeth, Jeff Linn, Bruce Miller, Linda Moeder, and Dan Sharps.

4.2 CHILD Model Development and Capabilities

One of the main aims of the project was to add new capabilities to the CHILD model. Here, these capabilities are summarized. Applications and results from sensitivity analyses appear in various sections below.

Improvements to mesh-generation algorithms, low-level routines, and utility functions include the following:

- Implementation and testing of the fast Tipper algorithm for Delaunay triangulation. This resulted in a mesh-generation speed improvement on the order of 10^2 .
- General performance tuning and removal of memory leaks.
- Improved input-file handling, with fast random (rather than sequential) access of input data files.
- Implementation of a network-accessible source code management, update and retrieval system using the open-source Concurrent Version System (CVS). The system allows for file modification by multiple, concurrent developers, for retrieval of past file versions, and provides many other developer features.
- Creation of a browser-accessible auto-documentation system for the source code using the Doxygen document generator.

- Improved cross-platform compatibility, including resolution of floating-point handling differences among compilers and chipsets. Recent versions of CHILD have been compiled for Linux, MacOS, Sun, and Intel platforms.
- Random number generator enhancements, including read/write of current random generator state (which allows runs to be interrupted and re-started from exactly the same state), and independent random-number sequences for different modules.
- Run-time (rather than compile-time) selection of erosion/transport formulas.

Other new capabilities include the following:

- Module to simulate channel sidewall erosion/sedimentation by slab failure (Istanbulluoglu et al., in review).¹
- Time Series handling module that provides a general input-file format and parsing capability to handle time-varying parameters, such as mean storm intensity or infiltration capacity.
- Module simulating plunge-pool erosion (Flores, 2004).¹
- Option for computing peak storm discharge based on catchment geometry and storm duration (Solyom and Tucker, in press).
- Addition of new alternative erosion and sediment transport algorithms, including the Bridge-Dominic formula and a modified form of the Meyer-Peter-Mueller formula (Tucker, 2004).
- In connection with a related project on alluvial valley evolution, a module has been developed to record depositional stratigraphy at high space-time resolution, and bugs in the stream-meander module that caused the model to crash under conditions of rapid sedimentation have been fixed.

4.3 Origins and Controls on Arroyo Networks: Results from Paleohydrology and Aerial Photograph Analysis

Introduction

Understanding erosion and sediment transport in rangeland landscapes is important for a variety of reasons. From the perspective of land management, effective erosion control requires an understanding of the nature, frequency and magnitude of the climatic, hydrologic, biotic, and geomorphic drivers. From the perspective of long-term landscape evolution, a quantitative understanding of the "rules of the landscape" is needed in order to answer questions such as: What are the frequency and magnitude properties of sediment movement, and how do these change with scale? How sensitive are rates of sediment movement and topographic change to climatic, tectonic, or human forcing? What interpretations of the Quaternary landscape-change record are consistent with the mechanics and chemistry of the driving processes? In addition, in the particular case of the central Rocky Mountains piedmont, which we investigate here, quantitative models of rangeland dynamics are needed to test the plausibility of the hypothesis that climatic oscillation has driven accelerated denudation along the margins of the Rocky Mountains (e.g., Zhang et al., 2001).

¹ Implemented in MIT version; merger with CU-Oxford code base pending.

In this contribution we focus on the dynamics of ephemeral headwater (low-order) channel networks. Ephemeral headwater channel systems are important to understand because they are primary conduits for water and sediment movement. They also tend to be highly dynamic, with gully systems capable of growing rapidly into formerly unchanneled valleys and generating high sediment yields.

Vegetation plays a crucial role in controlling ephemeral channel incision. Field experiments in semi-arid grassland environments in Australia, California, and Arizona have revealed that an intact cover of herbaceous vegetation can effectively resist overland flow erosion even under shear stresses on the order of 100 Pa or more. Erosional vulnerability is substantially increased when the vegetation is damaged or removed; field tests on bare agricultural soils, for example, have shown that rilling can occur under overland-flow shear stresses on the order of only a few Pa. This evidence implies that the presence of an intact herbaceous vegetation cover can raise the effective erosion threshold by as much as two orders of magnitude, in addition to indirect hydrologic effects (such as increased runoff generation following vegetation loss).

The strong role of vegetation raises an important question regarding headwater dynamics: in a natural system, what are the relative roles of extreme runoff events versus vegetation damage events (e.g., droughts, damage by herbivory or disease) in controlling the tempo of channel network extension and retreat? Modern gully networks are often attributed to human impacts (typically heavy grazing by livestock). For example, Dietrich et al. (1993) found that the extent of channels in a California grassland catchment corresponded to an overland flow erosion threshold of 16-32 Pa, while a flume study in the same catchment suggested an effective erosion threshold of over 100 Pa under complete grass cover. Montgomery and Dietrich (1992) interpreted the extension of gullies in the catchment as a response to overgrazing. Yet the fact that this and other gully networks typically occupy dry valley systems suggests that periodic sediment evacuation by channel extension is a common natural process that does not require human disturbance. In order to understand the dynamics of headwater extension and retreat over geologic time scales, and the sensitivity of the system to environmental change (e.g., Rinaldo et al., 1995; Tucker and Slingerland, 1997), we need to understand the natural trigger factors for channel growth and retreat. To what degree is channel network extension driven by rare, intense storms, as opposed to episodes of vegetation disturbance due to drought, grazing, and disease? What controls the frequency and magnitude of extension events? And what are the implications of these controls for catchment sensitivity to climate change?

Here, we report observations from ephemeral channel networks in Colorado, USA, to address these questions and provide data for testing quantitative models. Analysis of aerial photographs and recent erosion events provides insight into the tempo of channel extension. Paleohydrologic reconstructions provide evidence for the magnitude of shear stresses generated during convective summer storms, and the relative frequency of these events. From these observations, inferences are drawn regarding the geomorphic impact of localized, high-intensity storm cells.

Background

The term rangelands is usually defined on the basis of vegetation (predominantly grasses, shrubs and similar groups) or land use (suitable for grazing animals but not arable agriculture) or both. Here, we use a looser, geomorphically based definition: terrain with low to moderate relief in which either present-day or glacial maximum climate supported a climax vegetation of predominantly low-

growing species such as shrubs and grasses. This definition includes much of the piedmont landscapes of the North American west, much of southern Africa, large areas of Australian lowlands, Mediterranean regions, South American pampas, and similar regions.

The geomorphology of rangelands is commonly characterized by ephemeral or intermittent stream channels and unchanneled valleys. Dry channels, variously called "gullies," "arroyos," "wadis" or other regional terms, are common. Whatever the name, ephemeral channels in rangelands are often incised into valley-floor alluvium or occasionally bedrock (e.g., Cooke and Reeves, 1976; Graf, 1983; Bull, 1997; Prosser and Slade, 1994; Boardman et al., 2003). Here the term arroyo is used to refer to incised, ephemeral channels with steep sidewalls and a rectilinear to U-shaped cross section. (Note that by including incised ephemeral channels of all sizes we depart from the definition of Graf (1988), who preferred the term "gully" for smaller channels. However, "gully" is commonly used to refer to any small, incised channel regardless of morphology, and is therefore too general for our purposes).

Arroyos networks are zones of concentrated geomorphic activity, and an understanding of sediment budgets and landscape sensitivity therefore requires a quantitative understanding of their governing mechanisms. A great deal has been written on arroyo networks, particularly those in the U.S. west. The bulk of the literature, however, has concentrated on understanding the trigger factors (e.g., grazing, subtle climate change, or other causes) for widespread arroyo incision near the close of the 19th century (e.g., Cooke and Reeves, 1976; Graf, 1983; Antevs, 1952). Although "ultimate causes" have proven difficult to untangle, it is clear that (a) there usually is a strong correlation between the advent of intensive grazing and widespread channel incision (e.g., Graf, 1988), but equally, in some parts of the world, ancient filled channels indicate that incision has occurred repeatedly during the late Quaternary, indicating that European-scale livestock grazing is not the only possible trigger.

A number of studies have focused on documenting patterns of channel change in drylands, using repeat channel surveys, space-time substitution and other methods. These studies have yielded a valuable database of observations and led to the development of conceptual models to describe a typical "arroyo cycle". Schumm (1977) argued that arroyos commonly undergo a phase of rapid incision, followed by widening and subsequent aggradation as stream power decreases and sediment supply from sidewalls increases. This view was modified by Elliott et al. (1999) to include the possibility of subsequent phases of incision. Leopold (1951) showed that arroyo trenching in the U.S. southwest was correlated with a period of increased rainfall intensity and decreased mean rainfall, and argued that this subtle climate change was sufficient to drive widespread incision. This view was challenged by Schumm and Parker (1973) and Patton and Schumm (1975), who argued on the basis of field observations and laboratory experiments that repeated episodes of incision and infilling can occur due to internal dynamics within a drainage network and do not require external forcing. If correct, this means that past episodes of incision or infilling will not necessarily provide any information about environmental change. (It would not imply that channel incision is unpredictable, but that the driving factors are predominantly internal (e.g., patterns of channel width, gradient, stream power, etc) rather than external.) Bull (1997) developed a conceptual model for discontinuous ephemeral streams in which deposition of a fan-like deposit below a discontinuous channel leads to a gradual increase in gradient, until stream power is sufficient to drive incision.

Despite these advances, we still lack a quantitative, process-based theory for arroyo formation and development, though recent models have begun to address this issue (Howard, 1999; Bull et al., 2000; Kirkby and Bull, 2000; Istanbuloglu et al., in review) and related problems such as the role of vegetation dynamics in ephemeral channel networks (Collins et al., in press). To develop and test such a theory, quantitative observations are needed on arroyo hydrology, kinematics (rates of morphologic change), vegetation patterns, and erosion and sedimentation rates. Here we report on observations collected from gullied drainage basins in central and southern Colorado, USA. These observations, together with inferences drawn from numerical modeling, point toward (a) a highly episodic pattern of arroyo initiation and growth, (b) the importance of intense, convective storms in driving channel incision and advance, and (c) the central role of rangeland vegetation as an erosion mediator.

Field setting

The primary field settings are Fort Carson, Colorado, and its satellite training facility, Pinon Canyon Maneuver Site. Our primary study sites within these installations are shown in Figures 1 and 2.

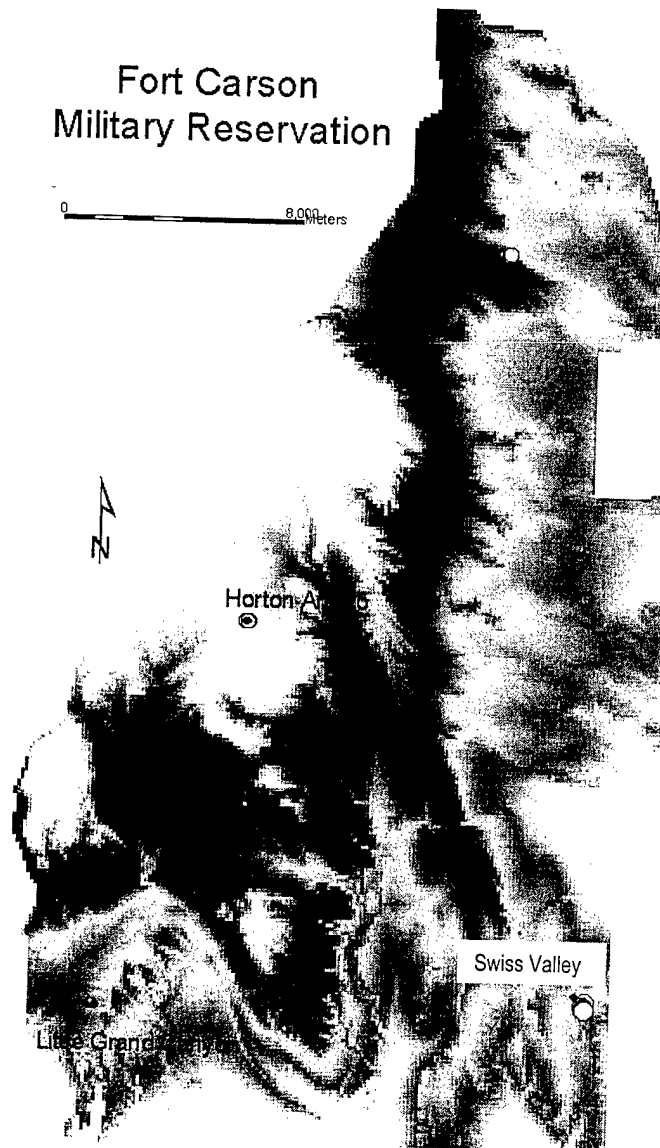


Figure 1: Location of study areas within Fort Carson.

Site FC-1: Little Grand Canyon

This is a several hundred meter long and deeply incised arroyo in Training Area 42 (Figure 3). It is incised into a combination of Quaternary alluvium and interbedded shales and fine sands of the Cretaceous Carlile shale and Greenhorn limestone formations. The head of the arroyo has multiple branches. The

northernmost of these is the deepest (10 to 15m just below the main headscarp); below this, the channel gradually shallows until the channel floor intersects the valley floor about half a kilometer below the largest headscarp. A portion of the northern branch trends almost perpendicular to the valley axis. Within the wall of this branch are three prominent filled paleochannels; the base of the largest of these is on the order of 10m below the valley floor. The alluvial infill exposed within these channels is also exposed throughout the sidewalls of the main channel. The eastern side of the basin contains cliff-forming outcrops of the Fort Hays limestone member of the Niobrara formation. Examination of 1937 aerial photographs reveals that the gully was present in 1937. Between 1937 and 1999 the headcut in its main active branch extended about 30 meters, at an average rate of about 50cm/yr. Since 1937, a shallower channel formed upstream of the main headcut. As of 1999 this upper channel was about 80 meters long; its minimum average extension rate is 1.3 meters per year.

Three large filled paleochannels are exposed along a section of the deep main channel (Figure 4). Three preliminary OSL dates of fill near the base of one of these yields an estimated ages in the early-mid Holocene. It is interesting to note that these dates correspond with the Altithermal period, a time of heightened aridity throughout the southwest.

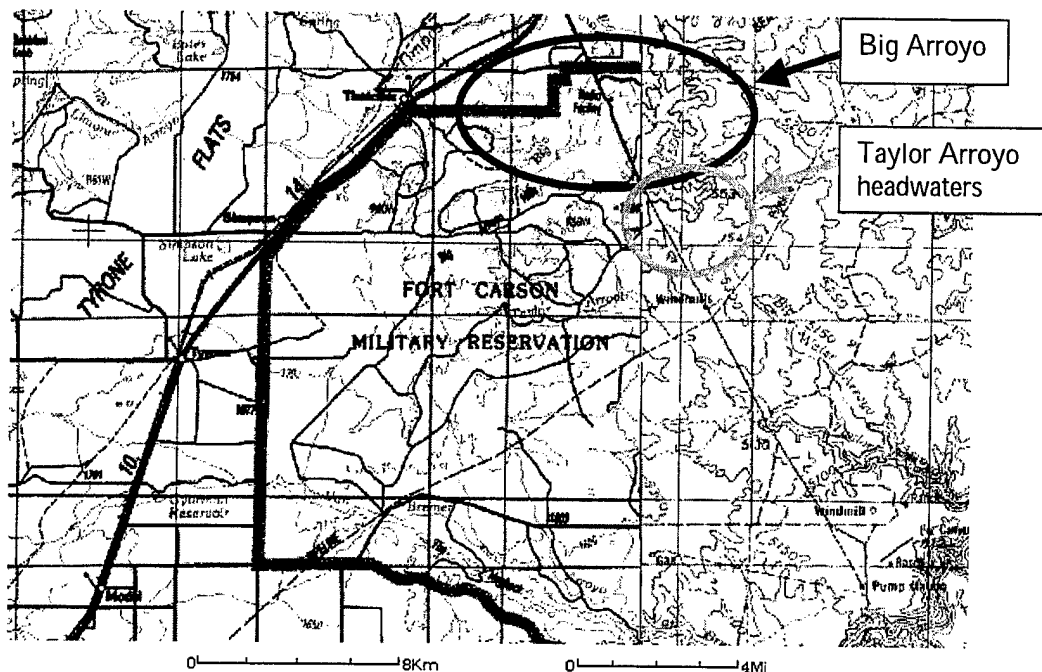


Figure 2: Location of main study areas at PCMS.

Site FC-2: Swiss Valley (also known as "Big Valley")

This site is an east-southeast oriented drainage basin along the eastern base perimeter in the south of Fort Carson (Figure 1, 5). It contains a branching arroyo network whose channels extend nearly to Route 1. The main channel is interrupted by

two large check dams, one near the perimeter fence and one upstream. The catchment is underlain predominantly by sub-horizontal shales and interbedded limestone-shale sequences belonging to the Smoky Hill shale member of the Niobrara formation. Capping this along the basin-margin ridges is an unconsolidated deposit of gravelly alluvium (Quaternary Nussbaum alluvium) sourced from red granites within the Front Range. The presence of this unit implies that the basin rim is a remnant of one of the lower pediment surfaces that occur along much of the Front Range. Within the central part of the valley is a clay-rich (shale-derived) alluvial infill. To the north of the main channel and beginning just below the upper check dam, this clay-rich alluvium is incised by a series of narrow, north-south oriented channels. These channels contain abundant evidence of active piping, including sinkholes and arches. Other piping-associated features, such as pillars and subterranean plunge-pools (?) are present along the walls of the main channel.

The main channel below the upper check dam locally cuts into bedrock, but more commonly is incised into valley-floor alluvium. Multiple, inset filled paleochannels outcrop along the channel walls (Figure 6). The fill within these channels is variable, ranging from stratified granite-derived sands and gravels to massive to stratified platy shales and fine sandstones (?).



Figure 3A: Little Grand Canyon in a 1999 USGS aerial photograph. Length from head to EC dam is about 800m.



Figure 3B: Little Grand Canyon in 1937. Note extension of northernmost branch between 1937 and 1999.

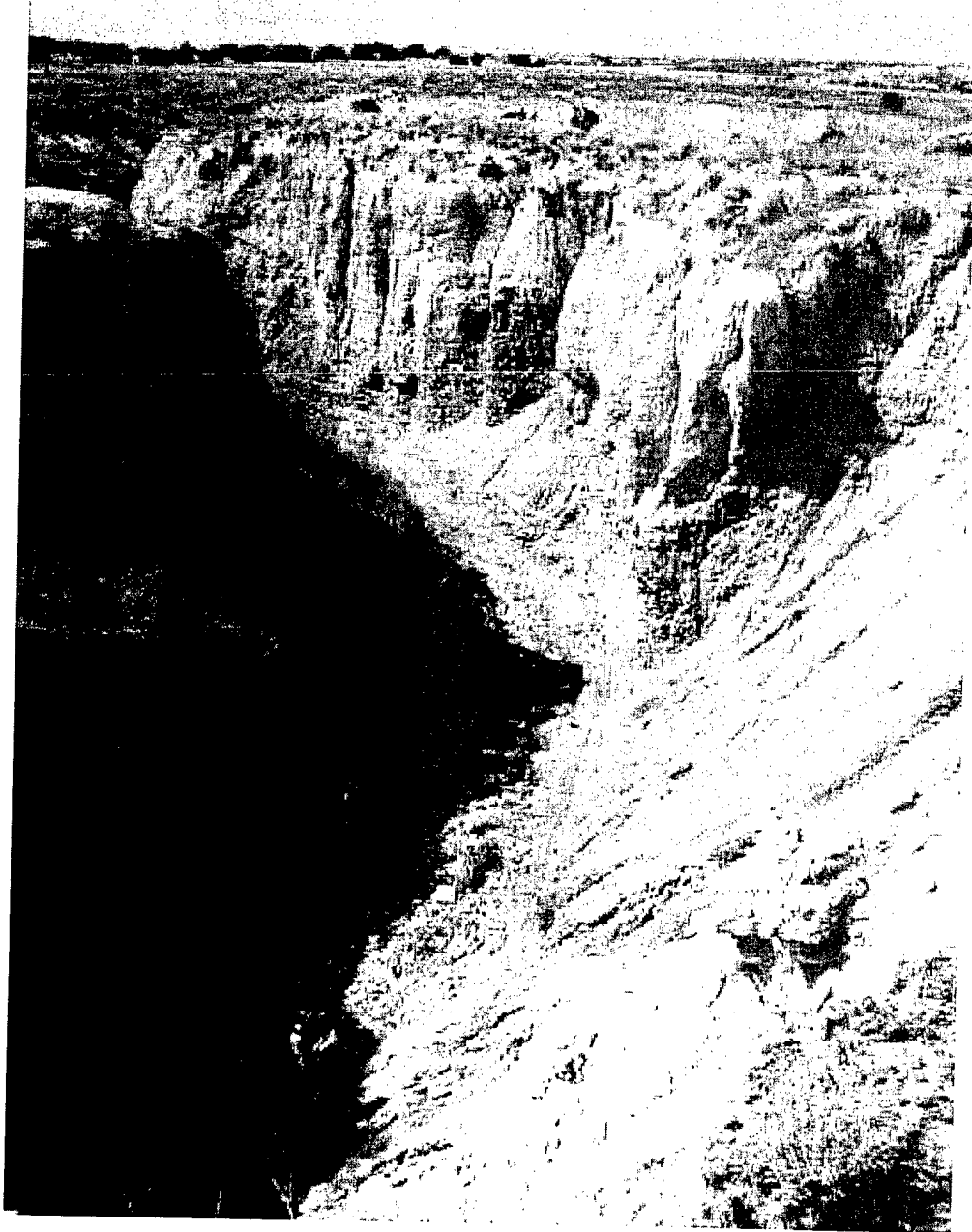


Figure 4: View looking southwest along main upper branch of Little Grand Canyon, showing three large, filled paleochannels (left-most one is partly obscured). The buff-colored channel fills contrast with the dark shale bedrock.

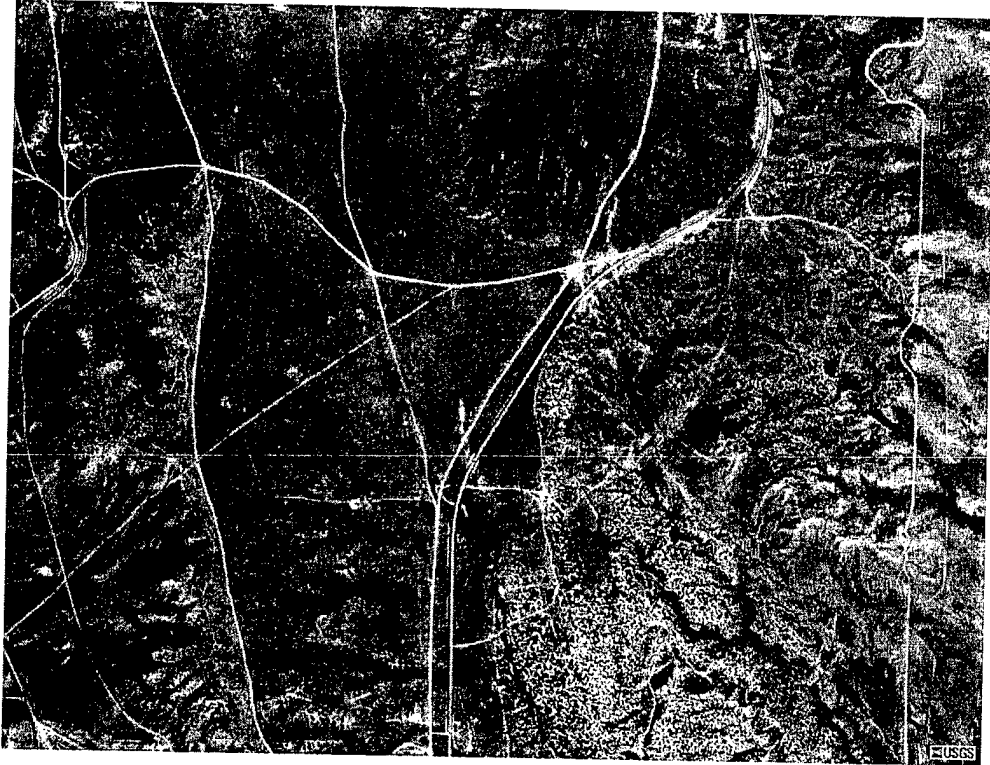


Figure 5: Swiss Valley. The channel network begins south and east of Route 1, which is the prominent paved road. Note path along base perimeter at right. The upper check dam is right of center.

Site FC-3: Horton Arroyo

This is a small drainage basin just east of Route 11 (Figure 7). It contains a wide but short (few hundred meters) arroyo that deepens upslope toward the main headscarp just below a large juniper tree. A shallower channel continues upslope of this. (The underlying lithology is mapped as "landslide deposit" but given the stratified nature of the fill exposed in the channel walls, this is clearly incorrect).

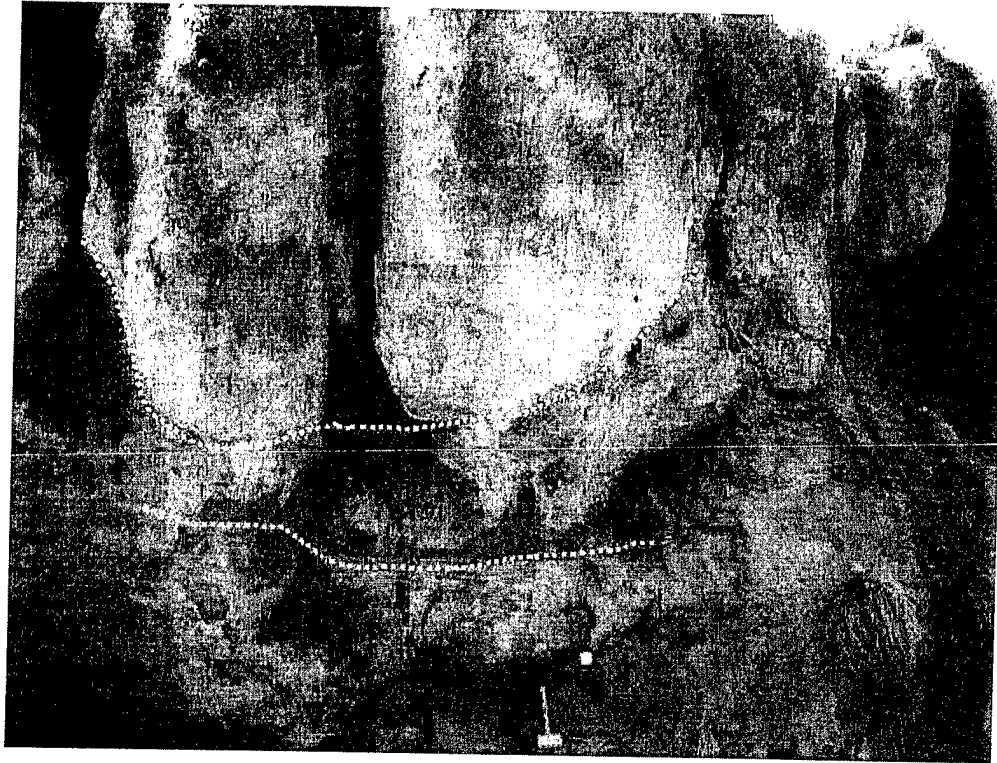


Figure 6: Paleochannels exposed in the side wall of a large gully in southeastern Fort Carson (Training Area 48). Dashed lines indicate two different generations of cut and fill. Note mallet for scale. OSL dating samples have been collected from this site.



Figure 7: Horton Arroyo seen in a 1999 USGS aerial photograph. Gully is about 200m long.

Site PC-1: Big Arroyo

This is a large drainage basin (15.5 square miles at the gaging station near the site boundary) underlain by upper Cretaceous sedimentary rocks (Figure 2). We report on observations from several locations within the Big Arroyo watershed.

Site PC-2: Taylor Arroyo

Taylor Arroyo is a tributary to the Purgatoire River. The watershed above the Rock Crossing gaging station is 48.4 square miles in area. Below we report on observations and measurements obtained from the headwaters area of Taylor arroyo in the vicinity of Burson Camp (Figure 2).

Channel forms, processes and occurrence

Occurrence and lithology

A variety of different channel forms have been observed in these field areas. As discussed above, we focus here on incised ephemeral channels with distinct, steep to vertical sidewalls. Based on aerial photograph analysis and field reconnaissance, it is clear that these channels occur predominantly in valley alluvium and/or shale bedrock. Texture analysis of incised alluvial fills show that these range from clay to sandy loam; the average median grain size from 41 field samples is 0.03mm (medium silt; $\phi = 5.9 \pm 1.8$; Flores, 2004). Incised channels are rare or absent in more competent lithologies (e.g., the Fort Hayes limestone member of the Niobrara formation), though they often do occur in alluvial valley fills that overlie these lithologies. Where channels have been observed to cut into bedrock, the bedrock is typically shale-rich. In several cases, we have observed vertical walls of alluvium overhanging fissile shale bedrock, suggesting that the fill is typically more cohesive

than the shale. Incised ephemeral channels are also rare on Quaternary gravel-capped pediments, which are common along the Front Range.

Channel morphology

By definition, the channels investigated here are rectilinear to U-shaped in cross-section. Sidewalls typically show a near-vertical wall section above a sloping rampart. Vertical wall height is correlated with substrate cohesion (Istanbulluoglu et al., in review). Unlike the valley and channel floods, and to a lesser extent ramparts, near-vertical walls are nearly always devoid of vegetation. Vegetation on channel floors ranges from essentially absent to a full cover of woody and herbaceous riparian species.

Channel heads

We have observed three types of channel head morphology, which often intergrade with one another.

1. Channels or channel segments that terminate abruptly with steep, vertical headcuts (ranging from "large step" to "large headcut" in the classification of Dietrich and Dunne, 1993).
2. Channels in which a narrower, shallower reach extends tens of meters above a prominent, broader and deeper headcut. In these cases, the headcut is typically supported by tree roots or by a resistant rock unit.
3. Flights of arcuate, discontinuous steps. Steps often lack discernable banks; where present, these rarely extend more than a few meters below the step. Step-flights often occur up-valley from a continuous channel showing morphology type 1 or 2. In other cases, they grade gradually downstream into increasingly long discontinuous channel segments. Evidence from historical air photos (discussed below) shows that step-flights are sometimes precursors to continuous incised channels.

Hydrologic analysis and flash flood discharge reconstruction

Our understanding of the hydrology of ephemeral channels in small headwater drainage basins ($\leq 10 \text{ km}^2$) is hampered by a lack of stream-gaging data. For example, although the USGS Surface Water database lists nearly 1200 gaging stations in the state of Colorado, fewer than 50 are in basins smaller than 3 square miles ($\sim 9 \text{ km}^2$), and only 17 of these are in basins smaller than one square mile ($\sim 3 \text{ km}^2$). Most have fewer than 10 years of record. In documenting the hydrology of arroyo networks in headwater areas, we are therefore forced to rely on paleohydrologic analysis.

Observations at the study sites indicate that rainfall generated by summer convective storms can generate large volumes of overland flow. Because the water table in the study sites is normally tens of meters below the ground surface (von Guerard, 1987), storm runoff is presumable generated by infiltration-excess overland flow. In one instance at the Swiss Valley site, we observed overland flow and flow in a gully channel occurring within minutes of the onset of a ~ 30 min storm. The resulting wetting front penetrated only about 2 cm into the clay-rich soil at this site.

In the middle reaches of Big Arroyo, we have observed flood debris indicating 10-15cm deep overland flow within an unchanneled valley. In this instance, the overland flow appears to have been generated by a convective storm that struck the area on August 8, 2003, 46 days prior to our observation. The nearby Burson Camp

rain gage located near the site recorded 60mm of precipitation on that day. This rain resulted from a storm of a little over 90 minutes in duration, with a peak 15-minute average intensity of 86mm/hr.

Analysis of the July, 2001 Sullivan Park event

An intense convective storm struck the Sullivan Park area of Fort Carson on July 13, 2001. The event caused check dams to overspill, and the spillways of at least two of these dams were heavily damaged (Figure 8). Both spillways had been lined with geotextile and armored with ~9" diameter granite boulders. Flood marks along the check dam crest and spillway mouth immediately after the event indicate that the peak outflow filled the trapezoidal spillway mouth and extended as shallow flow over part of the dam crest (J. Kulbeth, personal communication). From the dimensions of the spillway mouth and the gradient of the spillway, it is possible to estimate peak discharge and corresponding runoff rate. The slope of the spillway was measured using a hand level, which is accurate to about 0.5 degrees. Spillway mouth dimensions were provided by J. Kulbeth (DECAM). Using the Manning equation for flow velocity and roughness in a channel, we estimated that total peak discharge was on the order of 20-60 cubic meters per second. Given the size of the catchment draining to Dam 134, this would have amounted to a peak rainfall rate in excess of 100 mm/hr. Although high, this is not without precedent. Other high short-term intensities have been reported in the literature (e.g., Goodrich et al., 1997; Bull et al., 1999). A tipping-bucket rain gage about one mile north of the E.C. dam recorded an average peak rate of about 60mm/hr lasting for about 20 minutes (Figure 9). On the steeper portion of the spillway, where 9" boulders were entrained and removed, the resulting peak shear stress exceeded 400 Pa (because this calculation assumes steady, uniform flow, it is likely to be a slight overestimate because it neglects flow acceleration). This is consistent with the estimated entrainment threshold (critical shear stress) of order 200 Pa for the boulder armor. On the upper spillway slope, the shear stress would have been lower due to the lower gradient. Using the same range of roughness values and allowing for uncertainty in gradient measurement, the estimated peak shear stresses in the upper spillway are below the entrainment threshold for the boulder armor. Thus, the flow reconstruction is consistent with the observed pattern of boulder entrainment (Figure 8).



Figure 8: Lower portion of the spillway of Dam 134, Sullivan Park, Fort Carson, which was damaged by an intense storm on 13 July, 2001.

The drainage area above the check dam is approximately 0.5 km^2 . Dividing the peak discharge by the drainage area gives an estimated peak runoff rate of 170 to 460 mm/hr. By comparison, a tipping-bucket rain gage located about 1 mile to the north recorded a peak 15-minute average rainfall rate of 78 mm/hr (Figure 9). Although the estimated peak runoff rates are considerably higher than this, we believe that lower range of the estimate (order 200mm/hr) is plausible because (a) convective cells are known to have narrow radii, and (b) peak rainfall intensities on the order of 200-350 mm/hr have been recorded in similar climatic settings (e.g., Goodrich et al., 1997; Bull and Kirkby, 2000). It is also noteworthy that an event of similar magnitude (peak 15-min intensity 61mm/hr recorded at Sullivan Park) struck the area in 1999, also damaging check dams.

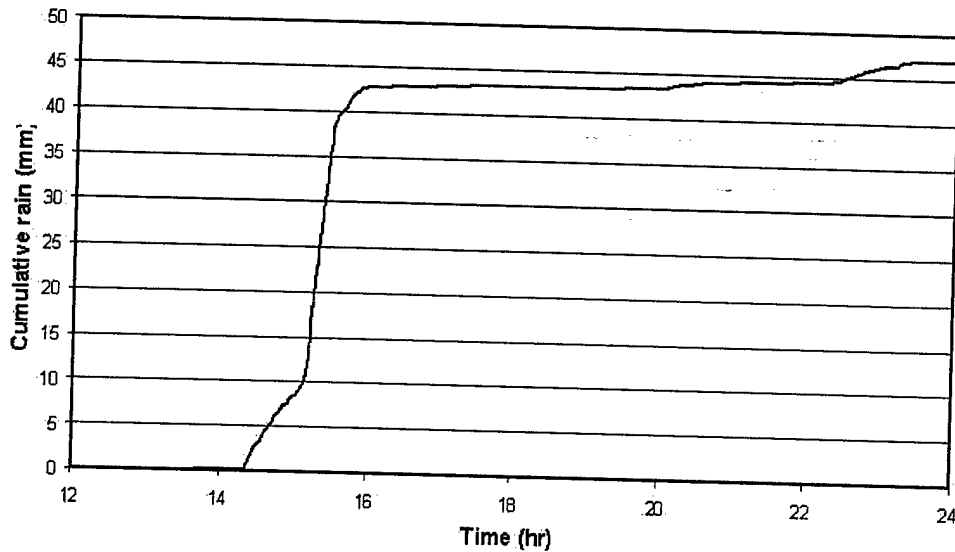


Figure 9: Cumulative rainfall plot at Sullivan Park meteorological station, July 13, 2001.

Peak discharge reconstruction in existing arroyo networks

Analysis of channel cross-sections and mapping of the height of recent flood debris allows reconstruction of peak in-channel discharges generated by short, intense convective storms. Here we describe peak-flow estimates from channel segments in the Little Grand Canyon, Big Arroyo, and Taylor Arroyo Sites.

Six channel cross sections were measured along the middle reaches of Big Arroyo. A preliminary estimate based on the downstream-most section indicates a peak flow of about 5 cms (shear stress ~ 40 Pa) associated with a storm on August 8, 2003. By contrast, the Big Arroyo gaging station, roughly 5 km downstream, recorded a peak discharge of only 22 cfs (0.6 cms), indicating significant in-stream losses during the event.

In Taylor Arroyo, four cross-sections were surveyed and analyzed for purposes of peak-flow reconstruction. Preliminary analysis indicates a peak discharge of about 1 cms, with an average flow velocity of ~ 0.6 m/s and resulting bed shear stress of 40-50 Pa.

In the Little Grand Canyon, survey in September 2003 revealed evidence of recent flow and channel incision. Near the upper part of the largest branch, the channel had incised about 1 meter (relative to a fixed OSL sampling site in the wall) since the previous survey in July 2002. Five cross-sections were surveyed for discharge analysis. Preliminary estimates of peak flow range from 1-3 cms, with associated shear stress ranging from 70 to 130 Pa.

Channel Pattern Analysis

Aerial photograph analysis

There are several lines of evidence that indicate that arroyo growth is highly episodic. Inspection of aerial photographs of portions of Fort Carson taken in 1937, 1962 and 1991 reveals that most (not all) channels that existed in 1937 had roughly the same extent in 1991. One example of this is the Little Grand Canyon (Figure 3A,B). Another is Horton Gully (Figure 10), the extent of which appears virtually unchanged over the 29-year period between 1962 and 1991. Field inspection shows that in fact the upper portion of the channel is still active and continuing to deepen, but that the wide, fork-headed portion of the channel retains essentially the same shape and size that it had over 40 years ago. The southern branch appears to be partly or largely inactive, as evidenced by slump deposits around the headcut. It is likely that this head was once fed directly by runoff from the dirt road adjacent, but that later most of this runoff was diverted into the northern head (where it is directed today). Examination of the base of a juniper tree growing within the main channel indicates recent aggradation (i.e., the primary roots are buried).

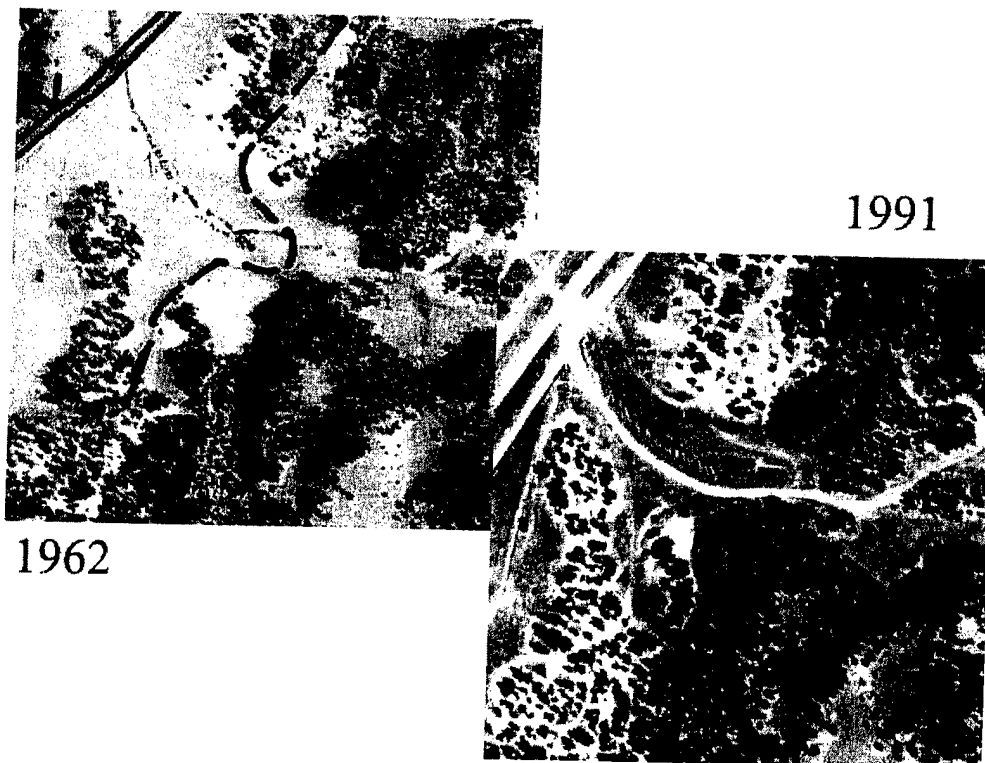


Figure 10: Comparison of the extent of Horton Arroyo in 1962 (left) and 1991.

Overall, this suggests a pattern long-term stability of wide, deeply incised channels. Note that the main limiting factor on the steep headwall in the north branch appears to be the roots of a large juniper tree. Once these are undermined it is possible that the headcut will propagate rapidly upslope.

Decadal-average rates of headward growth need to be quantified. This can be achieved by georeferencing the aerial photographs and plotting before-and-after

headcut positions. Much of Fort Carson is covered by 1937 USFS aerial photographs. In addition, further dendrogeomorphic analysis is needed to help reveal the timing of channel incision and/or aggradation at specific channel heads.

Ephemeral headcuts and discontinuous channel segments

Shallow (<1 m), often arcuate headcuts are common features in valley floors. In some cases these form the heads of short (order meters to tens of meters) discontinuous channel segments which grade in to the valley floor downstream (Figure 11). In other cases, there is no identifiable channel below the headcuts. A flight of shallow headcuts was mapped in a tributary of Big Arroyo (Figure 12). The headcuts run the length of the c. 700m long section of (otherwise unchanneled) valley that was surveyed; the average spacing between them is on the order of a few 10s of meters or roughly 100 times the typical headcut height. Headcuts are not always aligned with one another; often they occur on opposite sides of the same valley. Sediment exposed within headscarps is typically bare beneath the root zone (Figure 11).



Figure 11: Flight of shallow, ephemeral headcuts in a tributary to Big Arroyo. One headcut is in the foreground and two others in the background along the valley center.

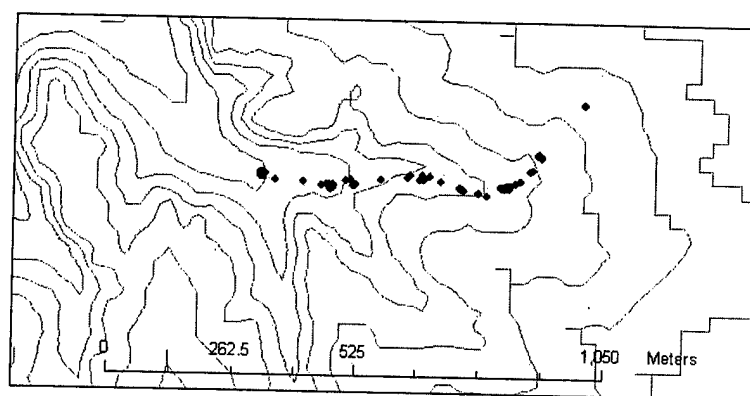


Figure 12: Map showing locations of shallow ephemeral headcuts along a tributary of Big Arroyo. (Dot clusters are multiple survey points around individual headcuts).

Discussion

Summer convective storms are able to generate very high peak runoff rates and discharges over a limited area. In the case of Sullivan Park, the discharge produced in a 0.5 km² catchment during a 30-minute downpour was able to generate hundreds of pascals in shear stress. Such shear stresses are able to entrain and transport 20cm diameter boulders, and are almost certainly high enough to penetrate tough grassland vegetation mats. Studies on vegetation resistance to erosion (Prosser and Slade, 1994; Prosser and Dietrich, 1995) have shown that undisturbed vegetation can resist flows of up to order 100 Pa. They suggested that flows much higher than this would likely be able to undermine low-growing dense vegetation, but were unable to demonstrate this in field experiments. Similar studies on clipped or degraded vegetation show that shear stresses on the order of tens of Pa are capable of breaking vegetation. Thus, two conclusions can be drawn. First, short, intense downpours associated with convective cells can be sufficient to exceed even the very high erosion thresholds associated with grassland vegetation. Second, because disturbance of vegetation can reduce the threshold by an order of magnitude, such disturbance (whether human or natural – e.g., bison grazing, drought) can leave a landscape highly vulnerable to summertime convective storms.

Although rainfall intensities high enough to initiate channels can occur, it is important to consider how frequent such events are. While a complete magnitude-frequency analysis has yet to be undertaken, it is instructive to examine the relative 24-hour frequency of the events described in this report. The peak 1 hour, 30 minute, and 15 minute rainfall totals at Burson Well (PCMS) were, respectively, 1.43, 1.37, and 0.85 inches. According to the NOAA Atlas 2 precipitation frequency database (using the short-duration ratios of Arnell and Richards, 1986), the corresponding 2-year values are 1.15, 0.95, and 0.71. Therefore, the August 8 storm had a recurrence interval of a bit more than two years. Using the graphical method described in Miller et al. (1973), the recurrence interval for the event is between 2 and 5 years.

The July 13, 2001 event at Sullivan Park produced 1-hour, 30-minute, and 15-minute peak depths of 1.35, 1.19, and 0.77 inches, respectively. These correspond closely with the 2-year recurrence interval depths for this location (1.18, 0.98, and 0.73 inches, respectively; values were derived from NOAA Atlas 2; Miller et al., 1973; Arnell and Richards, 1986). On the other hand, as noted above, the peak intensity within the small EC dam catchment is likely to have been 2-4 times the intensity recorded at the meteorological station, and thus would have a larger recurrence interval. This raises an important issue regarding the use of point-based rainfall records to estimate flash flood and erosion risks. Catchments cover a finite amount of space, and during a typical convective storm, a catchment as small as half a square kilometer can experience significant spatial variations in rainfall intensity (Goodrich et al., 1997). If the response to rainfall in semi-arid catchments were linear, the rainfall peaks and troughs would offset one another and the corresponding runoff would reflect an areally averaged rate. However, we know that at rainfall intensities comparable to or less than soil infiltration capacities, catchment response can be highly nonlinear (Goodrich et al., 1997). Thus, the spatial structure of rainfall plays an important role that is only captured by the densest of rain-gage networks.

The evidence discussed above suggests that rainstorms with a recurrence interval on the order of a few years are able to create flash floods that generate tens to a few hundred pascals of shear stress. This type of convective system is generally quite limited in aerial extent. A rainfall map for 8 August 2003, for example, suggests that the cell center had a radius of no more than 5 kilometers. Data discussed by

Goodrich et al. (1997) from Walnut Gulch in Arizona indicate typical convective storm-core sizes of 10^4 to 10^5 m². Thus, the effects of such flash floods will tend to be limited in extent. The fact that flash floods propagate downstream implies that small convective cells can have a much greater "geomorphic reach" than the storm radius. However, the reach is limited by run-on losses. For example, while our estimated peak discharge in Big Arroyo was 5 cms, the gaging station at the site perimeter recorded only about 0.6 cms (22 cfs) (D. Sharps, personal communication). While part of the difference may reflect different data collection methods (our estimate is an instantaneous peak value), it is clear that there were substantial in-stream losses as the flood wave propagated. The average sediment transport distance during this type of event will clearly be limited by this flood wave attenuation. Equally, it is clear that any models that predict erosion and transport in arroyo networks on the basis of a steady, uniform rainfall and discharge field will be widely off the mark.

There are some important implications for climatic controls on erosion and sediment transport. If localized, intense events are key drivers of sediment transport and land change, as we believe, then it becomes important to understand their frequency, magnitude and impacts. On a small scale, the episodic nature of sediment movement presents a challenge for prediction, because short-term average sediment yield measurements may not be representative of the decadal (or longer) mean. From a practical standpoint, it is worth exploring a risk-based, quantitative approach to erosion prediction in which the uncertainty in climatic drivers (and in other aspects, such as erosion thresholds) is accounted for. From a longer-term perspective, our findings raise a tantalizing hypothesis: does the rate of landscape change and denudation depend strongly on the degree of summer convective activity? If it does, then any changes in such activity (for example, suppression of monsoonal activity and/or increased zonality of circulation) could potentially have had a large impact on denudation rates in the Colorado piedmont during the Quaternary period.

Together, these observations reported here provide a useful basis for understanding the driving processes in arroyo development and for parameterizing and testing models. It is recommended that future research efforts be concentrated along two lines. The first is installation of flash-flood monitoring stations in order to build up a database of discharge frequency and magnitude. Second, development with the CHILD model should include an improved treatment of the unsteady hydrologic style associated with intense convective storms and flash floods.

4.4 Geochronology using Optically Stimulated Luminescence (OSL) Methods

As noted earlier, ancient channel fills appear in the sidewalls of many of the incised channels at Fort Carson and PCMS. These offered the potential to reveal a chronology of cut and fill episodes in the geologic past, which may be compared with paleoenvironmental records in order to test causative relations. We embarked on a program to test the use of OSL for dating these channel fills. OSL and related-luminescence methods have been widely used in dating eolian sediments; their use in dating fluvial sediments is relatively recent, and reflects technological advances in the method.

Briefly, OSL exploits the fact that buried mineral grains (quartz is the most commonly used) naturally tend to build up a weak electrical charge due to natural background radiation. This charge is released, and can be measured in the lab, by exposure to light or high heat. When a grain is exposed to daylight, the charge is released and the grain is "re-set." When re-buried, they begin to build up a charge again. If the rate of charge buildup and the total charge are measured, the elapsed time since burial can be calculated. OSL has an effective time window that depends on the nature of the local sediment and radiation doses, but is typically on the order of several tens to a few hundred thousand years.

Application of OSL to fluvial sediments is not completely straightforward, because there exists the possibility of "partial bleaching": an incomplete resetting of the clock due to weak light exposure, which could result from exposure at night or from radiation attenuation by muddy water. Thus, one of the first aims of this project was to examine the properties of channel-fill sediment and test for signs of partial bleaching. The second was to obtain a suite of preliminary dates from channel fills at several locations in PCMS and Fort Carson. The initial results are promising. They are presented in greater detail in Appendix A, which is an unpublished confirmation-of-status report by Lee Arnold (Oxford D.Phil. student).

4.5 Dendrogeomorphic Analysis

Dendrogeomorphology is the study of geomorphic processes and history using evidence obtained by plants. Methods include analysis of tree rings to identify times of stress associated with damage due to erosion of roots, assessment of erosion rates from root pedestals, and estimation of sedimentation rates from buried trunks.

Dr. Vanessa Winchester, an expert in dendrogeomorphology, has begun compiling a database from study sites on Fort Carson and PCMS. In order to provide a regional background with which individual tree-ring records can be compared, a regional ring-growth curve has been compiled from a set of field samples. The record extends back to the early 18th century. Western drought episodes in the late 19th century, 1930s, and 1950s are correlated with periods of reduced growth rates. The tree-ring graph along with detailed information on species and localities can be found in Appendix B.

4.6 The Role of Storm Duration and Size in Shaping Topography

Most models of landscape evolution over geologic time spans make an important simplifying assumption: discharge at any point in the channel network is in

steady state with a given excess-rainfall field, and therefore is equal to (average) runoff rate times drainage basin area. This assumption is appropriate for situations in which storms are relatively long and/or the catchment is relatively small. For example, if the average speed of runoff is 0.5 m/s, it will take runoff about 5 and a half hours to travel the full distance of a 10km long catchment. If rainfall persists longer than this (at a roughly steady rate) then the discharge at the outlet will be approximately equal to the rate of surface water input (runoff rate times basin area) minus any in-channel infiltration losses. This will not be true for smaller catchments or shorter storms. This is one reason why peak discharge typically shows a less-than-linear relationship with basin area, especially in arid settings (e.g., Goodrich et al., 1997 and references therein). Other contributing factors are run-on losses and limited storm cell size relative to catchment size.

From theoretical studies of drainage basin morphology and evolution, we know that the manner in which stream discharge increases (or decreases) downstream should have an important influence on basin and network shapes. In order to study and quantify these effects, we understood an analytical and numerical investigation of storm-duration effects. Using a simple model of peak-flow scaling with catchment length and area, we compared cases of short versus long relative storm durations, and discovered that the standard stream-erosion law predicts marked differences in topography between them. This brings important implications for climate controls on landscape evolution. The method and results are described in Appendix C, which is a preprint of a journal article in press with Journal of Geophysical Research F.

4.7 The Role of Entrainment and Erosion Thresholds in Evolving Drainage Networks

Another common simplification used in terrain evolution models is the neglect of a critical tractive threshold for particle detachment. It is well known from laboratory and field studies that sediment movement does not begin until the flow is sufficiently strong to lift or roll grains, and/or detach them from a cohesive or indurated substrate. Classic work by Shields showed that movement of loose grains only begins once a critical dimensionless shear stress has been exceeded.

Accounting for such thresholds in models of long-term topographic evolution is complicated by the wide range of different flows a typical channel or hillslope experiences over time. To deal with this, we have developed a stochastic theoretical framework for modeling erosion and sediment transport with a threshold term. Basic sensitivity analysis was conducted to develop a better understanding of the implications of the model. These can be profound: large thresholds (such as are associated with coarse gravel channels, for example) can have a demonstrable impact on the shapes and dynamics of stream profile response to climate and tectonic forcing. The results of the analysis appear in Appendix D, which is a reprint of Tucker, G.E. (2004) Drainage basin sensitivity to tectonic and climatic forcing: implications of a stochastic model for the role of entrainment and erosion thresholds. *Earth Surface Processes and Landforms*, 29, 185-205.

4.8 Analysis of Dynamic Interactions between Plant Growth and Erosive Flash Floods

Recent work has shown that plant stems and roots also impose an effective tractive threshold, which for intact grassland vegetation is on the order of a few hundred pascals – roughly equivalent to clasts of several tens of centimeters in diameter. Thus, vegetation can provide enormous resistance to erosion. Yet, when vegetation armor grows on an erodible substrate (e.g., fine-grained alluvium or soft shale bedrock, both of which are common in the Colorado piedmont), its removal can lead to very rapid erosion until the vegetation re-grows. This sets up a sort of competition between vegetation and runoff erosion, and this competition has a strong control on the extent of channel networks. In order to explore the dynamics that emerge from this system, we explored a simple model of vegetation growth and erosional loss. The results lead to some interesting findings, including the potential for a “memory effect” in the landscape. The results are presented and discussed in Appendix E, which is a reprint of Collins, D., Bras, R., and Tucker, G.E. (2004) Modeling the effects of vegetation-erosion coupling on landscape evolution: *Journal of Geophysical Research - Earth Surface*, v. 109, no. F3, F03004, doi:10.1029/2003JF000028.

4.9 Autocyclicity and climate impacts in arroyo network evolution

Two of the leading hypotheses for observed arroyo dynamics are the following:

1. Channels can and do undergo cut-fill cycles as a result of internal dynamics, rather than through external drivers such as grazing and climate change.
2. Subtle aspects of climate change, such as variations in rainfall frequency and magnitude, can and have driven accelerated arroyo incision during the historical period.

These two hypotheses are not mutually contradictory, though even if both are correct in some circumstances, we still need to understand what those circumstances are. To investigate both from a mechanics-based viewpoint, we have run sensitivity experiments with CHILD (including the vegetation module discussed above). An important finding is that the model produces periodic cut-fill cycles even in the absence of direct forcing, which supports the first hypothesis. To evaluate and quantify the second, an additional series of runs are being conducted to test the response to variations in rainfall frequency, intensity, and duration. This work is discussed in Appendix A.

4.10 Additional observations, notes and recommendations

Aerial photograph evidence

Analysis of aerial photographs of Fort Carson from 1937, 1962, and the 1990s indicates that the majority of incised ephemeral channels present today were also present in 1937, before the creation of the facility in 1942. Some channel heads have

advanced headward since 1937 at average rates on the order of 20-50 cm/yr; many others are either stable or have advanced too slowly to be detectable from photo pairs.

Preliminary examination of aerial photographs also shows, not surprisingly, that the majority of channels occur in valley alluvium or shale units (such as the Graneros shale which underlies the Little Grand Canyon). Limestone-rich units such as the Fort Hayes limestone member of the Niobrara formation appear to be generally resistant to deep and/or steep-walled channel incision. This does not mean that such channels are inactive, but rather that either (a) their development is less episodic and less prone to environmental disturbance, or (b) the materials composing the channel banks are poorly cohesive and unable to support steep sidewalls. We presently lack data necessary to distinguish between these two interpretations. Nonetheless, it is clear that steep-walled, rapidly eroding gully systems occur preferentially on alluvial soils and on shale bedrock units.

Value of meteorological and hydrological data collection

One of the difficulties in managing erosion and sedimentation hazards in a semi-arid landscape is the episodicity of erosion and transport. As discussed above, it is possible for features such as gullies to remain essentially stable for many years, only to experience rapid erosion during a single, intense storm event. To cope with the resulting uncertainty, managers need better estimates of event-based flood and erosion risks. However, risk-based management requires records of past events, and such records are generally quite rare for small drainage basins. For the past several years, DECAM has supported a program of meteorological and hydrological monitoring, which is run by the USGS, at Fort Carson and PCMS. As the length of record grows, these data will become increasingly valuable. The relatively dense rain gage network at PCMS is particularly useful because it places constraints on the spatial distribution of precipitation. In addition, the high frequency sampling rate of rainfall provides a useful window into the relationship between storm magnitude and duration. Furthermore, the rainfall and runoff data provide a basis for testing and calibrating hydrologic and erosion models, such as the one discussed in this report. For these reasons, we recommend that the monitoring program be continued.

Empirical testing of training impacts

On obvious application of erosion modeling is to assess the natural and degree of training impacts on erosion and sediment export. Indeed, a number of different models have been used for this purpose. Physically based models have an obvious advantage over purely empirical ones because they predict outcomes of basic processes (runoff, sediment transport) given a set of boundary conditions and material properties. Thus, in principle, if conditions or materials change, the effects of such change can be predicted. An important limiting factor, however, is in our ability to obtain key parameters (such as soil infiltration capacity and sediment detachability) from direct field measurements alone. This is a general problem in hydrologic and geomorphic modeling, and the subject of much current research. Despite many advances, it is still the case that a number of key model parameters must be calibrated. Confidence in model predictions of training versus non-training scenarios would be enhanced, therefore, if field examples of both impacted and "pristine" catchments were available and monitored in order to provide such calibration data. Such a paired-catchment experiment would require setting aside a portion of training land for a long period of time. However, the knowledge gain from such monitoring could, over the long term, result in significant cost savings. On the other hand, without a controlled

field experiment, quantifying (and, ultimately, costing) training impacts would be hampered by the difficulty in testing and calibrating models across a full spectrum of training conditions. Therefore, we recommend that the Army, and Fort Carson in particular, consider setting aside a representative drainage basin to serve as a controlled experiment in training impacts. This is probably best done at PCMS, where the terrain is more homogeneous than that of Fort Carson proper.

Use of process models as decision-support systems

Process-based models such as CHILD have the potential to serve as decision support tools that can provide estimates of the impact of engineering works (such as check dams, diversion structures, etc) and other land modifications, before those works are put into effect. One of the goals of this project has been to assess this potential. At present, there remain two barriers that need to be overcome in order to make this potential a reality. The first concerns modeling of distributed overland flow. In order to capture the transition from sheet flow to channel flow and channel incision, a numerical solution to an appropriately simplified form of the shallow-water (depth-integrated) hydrodynamic equations is required. Solutions capable of handling conditions particular to overland flow, such as run-on infiltration and surface wetting/drying, have been surprisingly hard to obtain. However, recent progress on regular-grid-based finite-difference methods (Fiedler and Ramirez, 2000) has shown promise. Methods to adapt these techniques to irregular grid schemes are still required. The second challenge is to obtain, in a cost-effective manner, digital terrain data of sufficiently high resolution (on the order of a few meters or less) and accuracy that individual structures can be resolved, and subtle influences on overland flow routing, such as road embankments, can be captured. Airborne laser altimetry is a natural candidate for this application.

References

- Antevs, E., 1952, Arroyo-cutting and filling: *Journal of Geology*, v. 60, p. 375-385.
- Arnell, R. E., and F. Richards, 1986, Short duration rainfall relations for the western United States: Conference on Climate and Water Management, p. 136-141.
- Bull, L. J., M. J. Kirkby, J. Shannon, and J. M. Hooke, 1999, The impact of rainstorms on floods in ephemeral channels in southeast Spain: *Catena*, v. 38, p. 191-209.
- Bull, W. B., 1997, Discontinuous ephemeral streams: *Geomorphology*, v. 19, p. 227-276.
- Cooke, R. U., and R. W. Reeves, 1976, Arroyos and environmental change in the American Southwest: London, Oxford University Press, 213 p.
- Dietrich, W. E., C. J. Wilson, D. R. Montgomery, and J. McKean, 1993, Analysis of erosion thresholds, channel networks, and landscape morphology using a digital terrain model, Centennial special issue, v. 101; 2: Chicago, IL, United States, University of Chicago Press, p. 259-278.
- Dietrich, W. E., and T. Dunne, 1993, The channel head, *Channel network hydrology*: Chichester, United Kingdom, John Wiley & Sons.
- Elliott, J. G., A. C. Gellis, and S. B. Aby, 1999, Evolution of arroyos; incised channels of the Southwestern United States, in S. E. Darby, and A. Simon, eds., *Incised river channels; processes, forms, engineering and management*.
- Goodrich, D. C., L. J. Lane, R. M. Shillito, and S. N. Miller, 1997, Linearity of basin response as a function of scale in a semiarid watershed: *Water Resources Research*, v. 33, p. 2951-2965.
- Graf, W. L., 1983, The arroyo problem; palaeohydrology and palaeohydraulics in the short term, in K. L. Gregory, ed., *Background to palaeohydrology; a perspective*, p. 279-302.
- Graf, W. L., 1988, *Fluvial Processes in Dryland Rivers*: Caldwell, NJ, Blackburn Press, 346 p.
- Boardman, J., A. J. Parsons, P. J. Holmes, R. Holland, and R. Washington, 2003, Development of badlands and gullies in the Sneeuwberg, Great Karoo, South Africa: *Catena*, v. 50, p. 165-184.
- Howard, A. D., 1999, Simulation of gully erosion and bistable landforms, in S. E. Darby, and A.

- Simon, eds., Incised river channels, John Wiley & Sons.
- Kirkby, M. J., and L. J. Bull, 2000, Some factors controlling gully growth in fine-grained sediments: a model applied in southeast Spain: *Catena*, v. 40, p. 127-146.
- Leopold, L. B., 1951, Rainfall frequency: an aspect of climatic variation: *Transactions of the American Geophysical Union*, v. 32, p. 347-357.
- Miller, J. F., R. H. Frederick, and R. J. Tracey, 1973, Precipitation-frequency atlas of the western United States, Silver Spring, MD, National Oceanic and Atmospheric Administration.
- Montgomery, D. R., and W. E. Dietrich, 1992, Channel initiation and the problem of landscape scale: *Science*, v. 255, p. 826-830.
- Patton, P. C., and S. A. Schumm, 1975, Gully erosion, northwestern Colorado: a threshold phenomenon: *Geology (Boulder)*, v. 3, p. 88-90.
- Prosser, I. P., and W. E. Dietrich, 1995, Field experiments on erosion by overland flow and their implication for a digital terrain model of channel initiation: *Water Resources Research*, v. 31, p. 2867-2876.
- Prosser, I. P., and C. J. Slade, 1994, Gully formation and the role of valley-floor vegetation, southeastern Australia: *Geology (Boulder)*, v. 22, p. 1127-1130.
- Rinaldo, A., W. E. Dietrich, R. Rigon, G. K. Vogel, and I. Rodriguez-Iturbe, 1995, Geomorphological signatures of varying climate: *Nature*, v. 374, p. 632-635.
- Schumm, S. A., 1977, *The Fluvial System*: New York, John Wiley, 338 p.
- Schumm, S. A., and R. S. Parker, 1973, Implications of Complex Response of Drainage Systems for Quaternary Alluvial Stratigraphy: *Nature*, v. 243, p. 99-100.
- Tucker, G. E., and R. Slingerland, 1997, Drainage basin responses to climate change: *Water Resources Research*, v. 33, p. 2031-2047.
- von Guerard, P., P. Abbot, and R. Nickless, 1987, Hydrology of the US Army Pinon Canyon Maneuver Site, Las Animas County, CO, U.S. Geological Survey, p. 84.
- Zhang, P., P. Molnar, and W. R. Downs, 2001, Increased sedimentation rates and grain sizes 2-4 Myr ago due to the influence of climate change on erosion rates: *Nature (London)*, v. 410, p. 891-897.

Appendix A

Optical Dating and Computer Modelling of Arroyo
Epicycles in the American Southwest

Unpublished Confirmation of D.Phil. Status Report by
Lee Arnold, March 2004

Optical Dating and Computer Modelling of Arroyo Epicycles in the American Southwest

**Lee J. Arnold
School of Geography and the Environment
University of Oxford**

**Confirmation of D.Phil Status Report
Submitted March 2004**

CONTENTS

1	Research aims and methods	3
1.1	<i>Research summary statement</i>	3
1.2	<i>Research aims and methodology</i>	4
2	Thesis structure and progress made	6
2.1	<i>Thesis structure</i>	6
2.2	<i>Individual chapter breakdown and progress made</i>	8
2.3	<i>Section I</i>	8
	<i>Chapter 1</i>	8
2.4	<i>Section II</i>	9
	<i>Chapter 2</i>	9
	<i>Chapter 3</i>	9
	<i>Chapter 4</i>	10
	<i>Chapter 5</i>	10
2.5	<i>Section III</i>	12
	<i>Chapter 6</i>	12
	<i>Chapter 7</i>	12
	<i>Chapter 8</i>	12
2.6	<i>Section IV</i>	13
	<i>Chapter 9</i>	13
	<i>Chapter 10</i>	13
	<i>Chapter 11</i>	14
2.7	<i>Appendices</i>	14
3	Plan for further work	17
4	References	18
5	Example of completed work	19

1. RESEARCH AIMS AND METHODS

1.1 *Research summary statement*

This research is concerned with improving the understanding of process-response relationships involved in Late Quaternary arroyo formation across the American southwest, and specifically within southeastern Colorado. The cause of Late Quaternary episodic incision and aggradation in the American southwest has been the subject of a long but inconclusive debate. Fluvial systems in this region are known to have adjusted and responded to a variety of external and internal forcings over the Late Quaternary, but the nature of these cause-effect relationships isn't well understood and our knowledge of these systems remains far from complete. Both modern and prehistoric cyclical arroyo formation has been attributed to a number of different causes by various authors. These include climate change (e.g. Bryan, 1928), climate variability (e.g. Waters and Haynes, 2001), changes in rainfall patterns under constant climates (e.g. Cooke, 1974), changes in sediment availability (e.g. Blum et al., 1994) and vegetation cover (e.g. Antevs, 1952), intrinsic threshold mechanisms (e.g. Patton and Schumm, 1975), anthropogenic factors (e.g. Bailey, 1935), and random storm events (e.g. Thornthwaite, Sharpe and Dosch, 1942). While it is acknowledged that an interaction of various factors controls arroyo formation, much still remains unanswered regarding the relative importance of these various factors at different spatial or temporal scales, the interactions between the various causality factors, and the exact nature of the various process-response relationships involved.

The multivariate nature of arroyo formation emphasises the need for solid evidence in proposing a mechanism of arroyo formation at a given site (Miller and Kochel, 1999). The majority of past studies devoted to explaining the causes of periodic stream aggradation and erosion have relied on correlating observed changes in the Quaternary alluvial stratigraphy with known or inferred changes in climate. Given the complexity of these geomorphic systems it is not surprising that the conclusions reached have often been contradictory (e.g. reviews by Antevs, 1952; Cooke and Reeves, 1976; Knox, 1983).

Resolution of the arroyo causality debate has been hampered by the lack of an accurate, widespread chronological framework for these systems. In the rather limited cases where chronology has been established, it has not been based on the most suitable dating techniques for this type of environment and so often remains too poorly constrained to invoke a causal association. Radiocarbon dating has been mainly used to provide absolute age control on arroyo formation, which is particularly problematic in this context given that it relies on dating circumstantial evidence associated with the sediment under consideration. Luminescence dating circumvents this problem by directly dating the sediment itself, providing an absolute chronology that has the potential to offer greater constraint on causality.

Previous stratigraphic studies of episodic degradation and aggradation have also only provided limited insight into the complex and coupled physical mechanisms and feedbacks that have resulted in the observed geomorphic patterns (Tucker and Slingerland, 1997). Causal attribution has been made difficult by the fact that potential causal factors have often occurred in coincidence. In particular this has resulted in virtual stalemate being reached in the 'human versus climate change' debate of modern arroyo formation in the southwest. Similarly, it is difficult to distinguish between Late Holocene cut and fill cycles created by

intrinsic geomorphic parameters from those that have resulted from short-term climate change/variability on the basis of stratigraphy alone.

Understanding these complex fluvial systems, their formation, dynamics, and evolution requires a more quantitative framework. Computer modelling of drainage basin evolution has the potential to provide such a framework, enabling the unravelling of complex drainage basin responses to climate changes (and other variables) that usually involve the simultaneous alteration of a number of variables. Numerical modelling is used in this research for the development and testing of conceptual models and theories about arroyo formation, and to provide valuable insight into the *nature* of the geomorphic response to changes in controlling factors (e.g. response magnitude, sensitivity, lag).

It is widely recognised that much more research into arroyo formation is needed. The approach adopted in this research is to apply some of the most recently developed, quantitative geomorphological techniques to an old problem. Through a combination of luminescence dating of alluvial sequences and computer modelling of drainage basin evolution, this research aims to provide an additional dimension to the "arroyo debate" that has raged for over a century in the American southwest. In addition to establishing accurate chronologies of Late Quaternary arroyo epicycles in the American southwest, the study aims to resolve some of the uncertainty and speculation surrounding the relative importance and interaction of causality factors, and process-response complexity evident in these systems.

1.2 Research aims and methodology

My D.Phil research aims to remodel, redat and rethink arroyo development in the American southwest. The main objective is to improve understanding of arroyo epicycle histories and the process-response relationships involved in arroyo formation in the American southwest. The project focuses in particular on small to medium sized arroyos found across southeastern Colorado, specifically those located at Pinon Canyon Manoeuvre Site and Fort Carson Military Reserve. This part of the southwest remains largely unstudied and hence little is known about the history and nature of arroyo epicycles in this sub-region, or how they relate to arroyo histories elsewhere across the southwest. This is combined with studies of arroyo systems from southern California (Cuyama River) and southeastern Arizona (Murray Springs, Curry Draw). Together this sampling strategy provides good representation of the range of different size and types of arroyos found across the southwest, and covers a wide geographical area of the region.

The research aims to establish a more suitable, robust and accurate chronology for both past and present arroyo epicycles in the American southwest. Optical dating is used to systematically evaluate and constrain the timing of Holocene arroyo activity in individual basins. The temporal patterns of arroyo histories for specific basins are then used to determine spatial patterns of past arroyo histories across the region. Comparison of alluvial chronologies between different arroyo systems in southeastern Colorado enables interbasin and sub-regional histories to be established. Comparison of chronologies from all the studied basins across the southwest provides insight into regional responses throughout the Holocene.

Once accurate time frames have been established for the series of Late Quaternary aggradation and incision events of individual basins, the causal factors responsible for these episodes are established from:

- i) Correlation with independently derived palaeoclimatic and palaeoenvironmental records from across the region
- ii) Inter-basin comparison of arroyo epicycle timing (synchronous or diachronous)
- iii) Comparison of alluvial histories and epicycle timing at different locations within individual basins

An integral part of the research aims to determine and demonstrate the suitability of optical dating in this fluvial context. This is vital to ensure that both accurate and precise chronologies are produced, and is particularly important given that optical dating of arroyo sediments is unprecedented. In particular it is necessary to test whether light exposure of mineral grains during fluvial transport was sufficient to reset the optical signal of all or some of the grains prior to deposition. In order to assess the bleaching characteristics of the fluvial samples being sampled, a two-fold field approach is adopted, involving:

- i) Redating sections with independently established robust ^{14}C age control
- ii) Analysing modern channel sediment for residual OSL signals. This also provides information on how optical resetting varies downstream and between tributaries and main channels

A variety of statistical and analytical techniques are also tested and subsequently used to assess the bleaching characteristics of each sample. These are based on either an analysis of the degree of scatter in the sample's accumulated optical signal or an analysis of different temporal components of this signal.

Chronological analysis is complemented by numerical modelling investigations into ephemeral system evolution and dynamics. The main aim of the modelling simulations is to enable further insight into the relative importance and interaction of various controlling variables thought to be involved in arroyo formation. In particular this work focuses on the role of more 'subtle' intrinsic and extrinsic control factors. The importance of control factors such as intrinsic geomorphic controls and rainfall frequency-magnitude patterns have often been overlooked in previous studies owing to difficulties in identifying their signatures in field and stratigraphic records. The ability to control and explore individual controlling variables in a 'virtual space' is exploited in the modelling simulations to help further understanding of the more complex, coupled fluvial responses observed in reality.

2. THESIS STRUCTURE AND PROGRESS MADE

2.1 Thesis structure

OPTICAL DATING AND COMPUTER MODELLING OF ARROYO EPICYCLES IN THE AMERICAN SOUTHWEST

Abstract

Acknowledgements

Table of contents

General Introduction: New approaches to an old problem

Section I Research context: the arroyo causality debate

Chapter 1 The Arroyo debate in the American southwest: A review of previous and current interpretations, existing chronological control, and the potential for improved understanding using optical dating and numerical modelling.

Section II Optical dating of ephemeral fluvial sediments: verification of the technique

Part A Single aliquot and single grain Equivalent dose (D_e) calculation.

Chapter 2 The suitability of the modified Single Aliquot Regenerative-dose (SAR) protocol for D_e estimation of Arroyo sediments from the American Southwest.

Chapter 3 Single grain analysis of arroyo sediments using an Annealed Single Aliquot Regenerative-dose (ASAR) approach: Initial results.

Part B Assessing optical resetting and characterising dose distributions

Chapter 4 Evaluation and analysis of bleaching histories in ephemeral fluvial samples part I: Investigating optical resetting using modern sample analogues and independent age control

Chapter 5 Evaluation and analysis of bleaching histories in ephemeral fluvial samples part II: Analytical techniques and the selection of representative equivalent Dose (D_e) values for age calculations.

Section III Chronologies of Late Quaternary arroyo epicycles in the American southwest

Chapter 6 Redating and extending arroyo epicycle chronologies at Murray Springs-Curry Draw, southeastern Arizona

Chapter 7 Reconstructing the Late Quaternary alluvial history of the Cuyama River, Southern California, using optical dating

Chapter 8 Optical dating of arroyo sequences across southern Colorado: an inter- and intra-basin comparison

Section IV Numerical modelling of ephemeral river basin cut-fill cycle dynamics

Chapter 9 Numerical modelling of ephemeral stream epicycles of erosion and aggradation: Introduction and model overview

Chapter 10 Autogenic cut-fill cycle behaviour in ephemeral streams: Numerical modelling insights into the role of geomorphic thresholds and complex responses in the context of fluvial epicycles

Chapter 11 The importance of rainfall characteristics in the development of ephemeral basin cut-fill cycles: Results from numerical modelling investigations using CHILD

Conclusions and future directions

Appendices

Appendix A

Paper I Arnold, L.J., Stokes, S., Bailey, R., Fattahi, M., Colls, A.E., Tucker, G., 2002. Optical dating of potassium feldspar using far-red ($\lambda > 665\text{nm}$) IRSL emissions: A comparative study using fluvial sediments from the Loire River, France. Quaternary Science Reviews 22, 1093-98

Paper II Lai, Z.-P., Arnold, L.J., Stokes, S., Bailey, R., Fattahi, M., 2002. Detection of far-red IRSL from loess. Ancient TL 20(2), 41-46.

Appendix B

Section III CHILD simulation parameterisation details

2.2 Chapter breakdown and progress made

This section summarises the contents of each chapter and the progress made so far in each of these chapters. As can be seen, I am pursuing the traditional thesis approach, with the intention of submitting much of the work for publication either in its original form, or in a modified form (i.e. combined with parts of other chapters or in a shortened form) where most appropriate.

The main body of my completed D.Phil thesis will comprise 13 chapters in 4 sections. These will be preceded by an introduction to context, scope and aims of the research and followed by a separate conclusions section at the end of the thesis, drawing together the ideas discussed in each of the chapters and future directions. The appendices to the thesis will be made up of further papers of which I am either first or second named author. These papers are the outcome of more practical research associated with the continuous development of optical dating that accompanies research using the technique. In particular they relate to the development and application of the newly developed technique using far-red IRSL emissions in potassium feldspars. The appendices to the thesis will also include a section comprising data tables and notes regarding the choice of parameterisation used in the CHILD model.

2.3 Section 1 – Research Context: the arroyo causality debate

Chapter 1 – The Arroyo debate in the American southwest: A review of previous and current interpretations, existing chronological control, and the potential for improved understanding using optical dating and numerical modelling.

The first chapter of my D.Phil thesis is a review paper. A first draft of this paper is currently in preparation. The paper provides an overview of the arroyo debate, from the earliest theories invoking single causal factors to the more recent multiple causality conceptual models emphasising complex interactions of factors and equifinality. Despite the vast amount of literature devoted to arroyo dynamics our understanding of arroyo system process-response relationships remains far from complete. This is discussed in the context of the limited methods of analysis that have been employed in previous studies. The majority of past studies devoted to explaining the causes of periodic stream aggradation and erosion have relied on correlating observed changes in alluvial stratigraphy with known or inferred changes in climate. Process studies and the monitoring of field basins introduced since the 1950's have provided valuable insights into the dynamics of these systems over short time scale. Our understanding of long-term arroyo system dynamics and arroyo epicycle histories, however, remains somewhat limited owing to the lack of widespread and accurate chronological control. The types of dating methods employed in the past and their limitations in arroyo contexts are reviewed. Achieving more accurate chronologies requires a dating method that is better suited to this type of environment. The benefits and limitations of optical dating in this context are discussed. It is suggested that recent methodological advancements in this technique now mean that optical dating has the potential to provide accurate and precise arroyo epicycle chronologies. There is also a strong need for linking short-term field and process observations to the longer-term evolution of arroyo systems. This would be invaluable in assessing the relative importance and interactions between various potential controlling factors responsible for arroyo epicycles. Numerical modelling of ephemeral catchments offers an ideal framework for this, providing a unique quantitative tool for arroyo causality theory testing. It is suggested that readdressing the arroyo debate

using these latest geomorphological techniques could provide new dimensions to the discourse.

2.4 Section II – Optical dating of ephemeral fluvial sediments: Verification of the technique

Part A – Single aliquot and single grain Equivalent dose (D_e) calculation.

Chapter 2 – The suitability of the modified Single Aliquot Regenerative-dose (SAR) protocol for D_e estimation of Arroyo sediments from the American Southwest.

The paper describes the details and performance of the optical dating protocol used in equivalent dose determination for the arroyo samples in the research. All of the measurements required for the writing of this paper have already been completed. Equivalent dose calculation is made using the modified Single Aliquot Regenerative-dose (SAR) protocol recently proposed by Duller (2003). This entails the measurement of a second additional repeat dose cycle with prior IR exposure at the end of the standard SAR procedure (Murray and Roberts, 1998) to check for feldspar contamination. Internal checks on the modified SAR procedure performance (recuperation ratios, recycling ratios, ability to recover known doses) reveal that the southeastern Colorado samples behave well under these conditions of optical stimulation and growth curve construction. The southern California samples, however, display particularly low sensitivity, and are characterised by very dim natural and laboratory dose signals. Poor recycling ratios and large errors on growth curve construction are commonplace in samples from this particular region. In order to improve the performance of these samples, larger test dose values were administered and the second rather than the first laboratory dose points were used to monitor sensitivity corrections. The effects of these alterations on the performance of the modified SAR protocol were investigated before being routinely employed for dating. Laboratory doses can be successfully recovered following these procedural alterations. The natural equivalent dose values display much-improved precision, record acceptable recycling ratios and show no evidence of thermal transfer throughout. Following verification, these alterations are consequently incorporated into the modified SAR technique used for the dating of the insensitive Californian samples.

Further checks were made on improving equivalent dose estimates using an additional bleaching stage after each test dose cycle in the SAR protocol, as suggested by Murray and Wintle (2002). No distinct improvements in sample performance were observed following this alteration. This chapter also includes investigations into appropriate preheat selection on a number of representative samples. The choice of suitable preheating conditions may be of particular importance in the case of some of the younger samples. Tests involving measuring natural D_e 's in a number of samples at eight different preheat temperatures (160-300°C for 10s, at 20 °C increments) reveal no significant mean D_e dependence upon pre-heat temperature. Natural D_e scatter is generally smallest in the 220-260 °C range. Dose recovery experiments conducted over the same range of preheat temperatures also generally reveal successful measurements of laboratory doses over all but the most extreme temperatures measured. Consequently a fixed preheat (260 °C for 10s) and cut-heat regime (220 °C for 10s) is employed for all the samples measured in this study.

Chapter 3 – Single grain analysis of arroyo sediments using an Annealed Single Aliquot Regenerative-dose (ASAR) approach: Initial results.

Chapter 3 will describe the results of analyses currently in progress. Single grain analysis of samples with relatively insensitive optical signal characteristics can result in very limited number of grains being accepted on the basis of the rejection criteria used in the modified SAR technique. This was found to be particularly true of the Californian arroyo sediments. Low natural signal counts and poor fitting on growth curve construction means that relative errors on equivalent dose estimates of accepted grains in these samples is also subsequently high. Annealing is known to increase the sensitivity of quartz considerably from previous studies. The aim of this chapter is to investigate the effects of annealing samples on growth curve construction and the relative errors on D_e values, and to verify whether this technique could be used to improve routine single-grain dating of quartz.

The Annealed Single Aliquot (ASAR) technique involves annealing each disc (at 350°C for 240s prior to administering the first laboratory dose in the modified SAR technique (Duller, 2003). In the initial measurements made thus far, annealing significantly improves growth curve construction and fitting. In the Californian samples measured, the relative errors on equivalent doses do show some improvement, although much of this error is derived from the low natural signals and so still displays wide values. Additional work is planned to measure some of the much more sensitive Colorado samples to see whether relative errors are improved in these cases. Verification of the ASAR technique is undertaken using the internal checks and dose recovery experiments. Recycling ratios are greatly improved and thermal transfer is not detected throughout. Laboratory doses can be successfully recovered using ASAR in the measurements made thus far. Further work may be pursued to investigate the effects of annealing at different temperatures/durations.

Part B – Assessing optical resetting and characterising dose distributions

Chapter 4 – Evaluation and analysis of bleaching histories in ephemeral fluvial samples part I: Investigating optical resetting using modern sample analogues and independent age control

Chapter 5 – Evaluation and analysis of bleaching histories in ephemeral fluvial samples part II: Analytical techniques and the selection of representative equivalent Dose (D_e) values for age calculations.

Chapters 4 and 5 describe the various approaches used in the verification of optical dating in this geomorphological setting. In particular they relate to assessing whether complete or partial resetting of the optical signal has occurred in the arroyo samples being measured, and how to best represent resulting fully or partially bleached dose distributions in D_e estimates. Chapter 4 describes the field methods used and chapter 5 describes the analytical and statistical techniques used for investigating optical resetting characteristics and dose distributions.

In the first part of chapter 4 the single aliquot and single grain results of measurements made on the modern channel sediments collected downstream at Murray Springs will be presented. Implications for optical resetting characteristics of ephemeral stream sediments in a downstream direction will be discussed and related to theory and measurements of sediment transport rates and distances undertaken by previous authors in such systems. The modern channel samples have been prepared and are awaiting measurement over the Easter break. In the second part of this chapter, optical resetting is compared with independently derived ^{14}C ages collected from the same stratigraphic units at the Cuyama River and Murray Springs

sites. Minimum and mean optical ages calculated from both single grain and single aliquot equivalent dose measurements are compared with radiocarbon ages for associated units. In the case of the Cuyama samples, the Holocene channel terrace sediments display particular scatter and mean single aliquot ages are generally an overestimation in comparison to associated radiocarbon ages. Single aliquot minimum age calculations reveal better age correlation in a number of these samples. Single grain minimum and mean ages provide much better correspondence with independent age control. Results highlight the importance of using single grain analysis in the case of partially bleached samples, and demonstrate that single aliquot minimum ages may still not yield accurate ages in partially bleached samples. All single aliquot and single grain measurements of the Cuyama samples have been completed. Samples from the Murray Springs sites have been prepared and await measurement over Trinity term. Independent ^{14}C age control for both sites has been carried out by S. Delong and Vance Haynes at the University of Arizona. Work on the radiocarbon sample ages has been completed for both sets of samples.

Chapter 5 follows on directly from chapter 4, trying to determine the bleaching characteristics of the fluvial samples using an array of analytical techniques. Much of these investigations have been completed on the Cuyama and Colorado samples measured so far. Further measurements and analysis of the Murray-Springs samples will be added following equivalent dose determination measurements of these samples in Trinity term. The first part of this chapter concentrates on the range of both distributional and signal analysis methods available for identification of partial bleaching. Each method is applied to a number of samples from arroyo sites across the southwest and their suitability discussed. Although ideally suited for fluvial samples, $\text{De}(\text{t})$ analysis fails to discriminate seemingly obviously partially bleached samples in a number of the Colorado and Californian samples. This is investigated further and two possible reasons for this are put forward for the failings of $\text{De}(\text{t})$ analysis in partial bleaching identification: i) absence of medium components in sample natural signals ii) environmental bleaching conditions. Tests using artificially partial-bleaching measurements made in the lab and curve fitting reveal that in a number of sites in Colorado the sample's signals lack significant medium components. In the Californian samples this is not the case, and artificial laboratory partial bleaching is detectable. A possible explanation proposed for the failings of $\text{De}(\text{t})$ analysis in this ephemeral system is that much of the sediment bleaching may be occurring in the long dormant phases in between episodic flow events rather than during them in this and other ephemeral streams. If this were the case, samples would then have been bleached (partially or fully) directly rather than underwater, hence explaining the failure of $\text{De}(\text{t})$ analysis.

The suitability of alternative distributional methods for identifying partial bleaching are then investigated. Standardised intensity versus equivalent dose plots are shown to be of little use in the samples tested, owing to inhomogeneous grain-grain sensitivities revealed in single grain analysis. Analysis is therefore focussed on assessing dose distribution characteristics using histograms, PDF's and radial plots. Identification of non-normal distributions in these plots is often taken as being indicative of partial bleaching. Where non-normal distributions or scatter are present there are a number of possible methods that have been suggested for obtaining best estimates of true burial doses. Each of these techniques is reviewed and its suitability for the arroyo samples investigated. Given the fairly limited number of aliquot measurements made in a large number of the samples in this study, leading edge analysis is unsuitable. Taking the lowest fifth percentile/lowest D_e value may result in underestimations of true burial doses owing to experimental error scatter. A scheme is proposed based on the running mean analysis of Fuchs and Lang (2001). In this procedure the significance of dose

distributions are first tested using measures of skewness and comparisons of relative standard deviations on the burial dose distributions and experimental error distributions. Equivalent doses obtained by this method yield reasonable and stratigraphically sensible ages.

Additional work to be completed in this chapter includes comparing the final optical ages obtained from each of the dose distribution techniques reviewed with the independently derived ^{14}C ages. Further analysis using the common, central and minimum age models is also currently being undertaken on sample equivalent dose measurements already made.

2.5 Section III – Chronologies of Late Quaternary arroyo epicycles in the American southwest

Chapter 6 – Redating and extending arroyo epicycle chronologies at Murray Springs-Curry Draw, southeastern Arizona

Samples from the Murray Springs, Curry Draw site are awaiting measurement in Trinity term using both single aliquot and single grain methods. Once these are obtained the optical ages will be compared with the ^{14}C ages and interpreted in their geomorphic context. The history of this site is well known from one of the most extensive radiocarbon dating schemes undertaken in the southwest. It is hoped that the optical ages obtained from palaeochannel fill deposits will be able to consolidate current understanding of alluvial history at the site, and improve precision on the current stratigraphy chronology. In addition, the optical dates will extend the current chronology back to the initial Late Pleistocene valley filling episodes. Additional optical ages obtained from the previously undatable Sobiapuri and Millville units will indicate the timing of initial valley filling across the region.

Chapter 7 – Reconstructing the Late Quaternary alluvial history of the Cuyama River, Southern California, using optical dating

This chapter describes the application of optical ages obtained on the Cuyama samples to their geological context. All single grain and single aliquot measurements of these samples are nearing completion, and interpretation of the results is ongoing. Samples obtained from multiple alluvial terrace infills in the Cuyama basin have been dated simultaneously using both optical dating and radiocarbon dating. Through this multi-dating approach the Late Quaternary history of the Cuyama River is revealed. Interpretation of the chronological record against palaeoclimatic and palaeoenvironmental records in the Santa Barbara region reveal a strong correlation with major Late Quaternary climatic events. The current channel incision event is believed to be fairly recent, occurring within the last 1 ka. Prior to this, the valley experienced a period of aggradation lasting 2-3 ka. The second alluvial terrace was emplaced at the beginning of the Holocene or during the Late Pleistocene-Holocene transition (optical ages – 8.87 and 9.37 ka ages) when rainfall patterns and annual amounts are known to have varied in the region. Optical dating of the upper terrace infill suggests these deposits are Late Pleistocene in age (21.41 – 31.03 ka), resulting from a switch in river mode of operation to aggradation during this more humid period.

Chapter 8 – Optical dating of arroyo sequences across southern Colorado: an inter- and intra-basin comparison

This chapter describes optical ages obtained from a range of small scale arroyos across southern Colorado. Currently, about half of these samples have been dated, with encouraging

results. The remainder have been prepared and await measurement over Trinity term. Arroyos in this region display distinct and multiple palaeochannels in their side walls. Optical dating of sediments from these palaeochannels, along with intervening alluvial fill units enables the reconstruction of arroyo epicycle histories in the region. The dating of alluvial histories from within different parts of the same systems, and from different systems in the same vicinity enables an intercomparison of arroyo epicycles at a multitude of spatial scales. Both current and past arroyo cycles are dated. Numerous arroyos in the area display similar timing of arroyo epicycles around the mid-Holocene altithermal event. Ages of palaeochannel fill in the Little Grand Canyon, Fort Carson of 5.86-6.85 ka, correlate well with those from similar units in Big Arroyo, Pinyon Canyon which date back to 6.33 ka. These results suggest a regionwide external control for major Holocene arroyo epicycles in southeastern Colorado. The correspondence of arroyo incision timing within different reaches of the same system (Big Arroyo) support this suggestion further.

2.6 Section IV – Numerical modelling of ephemeral river basin cut-fill cycle dynamics

Chapter 9 – Numerical modelling of ephemeral stream epicycles of erosion and aggradation: Introduction and model overview

This will be a fairly short chapter, focussing on the technical details of the modelling procedure used in the investigations of chapters 10 and 11. The chapter serves two purposes. Firstly it presents an introduction to the numerical modelling investigations, outlining the suitability and limitations of modelling in providing quantitative insight into the operation of cut-fill cycle mechanisms and processes. The aims of the modelling investigations are summarised. An overview of the CHILD model is provided, describing the various erosion laws and parameters, along with climate and vegetation simulation modules etc. The second part of the chapter describes the parameterisation process of the CHILD model used in the investigations. Parameter values were chosen using a combination of empirical published values and calibrated values. The model is parameterised to closely represent semi-arid conditions in a small-scale ephemeral basin. Justification of parameter value choices are outlined along with information about simulation details and the steady state landscape conditions used in the simulations.

Chapter 10 – Autogenic cut-fill cycle behaviour in ephemeral streams: Numerical modelling insights into the role of geomorphic thresholds and complex responses in the context of fluvial epicycles

This chapter provides evidence for the existence and importance of autogenic ephemeral cut-fill cycle behaviour from the numerical modelling simulations undertaken using CHILD. All work towards this chapter has been completed and a first version of the chapter (including figures and tables) has been written.

The chapter focuses on intrinsic geomorphic thresholds that have previously been cited as important controls of cut-fill cycle initiation in numerous ephemeral streams across the American southwest. The types of controlling geomorphic thresholds involved and the mechanisms leading to the critical threshold crossing events are however not entirely revealed in the limited number of previous stratigraphic studies and laboratory/field-based experimental catchment investigations. In the following study, the importance of inherent landscape instability in ephemeral basin evolution is investigated within a numerical modelling framework. Numerical modelling simulations conducted on a small-scale semi-

arid basin using the CHILD model demonstrate the existence of alternating steady-state epicycles of aggradation and erosion without any prior changes in independent external variables. The two key *intrinsic control mechanisms* responsible for the autocyclic behaviour observed are found to be intrinsic geomorphic thresholds relating to critical channel slope gradients, and 'complex response' behaviour. Spatial and temporal analysis of the process-response relationships occurring within the catchment reveal the important environmental and basin conditions that promote autocyclic behaviour, and the sorts of channel-hillslope interactions and feedbacks that are an integral part of this dynamic steady-state activity. This numerical modelling study offers some of the first, truly quantitative evidence for the existence and importance of intrinsic controls of cut-fill epicycles in ephemeral systems. The implications of these findings are discussed in the context of the arroyo discourse and the interpretation of field records.

Chapter 11 – The importance of rainfall characteristics in the development of ephemeral basin cut-fill cycles: Results from numerical modelling investigations using CHILD

All the necessary modelling work towards this chapter has been completed. The chapter figures and tables have been prepared and a first version of the chapter is currently in writing. This chapter focuses on the importance of more 'subtle' aspects of climate in the formation of arroyo epicycles. Several researchers have suggested that changes in storm intensity, frequency and seasonality rather than simple changes in mean annual rainfall were the key controlling climatic factors in the modern phase of arroyo development seen in many parts of the American southwest (e.g. Leopold, 1951; Cooke, 1974; Balling and Wells, 1990; Molnar, 2001). Assessing the importance of changes in rainfall patterns under constant mean climatic conditions in nature is made difficult by the lack of detailed historical rainfall records around the time of the historic incision episode. In this chapter the importance of rainfall characteristics in cut-fill cycle development is investigated within a numerical modelling framework. Numerical modelling simulations conducted on a small-scale semi-arid basin using the CHILD model demonstrate the important role that even subtle changes in rainfall patterns may have had on cut-fill cycle development in the southwest during the past. Three types of sensitivity analysis are undertaken: i) Analysis of catchment morphology following alterations in rainfall characteristics under constant mean rainfall conditions. The catchment is parameterised using annual rainfall statistics from various different locations in the U.S. that share mean rainfall amounts, but display different rainfall patterns. Steady state basin morphologies show dramatic differences even though mean climate remains constant. ii) Analysing the effects of climate changes resulting from alterations to individual rainfall parameters. Simulating identical changes in mean rainfall following alteration of individual rainfall parameters (storm intensity, frequency, and duration) reveals the relative importance of these factors. Rainfall intensity is found to be a particularly dominant control variable compared to rainfall frequency or duration from this analysis. Non-linear, direction-dependent responses are also shown to be commonplace following alteration of rainfall parameters. iii) Investigating the nature of catchment responses in relation to the direction of changes in rainfall parameters. Given the important control exerted by rainfall intensity it is shown that channel incision epicycles can occur following both an increase or decrease in mean rainfall. These results are particularly important and suggest that emphasis should not be placed on changes in mean rainfall conditions alone when explaining ephemeral cut-fill cycles.

2.7 Appendices

Appendix A

- Paper I* Arnold, L.J., Stokes, S., Bailey, R., Fattahi, M., Colls, A.E., Tucker, G., 2002. *Optical dating of potassium feldspar using far-red ($\lambda > 665\text{nm}$) IRSL emissions: A comparative study using fluvial sediments from the Loire River, France*. Quaternary Science Reviews 22, 1093-98

This published paper is based on previous observations that UV-blue emissions from feldspars have often proved to be unacceptable dosimeters for age estimation given the intrinsic problem of anomalous fading. The potential of exploiting the far-red ($>665\text{nm}$) IRSL emissions from potassium feldspars as a means of avoiding the malign effects of anomalous fading has recently been proposed (Fattahi, 2001). While that research demonstrated that it was possible to detect the far-red signal in the coarse grain feldspar samples studied, it did not present any empirical data for actual geological samples with or without independent age control. The purpose of the present paper is to expand on the work of Fattahi (2001) by undertaking a direct comparison of SAR D_e 's and corresponding optical ages for a suite of Holocene through Late Quaternary Pleistocene fluvial terrace deposits from the upper reaches of the Loire River, France. Here we describe the behaviour of the far-red emissions for these samples and present some initial dating results. The far-red IRSL emission ages obtained are compared to UV-blue IRSL emission ages for the fluvial samples and to corresponding optical ages previously generated on quartz fractions from the same samples. Initial results are promising but show some inconsistencies. Basic experiments demonstrate that this is not attributable to insufficient sensitivity correction by SAR in the far-red emissions, neither was anomalous fading detected in either the far-red or UV-blue emissions over short storage times. It is suggested that refinement of pre-treatment and measurement conditions should enable more successful dating of feldspars with far-red emissions and that further research on the potentially stable far-red signal is necessary.

- Paper II* Lai, Z.-P.; Arnold, L.J., Stokes, S., Bailey, R., Fattahi, M., 2002. *Detection of far-red IRSL from loess*. Ancient TL 20(2), 41-46.

This published paper discusses the recent proposal that it may be possible to extend the age range of luminescence dating of loess using the far-red ($\lambda = 665\text{-}740\text{nm}$) emissions from feldspar, as it is thought not to exhibit anomalous fading. Studies on red luminescence have been hindered due to technical difficulties in suppression of background and other factors. Recent modifications to apparatus (esp. photo-multiplier plus filter combinations) have been reported demonstrating that red IRSL ($\lambda = 590\text{-}700\text{nm}$) may be observed from coarse-grained feldspar (Fattahi and Stokes, 2003). However, this modified system was not able to detect far-red IRSL ($\lambda = 665\text{-}740\text{nm}$) from old ($>800\text{ka}$) Chinese loess. In this short note we describe further modifications to the system which have successfully enhanced the far-red IRSL signal, and at the same time reduced background signal levels. As a result, routine measurements of far-red IRSL from loess are possible.

Appendix B

Section III CHILD simulation parameterisation details

This appendix contains the raw data used in the parameterisation of the CHILD model for the simulations undertaken in section III of the thesis. It includes the published values of various

physical and process parameters found from a wide search of the literature and more detailed explanations of how the values of some of the erosion law coefficients were calibrated or derived theoretically. This appendix is included to explain and give further details of the choices of parameter values used in the simulations. All data for this section has been collated into tables and needs only minor modifications.

3. Plans for further work

The main outstanding parts of work are associated with the production of equivalent doses and final ages for the Arizona samples and some of the Colorado samples, along with the final writing up of chapters. The remaining samples have all been prepared and are ready for measurement. The main work to be carried out over the following months is a systematic evaluation of these remaining samples using both single aliquot and single grain techniques. Given the fairly young ages of my samples it is practical to produce single aliquot equivalent doses for one sample in 24hr. Measuring the remaining 30 Murray Springs samples and 20 Colorado samples using this method should therefore take about 7 weeks of machine time. When taken in conjunction with additional measurements needed to validate the SAR technique and expanding equivalent doses on already measured samples with limited D_e 's, I expect to have completed all single aliquot measurements by the end of Trinity term. Single grain measurements of a number of the samples will also be ongoing. These will be prioritised for partially bleached samples, and particularly for the Cuyama and Murray-Springs samples. Practically, it is possible to produce equivalent doses for 2 samples in a week with the single grain reader. I anticipate spending a further three-four months carrying out these measurements, to produce a reasonable number of dates for thorough evaluation of the samples I have.

Dose rate evaluation for the majority of samples has already been carried out using in-situ gamma spectrometry. For more accurate beta dosimetry analysis, inductively-coupled plasma mass spectrometry will be undertaken. Preparation of the samples for this procedure takes 3 days per 30 samples. It is hoped, therefore that preparation and measurement of the samples by ICPMS will be undertaken fairly rapidly within 1-2 months. A detailed timetable outlining the objectives and timescales for the remaining D.Phil project is shown below. Throughout the following months, I will focus on both establishing the remaining ages and dose rate estimates. Writing up chapters is also currently an ongoing process and will become my sole focus from the end of Trinity term onwards.

Objective	Year 3 (2004/5)											
	Mar	Apr	May	June	July	Aug	Sep	Oct	Nov	Dec	Jan	
General and specific reading												
Equivalent dose measurements												
ICP analysis												
SAR and single grain protocol testing												
Analysis of chronology results												
Writing of chapter in section I												
Writing of remaining chapters in section II												
Writing of chapters in section III												
Writing of remaining chapters in section IV												
Writing of introduction and conclusion												
Bind and submit thesis												

Timetable for execution of remaining research

4. REFERENCES

- Antevs, E., 1952. Arroyo cutting and filling. *Journal of Geology* 60, 375-385.
- Bailey, R.W., 1935. Episodes of erosion in the valleys of the Colorado Plateau province. *Journal of Geology* 43, 337-355.
- Balling, R.C., Wells, S.G., 1990. Historical rainfall patterns and arroyo activity within the Zuni River drainage basin, New Mexico. *Annals of the Association of American Geographers* 80(4), 603-617.
- Blum, M.D., Toomey, R.S. and Valastro, S., 1994. Fluvial response to Late Quaternary climatic and environmental change, Edwards Plateau, Texas. *Palaeogeography, Palaeoclimatology, Palaeoecology* 108, 1-21.
- Bryan, K., 1928. Historic evidence of changes in the channel of Rio Puerco, a tributary of the Rio Gande in New Mexico. *Journal of Geology* 36, 265-282.
- Cooke, R.U., 1974. The rainfall context of arroyo initiation in southern Arizona. *Zeitschrift fur Geomorphologie (Supplement band)* 21, 63-75.
- Cooke, R.U. and Reeves, R.W., 1976. *Arroyos and Environmental Change in the American Southwest*. Clarendon Press, Oxford. 213 pp.
- Duller, G.A.T., 2003. Distinguishing quartz and feldspar in single grain luminescence measurements. *Radiation Measurements* 37, 161-65.
- Fattahi, M., 2001. Investigations into red luminescence emissions from quartz and feldspar. Unpublished D.Phil thesis, University of Oxford.
- Fattahi, M., and Stokes, S., 2003. Red luminescence from potassium stimulated by infrared. *Radiation Measurements*. Submitted.
- Fuchs, M., and Lang, A., 2001. OSL dating of coarse-grain fluvial quartz using single-aliquot protocols on sediments from NE Peloponnese, Greece. *Quaternary Science Reviews* 20, 783-87.
- Knox, J.C., 1983. Responses of river systems to Holocene climates. In, H.E. Wright (ed.), *Late Quaternary environments of the United States vol. 2. The Holocene*, Minneapolis, University of Minnesota Press, 26-41.
- Leopold, L.B., 1951. Rainfall frequency: an aspect of climatic variation. *Transactions American Geophysical Union* 32, 347-357.
- Miller, J.R. and Kochel, R.C., 1999. Review of Holocene hillslope, piedmont and arroyo system evolution in the southwestern United States: implications to climate-induced landscape modifications in southern California. In, Rose, M.R. and Wigand, P.E. (eds.), *Proceedings of the southern California Climate Symposium; Trends and Extremes over the 2000 years*. Natural History Museum of Los Angeles County.
- Molnar, P., 2001. Flooding in arid environments, and erosion rates. *Geology* 29, 1071-74.
- Murray, A.S., and Wintle, A.G., 2002. The single aliquot regenerative-dose protocol: potential for improvements in reliability. *Radiation Measurements* 36.
- Patton, P.C., Schumm, S.A., 1975. Gully erosion, northwestern Colorado: a threshold phenomenon. *Geology* 3, 88-90.
- Thornthwaite, C.W., Sharpe, C.F.S. Dosch, E.F., 1942. Climate and accelerated erosion in the arid and semi-arid Southwest with special reference to the Polacca Wash drainage basin, Arizona. U.S. Department of Agriculture Technical Bulletin. 808: 134 pp.
- Tucker, G.E., Slingerland, R., 1997. Drainage basin responses to climate change. *Water Resources Research* 33, 2031-2047.
- Waters, M.R. and Haynes, C.V., 2001. Late Quaternary arroyo formation and climate change in the American Southwest. *Geology* 29(5), 399-402.

5. Example of completed work

Chapter 10

Autogenic cut-fill cycle behaviour in ephemeral streams: Numerical modelling insights into the role of geomorphic thresholds and complex responses in the context of fluvial epicycles

Appendix B

Preliminary report on dendrogeomorphological studies in
Colorado

Unpublished progress report by Vanessa Winchester,
2002

Preliminary report on Dendrogeomorphological studies in Colorado
July 2002.

Vanessa Winchester,
School of Geography and the Environment, University of Oxford.

FORT CARSON

Fort Carson, 1655 m (5428 ft) a.s.l., and Piñon Canyon Maneuver Site (PCMS) 1635 m (5362 ft) a.s.l.

Material: 42 tree cores were taken with a 400 mm tree increment borer and 32 cross sections were cut from small trees, shrubs and shrub roots.

Tree species: Juniper (*Juniperus monosperma* and *Juniperus osteosperma*), a few Piñon pine (*Pinus edulis*) and Tamarisk (*Tamarix pentanda*).

Shrubs: Rubber rabbit bush (*Chrysothamnus nauseosus*) and Four-winged saltbush (*Atriplex canescens*).

Study sites:

Fort Carson - Horton Gully, Big Valley, and Little Grand Canyon, about 100 miles north-northwest of PCMS - Purgatoire Canyon and Big Arroyo

General observations on climate and tree growth at Fort Carson

There is significant statistical agreement between growth measurements of the majority of cross-dated cores at all the coring sites excepting Purgatoire Canyon. This suggests that climate has been the major factor controlling growth in the area.

The, mainly, juniper trees appear to be unaffected by the 1943 to 1957 drought period. However, growth was generally suppressed from the late 1850s to the 1970s with one release period between 1915 to 1925. Since 1930 when growth was (narrowly) at its lowest point for the last 165 years, growth has recovered reaching its highest point in the whole 285-year record in 2000; exceeding previous high points reached in 1790 and 1825 (*see climate graph*).

Conformable tree growth across the study area, where winters are cold and summers frequently drought ridden, may be owing to the high-stress factors and similarities in altitude and topography, with growth differences in Purgatoire Canyon due to the relatively, well-watered, sheltered river-valley site.

However, human impact could also account for suppressed growth from the 1850s until 1915. This period coincides with land settlement and the development of ranching across the area. Persistent growth recovery from the 1940s to the present could relate to further changes in land use associated with allocation of the area to the army. Further work is required to investigate the human and non-human factors influencing growth.

Events

There are at least four processes of gully activity that affect associated plants: (i) sapping (including piping induced by soil cracking, animal or insect burrowing) leading to

(ii) slumping; (iii) sliding, and (iv) filling. These processes will be accelerated by slope wash especially following intense storms after dry periods.

Gully activity and slope dynamics were investigated using both external and morphological characteristics of trees and shrubs. Slope soil accumulation rates were derived from distances between current ground surface and primary and secondary root structures, with annual rings used to date the different root/stem junctions. Similarly, minimum rates of soil loss were deduced from measurement of root exposure and by dating changes in ring eccentricity shown in trunk cross sections. Branch or trunk damage to trees growing by river channels date flooding events. In addition tree age provides a minimum date for events that clear surfaces of vegetation. The values in Table 1 show that it takes from 1-4 years for seedling trees to start growing, with the length of time depending on the amount of moisture available. Growth rates are similarly affected by moisture with juniper on dryer hill-slope sites growing 3.8 cm yr and on wetter sites 16.7 cm yr.

FORT CARSON

Horton Gully (Training Area 21). Aerial photos, from 1962, 1991 and 1995 show relatively stable gully walls. The gully's mid-section is eroded to a depth of 3.2 m. with some recent slumping and widening probably in the late 1990s. Retreat during the last growing season is marked by a tree dying from accumulation of too much soil at its base.

Big Valley (Training Area 48). This gully has dissected the rim of the valley and is advancing into the surrounding plateau, with the head wall currently relatively stationary. A tree, initially growing 1 m above the gully floor and fallen across the gully at its narrowest point where it pierces the valley rim, provides a minimum date for rim incision of 1901 and a date of 1989 for recent changes in the gully. The ages of rubber-rabbit and four-winged saltbushes growing around the enlarged head of the gully provide more detail. They suggest that active enlargement took place prior to the 1940s while the ages of shrubs (23 yrs) on the gully-head walls and a small juniper tree (16 yrs) growing on the gully floor suggest that, apart from some minor slumping, there have been few major changes since the 1940s (*see Big Valley figure*).

Little Grand Canyon (Training Area 42). Erosion is active on at least some of the head walls, with consequent accumulation of material in parts of the system. The most southerly head, unlike most of the other head walls, has a slope angle of 32° and is near a route junction; possibly this was back-filled by the army. A shrub growing on the head slide dates filling to 1996, with further slumping in 1997/8 since when, the gully head has probably been static. In the next gully to the north, the vertical headwall has been eroding over at least the last 9 years with increasing accumulation at its foot. Additional material has been carried down the main gully channel and deposited below a bedrock knick point, with at least 3 accumulation phases: before 1969 and in 1977 and 1988. A tree growing in a feeder channel on a small terrace below the north side of the main channel provides a minimum age for terrace creation of 80 years (1923). Ephemeral vegetation, grasses, small plants by the runoff channel and shrubs growing 26 cm above the channel suggest that there has been little activity at this point in the system, at least over the 2002 growing season. A further tree on the south side of the gully on its lip has exposed roots suggesting minor gully slumping and widening 25 and 4 years ago (1977 and 1998), with narrow tree rings forming in 1985, 1988 and 1992.

PCMS

Purgatoire Canyon is impressive with walls over 400 feet high. Apart from dinosaur footprints, it contains a wide river with 4 terraces on its east side, the highest standing approximately 25 feet above the river, certainly predating any of the trees growing on it (the oldest cored tree is 118-years old). A small gully-type wall, forming the upper terrace boundary, is receding at an approximate average rate of 1cm/yr over the last 100 years, estimated by the distance of an exposed root from the present wall. The average rate probably does not accurately represent wall recession which is more likely to occur in increments, as suggested by annual ring eccentricity and periods of narrow dark rings show by the branch cross-section of a dying trees standing on the lip of the wall, where its roots maintain a bastion, on one side of which severe sapping and cavitation is taking place (see *Purgatoire Valley figure*).

Tree ages and periods of damage on the lower terraces suggest flood dates. A number of tamarisks by the riverside date flood debris in 2000. Trees on the first rock-cut terrace (T1) above the river date to 1990 with narrow, dark rings suggesting further flooding in 1992/3 and 1998. On the next terrace (T 2), maximum tree age of 1984 suggests flooding before this date with rings becoming eccentric in 1986 and narrow dark rings in 1992/3/4 and 1998/9 indicating that floods in these years covered this terrace also. T3 is not represented.

Big Arroyo head. Tree ages in and beside the centre line of the valley may not exceed 1910, the construction year of the Pipeline Road crossing the valley head. According to Dan Sharps, wagons may have accessed the road by ascending the gentle 2-4° slope of the valley. The valley head begins in a dip in the road and there are indications that runoff draining down the opposed inclines washes down-valley at this point. Over the 1 km extent of the study section, there are intermittent scours of increasing depth down-slope. Near the road the scours have mini heads 8-10 cm high and are not more than 1-2 m across. Near the base of the study section where lateral valley focus additional runoff into the main valley, gullying becomes more persistent with walls up to 175 cm high and scours 3 to 4 m across. (see *Map of Big Arroyo and Sketch map*).

There is a knick point in the bedrock approximately 280 m down-slope where the vertical head is 80 cm high and erosion is taking place across the width of the valley floor at this its narrowest point (37 m). Some 588 m from the road and 275 m below the knick point, the valley becomes almost flat over a distance of approx. 125 m. Here, grasses of the *Geraniaceae* family indicate a clayey, moist, disturbed soil at the foot of side valleys joining the main Arroyo valley. Cattle may have created the disturbance.

At this point, a 12-year-old Pinyon pine, its roots in soil 43 cm above ground growing in the middle of an old multi-stemmed Juniper (aged over 59 years) suggests recent soil surface loss near the tree of 28 cm, presumably since 1990. This host tree and its 'cargo' nicely illustrate the ephemeral nature of the arroyo system, with frequent cycles of filling and soil loss (see *Sketch map*).

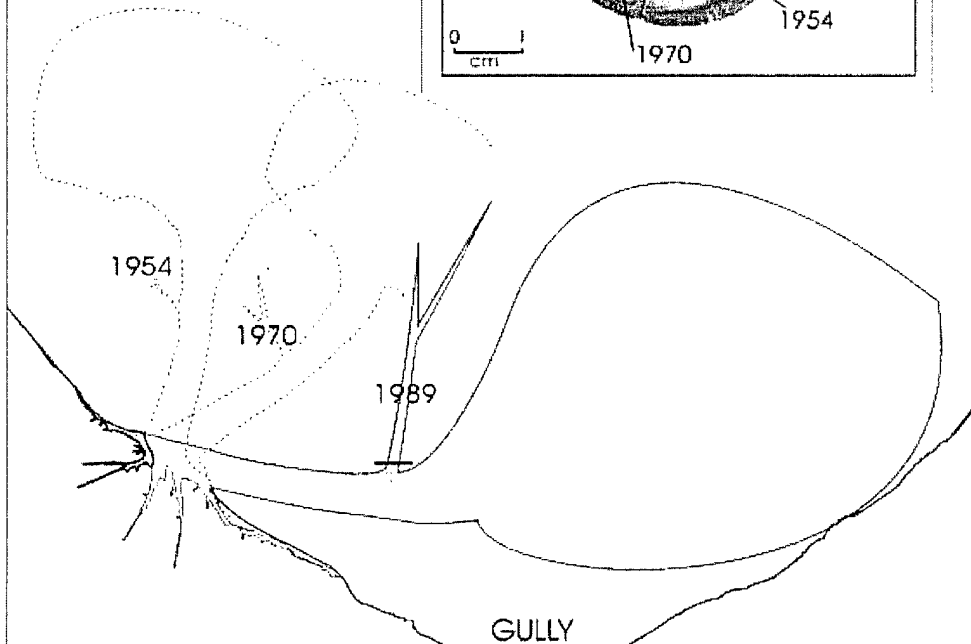
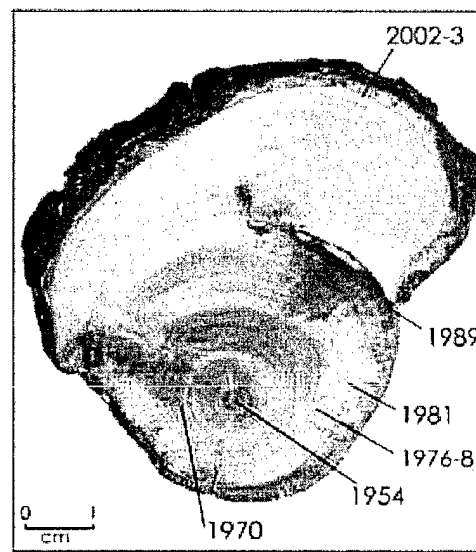
An additional factor that could repay further investigation is the existence of animal holes (pack rats?) below seedling trees and shrubs. These holes were often found during excavations of root systems not necessarily in main valley drainage channels. Such tunnels could act as focuses for moisture thus supplying both a good seedbed for plants and an initial focus triggering sapping and scouring.

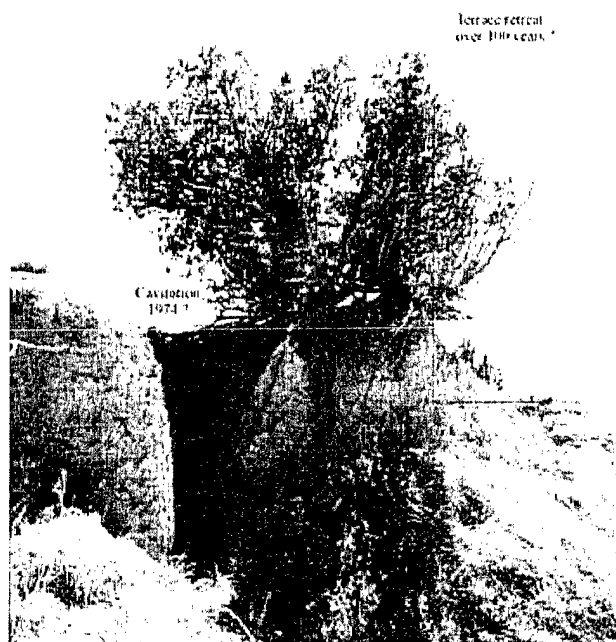
The present configuration of scours and mini gullies either focuses around tree stems or lays some metres up or down-valley from trees. The question is: what is the nature of the gully/tree relationship; are the gullies propagating uphill or downhill and what triggers uphill or downhill responses?

TABLE 1 shows tree height/age relationships at the head of Big Arroyo; 660 m down-valley in a moist gully and in the water tank ditch by the route from PCMS entrance. Growth rate vary according to environment, with rates from 2.5 to 4.7 cm/yr on dry slopes and from 13.6 to 20.5 cm/yr in moister areas. Estimate of years for juniper seedling establishment in water tank ditch, based on ditch excavation in 1984, is from 1 to 4 years.

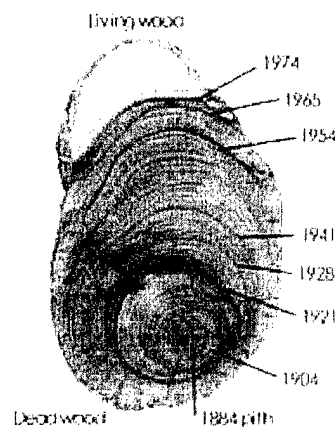
<i>Section (S) or Core (C) ID</i>	<i>Height above Primary root (pr)</i>	<i>Tree height (cm)</i>	<i>Tree age (yrs)</i>	<i>Growth rate cm yr⁻¹</i>
Big Arroyo head				
S1	pr	123	26	4.73
S3	pr	37	15	2.47
S4	pr	52	15	3.46
S6	pr	97	26	3.73
S8	pr	147	31	<u>4.74</u>
			0	3.83
Gully 660 m down-valley	<i>Core height above ground (cm)</i>			
C9	13	250	18	13.8
Water tank ditch dug 1984	<i>(S) or (C) height above ground (cm)</i>			
S3	Ground level	248	18	13.77
C4	19	270	13	19.28
C5	10	185	9	20.55
C6	33	250	12	19.23
S7	Ground level	195	14	13.93
S8	13	218	15	13.62
C9	63	282	14	<u>16.58</u>
			0	16.70

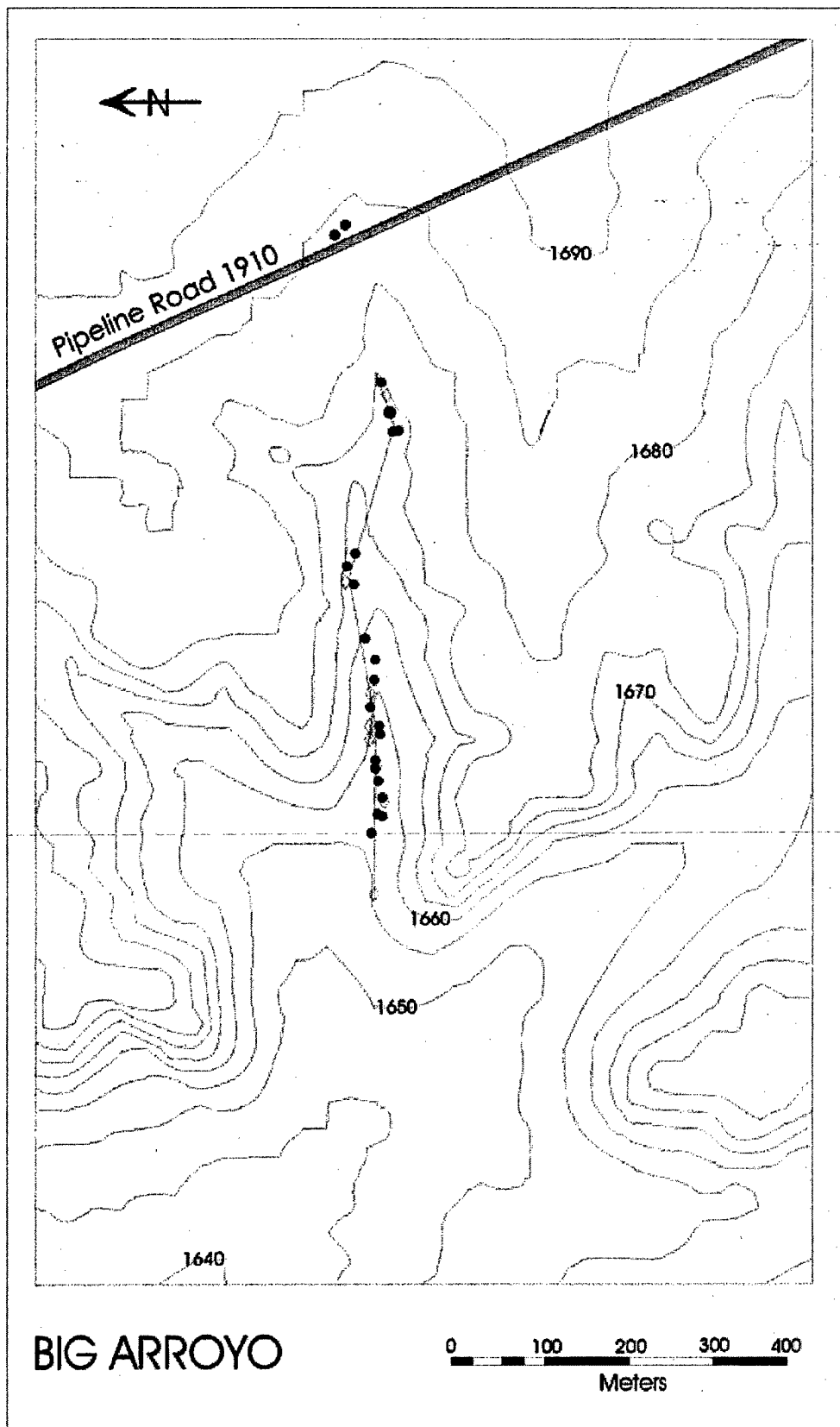
Section from a branch growing as new leading stem of tree taken across Big Valley gully where it has broken through the valley rim. 1976-78, 1981 and 2002-3 probably mark drought years and 1989 the year the tree fell. Darkened wood and ring eccentricity are reactions to slope movement starting in 1970, with the upper roots killed in 1989 (brown in time-lapse sketch below). Now only the lower slope roots remain to support growth.

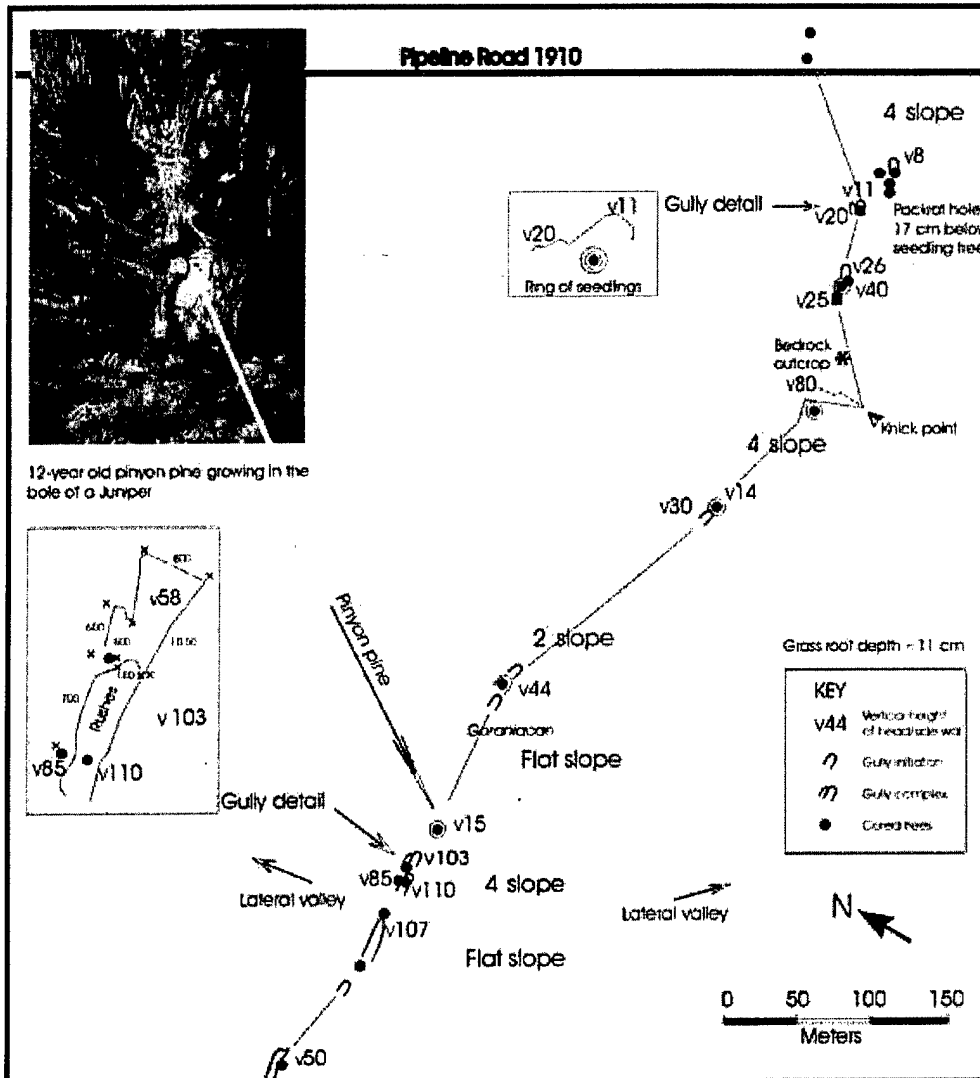




Purgatoire Canyon: retreating terrace wall with average retreat rate, of 1cm yr over 100 years, was extrapolated from length and age of exposed root. However, very narrow dark rings in the branch section (right) suggest that retreat has been episodic, beginning in 1904 when eccentric rings began to form. The first major change involved damage in 1921. In 1974 drastic terrace retreat, possibly including cavitation, exposed a large number of roots almost killing the tree - whose defoliated branches (above) are not to be mistaken for the healthy tree standing behind.







Appendix C

Solyom, P., and Tucker, G.E. (2004 in press) The effect of limited storm duration on landscape evolution, drainage basin geometry and hydrograph shapes: *Journal of Geophysical Research - Earth Surface*.

Effect of limited storm duration on landscape evolution, drainage basin geometry, and hydrograph shapes

Peter B. Sólyom and Gregory E. Tucker

School of Geography and the Environment, Oxford University, Oxford, UK

Received 26 February 2003; revised 1 April 2004; accepted 16 June 2004; published XX Month 2004.

[1] Landscape evolution models that calculate erosion as a function of discharge usually assume steady state runoff conditions and compute discharge as a power law function of the contributing area. This assumption is appropriate for small catchments and for regions in which the climate is characterized by long-lasting rainfall events. With larger catchments or shorter storms, however, the travel time of a water particle from the divide to the catchment outlet is typically longer than the characteristic storm duration. Hence a hydrologic steady state cannot be reached. This paper offers an analytic solution for nonsteady state peak discharge and investigates how changes in storm duration alter hydrograph characteristics and the shape of the resulting equilibrium landscape. An asymptotic function is used to incorporate the effect of storm duration into a landscape evolution model. We demonstrate with numerical simulations and analytical results that decreasing relative storm duration results in downstream-decreasing equilibrium channel concavity and decreasing valley density. It is also shown that this nonsteady state runoff system is less stable than the system of steady state runoff processes. Under certain conditions, no fixed dynamic equilibrium state exists. Furthermore, analysis of the shape of runoff hydrographs reveals feedback mechanisms manifested between hydrograph shape, erosion, and morphogenesis, demonstrating a compensatory mechanism between external precipitation input and internal runoff production. **INDEX TERMS:** 1815 Hydrology: Erosion and sedimentation; 1824 Hydrology: Geomorphology (1625); 1860 Hydrology: Runoff and streamflow; 3210 Mathematical Geophysics: Modeling. **KEYWORDS:** landscape evolution, storm duration, dynamic equilibrium, hydrograph shape

Citation: Sólyom, P. B., and G. E. Tucker (2004), Effect of limited storm duration on landscape evolution, drainage basin geometry, and hydrograph shapes, *J. Geophys. Res.*, 109, XXXXXX, doi:10.1029/2003JF000032.

1. Introduction

[2] One of the fundamental truisms of geomorphology is that the morphology of a catchment influences its hydrograph shape and that at the same time the catchment is shaped by the hydrograph via runoff erosion. This is one of the feedback mechanisms standing behind the self-organized character of landform development [Rodríguez-Iturbe and Valdez, 1979; Rodríguez-Iturbe et al., 1982; Rinaldo et al., 1993]. Landscape evolution models published in the past 2 decades have been successful in producing realistic-looking simulated landscapes [e.g., Ahnert, 1976, 1987; Howard, 1994b; Tucker and Bras, 1998; Willgoose, 1991a, 1991b], reproducing specific landform features [e.g., Howard, 1994a, 1997; Kirkby, 1971, 1986], and clarifying spatiotemporal causative relationships between model inputs and the resulting surface [Tucker and Slingerland, 1997; Tucker and Bras, 2000; Whipple and Tucker, 1999]. In these models the landscapes typically evolve in response to runoff expressed in terms of either mean annual, mean peak [e.g., Willgoose et al., 1991a, 1991b, 1991c], or

“effective” annual flow, without accounting for the shape of the hydrograph. This approach, which has the advantage of simplicity, ignores any interaction between hydrograph shape and erosion dynamics. Clearly, the incorporation of the hydrograph shape into landscape evolution models is not a necessary condition for landscape self-organization. However, the question of whether and how landscape evolution characteristics change when introducing the extra feedback between hydrograph shape and erosion remains unanswered.

[3] Hydrologic steady state occurs when a constant discharge is produced after a sufficiently long period of precipitation such that all runoff-producing portions of the catchment contribute flow to the point in question. It is convenient to assume this condition for purposes of long-term evolution modeling because it implies that the stream discharge at any point is simply the product of contributing area and a runoff coefficient. The assumption of steady state runoff may be quite reasonable for small catchments and for climates dominated by long-lasting, spatially extended precipitation events. However, it does not hold for large catchments and for regions in which short duration, small-scale convective storms provide the geomorphologically significant portion of the yearly precipitation. There are

several reasons for this. First, there are time-dependent losses during the rainfall-runoff transition. Interception and infiltration show decreasing rates during a storm event. These losses can entirely absorb the initial portion of a rainstorm, but after reaching saturation or a critical value, both interception and infiltration rate may attain constant values. Infiltration and interception are partly responsible for a time gap between the onset of the precipitation event and the buildup of the hydrograph peak discharge. If the precipitation event is shorter than this time gap, steady state (as defined above) cannot occur.

[4] Second, the relationship between the shape and the size of the rain cell and the shape and the size of the catchment determines the wetted proportion of the catchment during a storm event. If the rain cell does not entirely cover the catchment, the wetted proportion is less than one, and discharge cannot be assumed to be linearly proportional to the total drainage area. Third, the travel time of a water particle from the divide to the catchment outlet sets the time interval for the hydrograph to reach peak discharge and for runoff to reach steady state. If the characteristic storm duration is less than this timescale (which will depend on the longest storm flow travel time within the basin), steady state cannot occur.

[5] These effects have a direct influence on the spatial distribution of peak discharges within a drainage basin. They are responsible for two important hydrological phenomena that are likely to influence long-term drainage basin evolution. First, it is well known that in larger basins, peak discharge is commonly not linearly proportional to drainage area, even in humid temperate regions, where mean annual flow does vary linearly with basin size. For example, Figure 1 shows a linear relationship between mean annual discharge and drainage area for humid temperate drainage basins in Kentucky, United States. This is a common pattern in humid-temperate regions [e.g., Hack, 1957; Slingerland *et al.*, 1994]. By comparison, the relationship between basin size and mean peak discharge (i.e., the average annual maximum discharge) is clearly nonlinear (Figure 2). Non-linear relationships between peak flow and catchment size are particularly pronounced in dry climates, where in-stream losses are significant and rainstorms tend to be short lived

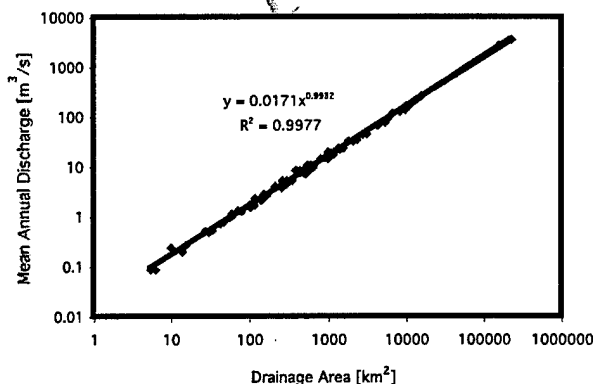


Figure 1. Mean annual discharge–drainage area relationship for river basins in Kentucky, United States. The exponent in the regression equation indicates a close-to-linear relationship between the two variables.

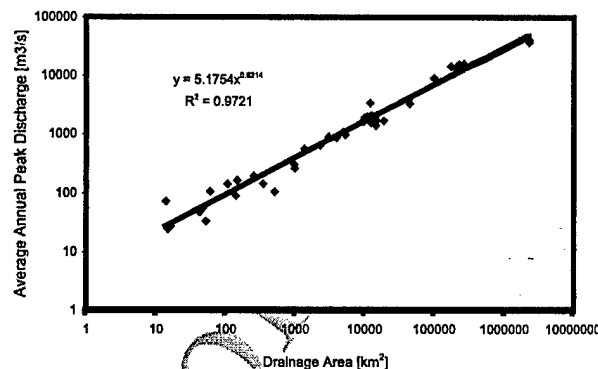


Figure 2. Average annual peak discharge–drainage area relationship for drainage basins in Kentucky. Note that the exponent in the regression equation is considerably less than unity, indicating the absence of a linear relationship.

and/or aerially focused [e.g., Leopold and Miller, 1956; Graf, 1988].

[6] A second important phenomenon is the observed relation between peak discharge and catchment shape. Strahler [1964] was among the first to point out the importance of drainage basin shape, arguing that all else equal, long, narrow basins will tend to have lower peak discharges at their outlet than more rounded ones. Such shape effects are commonly parameterized in synthetic unit hydrographs using a combination of area, mainstream length, and outlet-to-basin-centroid distance [e.g., Bras, 1990]. Shape effects are also implicit in the geomorphic instantaneous unit hydrograph concept [Rodriguez-Iturbe and Valdez, 1979] and in the well-known correspondence between hydrographs and catchment width functions [e.g., Rinaldo *et al.*, 1995b; Veneziano *et al.*, 2000; Dick *et al.*, 1997]. Given the importance of catchment size and shape effects in hydrology, it is natural to expect that they play a role in feedbacks between hydrology, erosion, and long-term basin evolution. This paper aims to develop a generalized theory to describe one of these key feedbacks, that arising from flow duration effects, and make predictions about its geomorphic consequences.

2. Background, Approach, and Scope

[7] By using landscape evolution models in geomorphic research, it becomes possible to forecast the reaction of the surface to changing climatic or land use conditions [e.g., Willgoose *et al.*, 1991a, 1991b; Howard, 1994a, 1994b; Kooi and Beaumont, 1996; Coulthard *et al.*, 2000; Tucker and Slingerland, 1997; Moglen *et al.*, 1998; Allen and Densmore, 2000]. However, most current landscape evolution models make these forecasts on the basis of a highly simplified representation of catchment hydrology. Typically, it is assumed that the discharge at any point in a channel network is a multiple of the drainage area. This implies that formative storms are larger in area than the catchment and that they last longer than the longest travel time of water particles within the largest basin, even when applied at scales of hundreds to thousands of square kilometers. Willgoose *et al.* [1991c] and Howard [1994a, 1994b] used

a more general approach, in which peak discharge is modeled as a power law function of basin area; in practice, however, a linear relationship is usually assumed. In some environments a limited travel time even for overland flow on hillslopes can have a significant influence on morphology. For example, *Dunne* [1991] showed how long, convex hillslopes arise as a result of characteristically short storm duration in Kenya. *Kirkby* [1993, 1994] constructed an erosion law with a characteristic scale parameter giving the distance traveled by overland flow during a dominant storm and found that equilibrium slope profiles are affected by this parameter; however, these analyses were restricted to hillslope profiles. *Niemann et al.* [1997] compared the predicted equilibrium morphology of catchments formed by long-lasting versus "impulsive" rainfall events and found that "impulsive" rainfall results in steeper slopes at higher contributing area than is the case under continual precipitation. Thus, although the steady state assumption has the appeal of simplicity, its application to larger catchments is problematic on both physical and theoretical grounds.

[8] In this paper we introduce a simple theory for peak discharge distribution within a catchment and use this theory to predict the long-term geomorphic consequences of nonsteady flood discharges. We do this in part by encoding the theory within a numerical landscape evolution model and running simulations of catchment evolution that compare steady and nonsteady hydrologic regimes. We begin by assuming that peak discharge of a given (but here unspecified) recurrence interval acts as a "dominant" discharge [*Wolman and Miller*, 1960]; in other words, it is the discharge which is most important in shaping the drainage basin. In adopting this assumption we note that annual peak flow is considered to be a better indicator of geomorphologically significant hydrologic conditions than annual mean flow. By doing so, the shape of the runoff hydrograph is explicitly represented in the model. The model offers a two-dimensional network framework to account for the geomorphological effects of the limited storm duration in the context of large-scale landscape evolution theory. Ideally, this will allow the modeling of more complex climate change scenarios and a better understanding of the hydrograph shape-erosion feedback mechanism.

[9] In sections 3–5 we examine both numerically and analytically the morphological changes to an evolving surface that occur when runoff conditions shift from steady toward unsteady and describe some features of the hydrograph shape-erosion interdependence. We show that reduced storm duration decreases the concavity of the fluvially eroded profiles, alters the slope-area diagram of the resulting equilibrium surface, and, in certain cases, results in convex equilibrium slope and channel profiles. At the same time we show that the hydrograph shape-erosion interaction provides a self-stabilizing feedback mechanism that dampens landscape response when the dominant storm duration changes.

212 3. Theory

213 3.1. Hydrology

214 [10] This paper focuses on the effects of short (duration <
215 travel time) and intense storms, which are typical of

semiarid climates, in which infiltration-excess runoff is often the dominant mechanism of runoff generation. Considering that theoretically, a hydrograph begins to rise at the very moment when the rain event commences (because raindrops fall in the stream) and that after cessation of the rainfall the time taken for the flood to leave the catchment is the longest travel time for storm runoff within the basin, the duration of a storm flow hydrograph can be given as the sum of the duration of the storm, T_r , and the time required for water at the most distant point of the catchment to reach the outlet, T_t :

$$T_h = T_r + T_t. \quad (1)$$

[11] Initial infiltration following the onset of a rain event can also be incorporated into the model by interpreting T_r as the runoff-producing duration of the event. The maximum travel time for storm flow can be obtained as

$$T_t = \frac{L}{U_f}, \quad (2)$$

where L is the longest flow path within the basin and U_f is routing velocity. The routing velocity is assumed here to be spatially constant. This assumption is consistent with the fact that bank-full flow velocity tends to show minimal increase downstream ($U_f \sim Q^{0.1}$ [*Leopold and Maddock*, 1953]) in most alluvial rivers. Our assumption ignores the fact that overland flow velocity is usually considerably slower than flow in open channels. One could account for this by using two distinct routing velocities, one for channels and one for hillslopes. However, if drainage density were relatively uniform, this would simply increase calculated travel times everywhere, without altering the scaling that we discuss in section 4 (to appreciate this, try replacing equation (2) with $Tt = (L - L_h)/U_f + L_h/U_h$, where L_h is hillslope length and U_h is overland flow velocity, in the derivations that follow). For the sake of clarity, therefore, we assume a constant routing velocity, recognizing that differential overland and channel velocities influence the model predictions only in detail and can, if desired, be easily incorporated.

[12] Following *Willgoose* [1989], the hydrograph, $Q(t)$ can be nondimensionalized by scaling with peak flow, Q_p , while time, t , can be normalized by flood hydrograph duration, T_h :

$$Q'(t') = Q(t)/Q_p, \quad (3)$$

where

$$t' = t/T_h. \quad (4)$$

[13] The total flood hydrograph volume, neglecting base flow, can be written as

$$V = \int_0^{T_h} Q(t) dt = Q_p T_h \int_0^1 Q'(t') dt', \quad (5)$$

where V is total volume and discharge is taken to include only storm flow (not base flow). In the case of infiltration-

267 excess runoff production, total volume can also be given as
 268 $V = (R - I)AT_r$, where R is time- and space-averaged
 269 rainfall intensity, I is time- and space-averaged infiltration
 270 rate ($I < R$), and A is contributing area. Combining
 271 equations (1), (2), and (5), and assuming constant R and I ,
 272 we can write Q_p as a function of runoff rate, storm duration,
 273 and basin length:

$$Q_p = \frac{(R - I)A}{F_{hs}} \frac{T_r}{T_r + L/U_f}, \quad (6)$$

275 where F_{hs} is a hydrograph shape factor equal to the integral
 276 in equation (5). $F_{hs} = 0.5$ for triangular hydrographs,
 277 whereas F_{hs} goes to 1 for steady state runoff conditions,
 278 indicating a rectangular hydrograph shape. This shape factor
 279 is assumed to be constant during our simulation runs. In
 280 other words, we assume self-similar hydrograph shapes,
 281 although, in fact, the evolving shape of catchments will
 282 continuously change the shape of the hydrograph to some
 283 extent as well. F_{hs} measurements using constant-velocity
 284 rainfall-runoff simulations on a synthetic surface (Figure 3)
 285 show that the value of F_{hs} changes only slightly when storm
 286 duration changes so that we can approximate F_{hs} as
 287 constant (here with the characteristic value of 0.4), without
 288 introducing a considerable amount of bias into the
 289 calculations.

290 [14] According to equation (6), peak discharge depends
 291 on both the basin's area-length ($A-L$) relationship and on the
 292 ratio of storm duration (T_r) to longest travel time within the
 293 basin (L/U_f). The fraction $T_r/(T_r + L/U_f)$ is a nondimensional
 294 number, here termed the storm duration number (SDN). The
 295 storm duration number is unity for steady state conditions
 296 and approaches zero as the storm duration-travel time ratio
 297 decreases. The storm duration number is a suitable variable
 298 to measure the combined effect of storm duration, flow path
 299 length, and routing velocity on runoff conditions and
 300 therefore to enumerate the deviation of the runoff conditions
 301 from the steady state.

302 [15] The link between catchment geometry and hydrology
 303 is reflected in the $A-L$ relationship (numerator and denom-
 304 inator of equation (6)). All else equal, for a given storm
 305 duration in a nonsteady state runoff environment, round
 306 catchments with a high area-length ratio will produce higher
 307 peak discharges than elongated catchments with a low area-
 308 length ratio.

309 3.2. Fluvial and Overland Flow Erosion

310 [16] The erosion model used in this paper is detachment
 311 limited in the sense that incision rate, ϵ , is only a function of
 312 excess shear stress and does not depend on the sediment
 313 content of the runoff. It is assumed that once material is
 314 detached from the surface, it leaves the basin with the flood
 315 wave, and therefore eroded material is immediately re-
 316 moved from the system with no possibility of redeposition.
 317 Shear stress, τ , under steady, uniform flow is modeled as a
 318 power law function of discharge and slope:

$$\tau = Ktq^\alpha S^\beta, \quad (7)$$

320 where K , α , and β are positive constants, q is discharge per
 321 unit contour length or channel width, and S is slope.
 322 Equation (7) assumes either the Manning or Darcy-

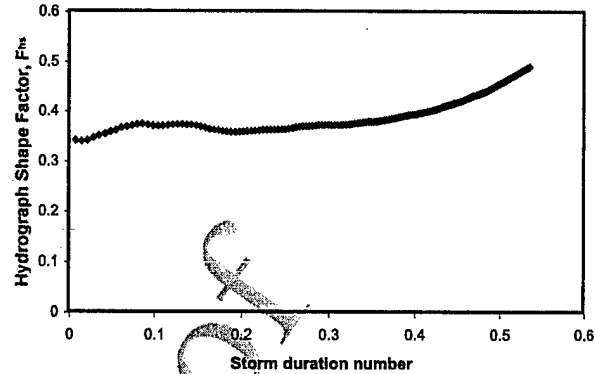


Figure 3. Hydrograph shape factor values (F_{hs}) for different storm durations measured from numerical rainfall-runoff simulations. On a synthetic catchment produced by a landscape evolution model, runoff was generated with a constant-velocity rainfall-runoff simulator, and the catchment was precipitated with rainfall events with increasing length. F_{hs} values of the hydrographs produced at the outlet of the catchment were recorded. As the storm duration number (SDN) representing nondimensional storm duration goes from 0 to 1 (0 and 1 are end cases for infinitely short and long storms), F_{hs} goes to 1 as well, but in the region where SDN is between 0 and 0.5, F_{hs} is relatively stable around 0.4.

Weisbach roughness relation for fully turbulent flow; in the latter case, both α and β are $2/3$ [Howard *et al.*, 1994; Tucker and Slingerland, 1997]. Incision (detachment) rate ϵ is modeled as

$$\epsilon = K_e(\tau - \tau_c)^\gamma, \quad (8)$$

where τ_c is a critical shear stress representing surface resistance to erosion and K_e and γ are positive, empirical constants [Howard and Kerby, 1983], with $\gamma = 3/2$ [Whipple and Tucker, 1999].

[17] Combining equations (5)–(8) and assuming τ_c to be 0, e.g., for fine-grained dispersive soils, we can write the storm-averaged erosion rate as

$$E = \frac{1}{T_h} \int_0^{T_h} K[Q(t)]^m S^n dt = KQ_p^m S^n \int_0^1 Q'(t')^m dt' \\ = \frac{K(R - I)^m A^m S^n F_{he}}{F_{hs}^m} \frac{T_r^m}{(T_r + L/U_f)^m}, \quad (9)$$

where $K = K_e K_\epsilon$, $m = \alpha\gamma$, $n = \beta\gamma$, and F_{he} is a constant (between 0 and 1) equal to the integral of $Q'(t')^m$. Note that there are two end-member cases. For small basins or long-lasting storms, $T_r \gg L/U_f$ and hydrographs tend to be flat ($F_{he} \sim F_{hs} \sim 1$) so that equation (9) reduces to the steady state erosion equation

$$E = K(R - I)^m A^m S^n. \quad (10)$$

[18] For large basins or short storms, $T_r \ll L/U_f$. In order to simplify equation (9), we need to find a relationship

between the contributing area and flow path length. An empirical relationship based on real catchments is provided by Hack's law [Hack, 1957], where $L \sim A^h$ and $h \sim 0.5-0.6$ [e.g., Montgomery and Dietrich, 1992; Rigon et al., 1996]. Using this relationship, equation (9) reduces to

$$E \sim A^{m(1-h)} S^n. \quad (11)$$

[19] This means that the degree of drainage area dependence becomes systematically smaller in larger basins, approaching about half the sensitivity of the smaller basins, because $(1-h) \sim 0.4-0.5$ [Niemann et al., 1997]. Different exponents for the length-area relationship, which are applicable to overland flow on hillslopes with various geometries, also merit consideration. On planar slopes, for example, L is linearly proportional to area ($h = 1$), which reduces equation (11) to $E \sim S^n$. On divergent slopes, where $h > 1$, erosion rate can actually decrease as the contributing area increases downslope. Aspects of these relationships will be explored in section 4.1.3.

3.3. Numerical Implementation

[20] The above erosion equations were used in the Channel Hillslope Landscape Development model (CHILD) [Tucker et al., 2001] to simulate topographies developed under different dominant storm durations. Simulations were carried out on a 80×80 lattice, with a single outlet point (fixed altitude, open to mass flux) in one corner. In the simulations an initial random topography is uplifted with a constant velocity relative to the outlet point. Water entering each node is routed toward the steepest flow direction, and contributing area for each node is computed in each iteration. Given the detachment-limited framework for wash processes, wash load defined in equation (9) is totally removed. To model diffusion, CHILD applies a point-to-point transport of diffusive sediment flux, but in our simulations, diffusion is turned down to zero in order to gain an unbiased picture about the effects of storm duration on the drainage network. Model calculations were run long enough to reach an equilibrium state, in which downwearing at any point of the surface balances tectonic uplift. In section 4, simulation results and corresponding statistics are presented.

4. Effect of Relative Storm Duration on Drainage Basin Morphology

[21] Beside the qualitative, visual characterization of landscapes, morphometric statistics offer a tool for quantitative description. One of the most common morphometric properties is the slope-area diagram [e.g., Montgomery and Dietrich, 1988, 1994; Willgoose et al., 1991a; Tarboton et al., 1992], which plots on a log-log scale the slope versus the contributing area of the points of the surface. In the following, we will use the slope-area diagram to measure the effect of storm duration change on the resulting equilibrium surface. With this diagram, one can visualize both (1) the degree of channel or slope profile concavity and (2) the transition point between diffusion-dominated convex hillslopes and the wash-dominated concave hollows and channels [Tarboton et al., 1992; Montgomery and Foufoula-Georgiou, 1993], although given the lack of diffusion

processes in our model, we do not exploit the second characteristic of the slope-area diagram.

[22] Figure 4 shows simulated equilibrium (erosion = uplift rate) landscapes, and Figure 5 provides the corresponding slope-area diagrams, illustrating the geomorphic effect of storm duration change. Figure 4a represents steady state runoff conditions, while Figures 4b and 4c show nonsteady state conditions caused by limited storm duration.

[23] The two most obvious visual outcomes of decreased storm duration are the reduced channel and slope concavity and the lower valley density. The first reflects the decreased weighting of drainage area. The second arises from reduced efficacy of runoff erosion as peak discharges decline.

4.1. Stream Profile Concavity

[24] Equilibrium profile concavity under nonsteady state runoff conditions is altered by two additional effects which are not present in the steady state framework: by the storm duration-travel time relationship captured in the storm duration number and by the area-length relationship hidden in the peak discharge function. We discuss these two effects in sections 4.1.1 and 4.1.2, respectively.

4.1.1. Effect of Storm Duration Number (SDN):

Downstream Decreasing Concavity

[25] Using the steady state detachment-limited erosion law of equation (10), we can express the equilibrium slope-area relationship as [e.g., Moglen and Bras, 1995; Whipple and Tucker, 1999]

$$S = \left(\frac{U}{K}\right)^{\frac{1}{n}} A^{-\frac{m}{n}} (R - I)^{-\frac{m}{n}}, \quad (12)$$

where $-m/n$ is often referred to as an intrinsic concavity index (θ). Plotting this relationship between S and A on a log-log graph, θ gives the slope of the resulting straight line.

[26] Expressing S from equation (9) gives an equivalent expression for nonsteady state hydrology:

$$S = \left(\frac{U}{KF_{he}}\right)^{\frac{1}{n}} F_{hs}^{\frac{m}{n}} (R - I)^{-\frac{m}{n}} A^{-\frac{m}{n}} \left(\frac{T_r}{T_r + L/U_f}\right)^{-\frac{m}{n}}. \quad (13a)$$

It is also useful to examine a dimensionless form of equation (13a), in which drainage area of subbasins is normalized by maximum basin stream length L_b (a constant) and parameters are grouped in dimensionless quantities:

$$S = \left(\frac{UF_{hs}^m}{K(R - I)^m L_b^{2m} F_{he}}\right)^{\frac{1}{n}} A_*^{-\frac{m}{n}} \left(1 + \frac{L}{U_f T_r}\right)^{\frac{m}{n}}, \quad (13b)$$

where $A_* = A/L_b^2$. The term $L/U_f T_r$ on the right-hand side represents the ratio of local (subbasin) mainstream length to the distance that runoff travels during a rainfall event.

[27] The storm duration effect (expressed by the right-most terms in equations (13a) and (13b)) introduces additional features to the slope-area graph. Because of the asymptotic character of SDN, the effect of flow path length in equation (13) appears gradually as flow path length increases downstream, with the result that the equilibrium slope-area relationship is no longer log-log linear. Instead, the curve will tend to flatten toward higher drainage area

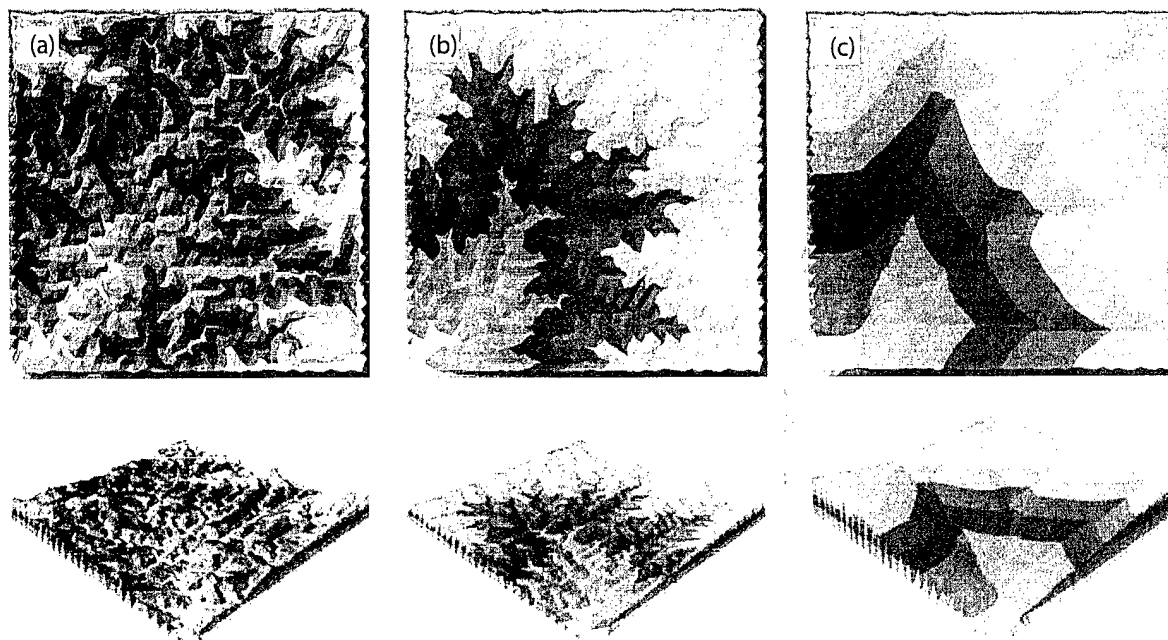


Figure 4. (a) Simulated landscape with steady state runoff conditions. Note the high valley density and the incised concave channels. (b) Landscape simulated under nonsteady state runoff conditions. SDN at the sidelength of the simulation field is 1/3. Note the decreasing valley density and the less concave channel profiles relative to Figure 4a. (c) Landscape simulated under nonsteady state runoff conditions. SDN at the length of the simulation field is 1/26. Note the low valley density and the convex channel profiles.

values. Figure 5a shows simulation outcome where runoff is in steady state, and Figures 5b and 5c present simulation outcomes in which the storm duration numbers at characteristic scale (side length) of the simulation field are 1/3 and 1/26, respectively. The given SDN values were chosen because they represent characteristically different stages of a continuous scale. The initial condition for all of the three cases was a randomly perturbed flat topography; diffusion in all cases was set to zero in order to get a clearer picture about the effects of nonsteady state runoff on equilibrium landforms.

[28] In Figures 5b and 5c the nonsteady state slope-area curves flatten toward positive values, meaning that channel gradients are steeper than for the steady state case. In Figure 5b the hydrograph duration at a scale equal to the width of the model domain is about three times the storm duration (i.e., the storm duration number equals 1/3). As a result, peak discharge in the upper parts of the network scales roughly linearly with drainage area, while in the largest branches of the network, Q_p grows less than linearly with drainage area. This produces a small inflection in the slope-area graph, reflecting decreased concavity in the larger valley profiles. At a storm duration number 1/26 the channel profile in certain links also turns slightly convex, as shown by individual dot lines on the graph. These represent channel links and indicate downstream-increasing slope values. SDN = 1/26 results also in a strong disintegration of the slope-area plot. This indicates the importance of the individual A - L and T_r - T_i relationships

for the different tributaries and hence the importance of catchment shape in governing drainage basin evolution. In sections 4.1.2 and 4.1.3 the role of catchment shape is analyzed in more detail.

4.1.2. Effect of the A-L Relationship: Convexity

[29] We devote special attention to the issue of profile convexity. This phenomenon is rather surprising for a landscape shaped by detachment-limited wash erosion without diffusion processes, and its occurrence in the model reflects interaction between peak discharge distribution and flow path geometry. The physical explanation for slope and channel convexities in low-SDN environments is that while increasing flow path length increases the duration of the hydrograph, the peak discharge can not grow proportionally with area. In certain cases, peak discharge is predicted to decrease with increasing flow path length. In order to maintain equilibrium, the slope must therefore increase downstream to maintain a uniform erosion rate. Obviously, storm duration can alter a number of further elements of runoff erosion, such as channel cross section shape, bed load grain size distribution, and associated critical shear stress. Although we acknowledge the possible counteracting feedbacks of these factors, our analysis remains focused for the sake of clarity on the interpretation of the effect of the limited storm duration.

[30] We explore the conditions under which Q_p decreases downstream. Differentiating the peak discharge function (6) with respect to L and substituting A with $K_p L^x$ by assuming a power law relationship between the contributing area and

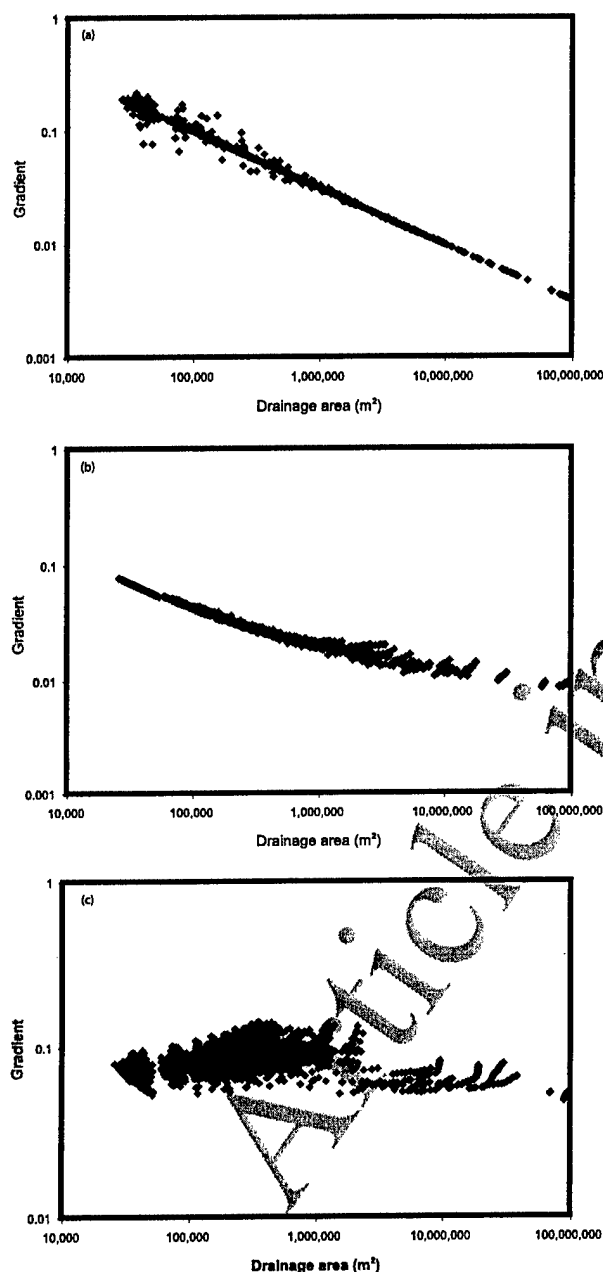


Figure 5. (a) Slope-area diagram for Figure 4a. The points of the graph organize themselves into a straight line, the slope of which characterizes the concavity of the surface, corresponding to $-m/n$ of the erosion law. (b) Slope-area diagram for Figure 4b. The points are organized into a loose line, the slope of which decreases for higher contributing areas. Note that the slope values are generally higher than in Figure 5a, but the slope range is smaller. (c) Slope-area diagram for Figure 4c. The points of the graph are disorganized, and slope-area relationships of individual valleys depend more on the local length-area and storm duration-travel time relationships than on the contributing area. Note also the small range of slope values as a result, with area only slightly increasing discharge.

flow path length, where x is the inverse for Hack's h [Hack, 1957] and K_h is the proportionality coefficient, 513 514

$$\frac{dQ_p}{dL} = (R - I)K_h F_{hs}^{-1} T_r U_f L^{x-1} \frac{x(T_r U_f + L) - L}{(T_r U_f + L)^2}. \quad (14)$$

This equation implies that reduction in storm duration alone 516 is not sufficient to decrease peak discharge with increasing 517 flow path length. Rather, two conditions must apply: (1) the 518 area-length exponent x needs to be less than 1 and (2) $T_r U_f$ 519 has to be small compared to L in order to obtain downstream 520 decreasing peak discharge values. 521

[31] We now explore possible conditions under which x 522 (which for most river basins lies in the range 1.7–2.0 [e.g., 523 Rigon *et al.*, 1996]) is less than unity. The condition $x < 524$ 1 corresponds to a case in which mainstream length 525 increases faster than drainage area. This is, of course, what 526 normally occurs between tributaries within a drainage basin. 527 Our model implies therefore that some upward convexity is 528 plausible between tributaries. 529

4.13 Flow Path Effects on Hillslopes and Low-Order Basins 530 531

[32] The basin-averaged length-area relationship is quite 532 robust for medium to large (third-order and higher) drainage 533 basins, with x departing relatively little from the geometric 534 value of 2. This is consistent with the hypothesis that 535 drainage basins are self-similar over a wide range of scales 536 [Rodríguez-Iturbe and Rinaldo, 1997]. However, observa- 537 tions of flow path structure on gullied hillslopes and small, 538 low-order basins suggest that these often depart markedly 539 from the geometry of larger basins. In this section we briefly 540 consider potential feedbacks between morphology and flow 541 path geometry (in particular, the area-length relation) at the 542 hillslope to first-order basin scale. Figure 6 illustrates how 543 simple and plausible flow path structure geometries deter- 544 mine the at-a-point area-length relationship. Figures 7–9 545 demonstrate manifestations of different flow path geometries 546 in nature. We do not intend to interpret these differences; they 547 are merely illustrations for possible flow path geometries (see 548 figure captions for explanation). Given the universality of the 549 stream-network hierarchy and of the associated hillslope 550 features such as hollows, spurs, or planar slopes, the flow 551 path structure geometries of Figure 6 are common to a wide 552 variety of climatic and lithological environments. According 553 to Figure 6, divergent hillslopes, and channels in catchment 554 tips, have at-a-point area-length exponents (x in equation 555 (14)) < 1 . On these locations, peak discharge can, according to 556 equation (14), decrease downslope if storm duration and 557 runoff velocity are small enough. This will tend to produce 558 convex slope or channel profiles. This effect corresponds 559 with the simulation outcome in Figure 4c, in which hillslopes 560 with divergent flow path structure and channels in catchment 561 tips show convex profiles as a result of the low storm duration 562 number. The latter convexity can also be traced on the slope- 563 area graph (Figure 5c), where individual dot lines at higher 564 drainage area point to the convexity of individual channel 565 links. At lower drainage area the dot cloud hides the individ- 566 ual flow lines. 567

[33] In the simulations this convexity has been further 568 accentuated by the boundary conditions of the model. The 569 square shape of the simulation field and the one-corner 570 outflow structure forces to some extent the area-length 571

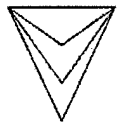
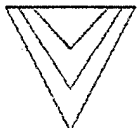

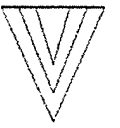
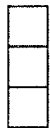



			
a) $x=1$. The topography is concave in the planform, flow path structure is passively convergent (no downstream change in width); characteristic of first order channels.	b) $1 < x < 2$. Actively convergent flow path structure (width changes downstream as a result of convergence); appears in hollows above channel heads.	c) $x=2$. Both width and length change with the same rate, therefore nested catchments are self-similar. Active convergence; appears in hollows.	d) $x > 2$. Width changes faster than length. Active convergence; appears in hollows.
			
e) $x=1$. Refers to parallel flow path structure; appears on hillslopes and plains with zero plan curvature.	f) $x > 1$. An extended version of b)-d). Characteristic geometry of hollows.	g) $x < 1$. Flow path structure is divergent. Appears on divergent hillslopes and on triangular slope facets between neighbouring catchments.	h) $x < 1$. Width decreases downstream shifting x below unity. Characteristic geometry of first order drainage basins.

Figure 6. At-a-point area-length relationships for basic geometries of nested contributing areas. The inverse of Hack's h , x , is set by the downstream rate of change of catchment width and shape. Figures 6g and 6h show geometrical patterns, with x below unity. In landscapes they correspond to divergent hillslopes (or triangular slope facets) and lower reaches of first-order channels with converging divides, respectively. (a) $x=1$. The topography is concave in the planform, and flow path structure is passively convergent (no downstream change in width); characteristic of first-order channels. (b) $1 < x < 2$. This shows an actively convergent flow path structure (width changes downstream as a result of convergence); appears in hollows above channel heads. (c) $x=2$. Both width and length change with the same rate, and therefore nested catchments are self-similar. This shows active convergence; appears in hollows. (d) $x > 2$. Width changes faster than length. This shows active convergence; appears in hollows. (e) $x=1$. Refers to parallel flow path structure; appears on hillslopes and plains with zero plan curvature. (f) $x > 1$. An extended version of Figures 6b–6d; characteristic geometry of hollows. (g) $x < 1$. Flow path structure is divergent; appears on divergent hillslopes and on triangular slope facets between neighboring catchments. (h) $x < 1$. Width decreases downstream, shifting x below unity; characteristic geometry of first-order drainage basins.

relationship. Close to the outlet, length will tend to grow faster than area ($x < 1$), and this effect increases the relative length of the convex channel reaches.

4.2. Storm Duration and Valley Density

[34] Valley density is a measure of the degree of dissection of the landscape. For landscapes in which valley

density is controlled by a competition between diffusion-like soil creep and channel incision, it can be approximated by a critical contributing area that separates the diffusion-dominated convex surface elements from concave surface elements dominated by wash processes [Tarboton *et al.*, 1992; Moglen *et al.*, 1998; Tucker and Bras, 1998]. On surface points that have this contributing area, half of the



Figure 7. Small-scale first-order catchments in an arid climate (Lanzarote, Canary Islands). Note the self-similar hollow shape illustrating Figure 6c and the characteristic hollow-triangular slope facet geometry. There are many remarkable planar slope segments in this landscape, showing the occurrence of parallel flow path structure (Figure 6e) in nature.



Figure 9. First-order catchments draining into a meandering main valley in a humid (subtropical) climate (La Palma, Canary Islands). The broad and extremely planconcave hollows show the geometry of Figure 6f. Note the lack of triangular slope facets.

erosion is attributed to diffusion-related processes and half to wash-related processes. Expressing equilibrium slope for wash processes of equations (13a) and (13b) and equilibrium slope for diffusion processes [Tucker and Bras, 1998] and solving them for the critical contributing area results in a value that is an inverse approximation for the dissection of the landscape:

$$A_{cr} = U^{\frac{1-\alpha}{\alpha}} (KF_{hc})^{-\frac{1}{\alpha}} K_d^{\frac{\alpha}{\alpha}} F_{hs} (R - I)^{-1} \left(\frac{T_r}{T_r + (L/U_f)} \right)^{-1} \quad (15)$$

If the contributing area of a given point is bigger than A_{cr} , the point is expected to be in a valley with concave profile curvature, while if the area is less than A_{cr} , the point lies on a convex hillslope. The effect of storm duration on valley

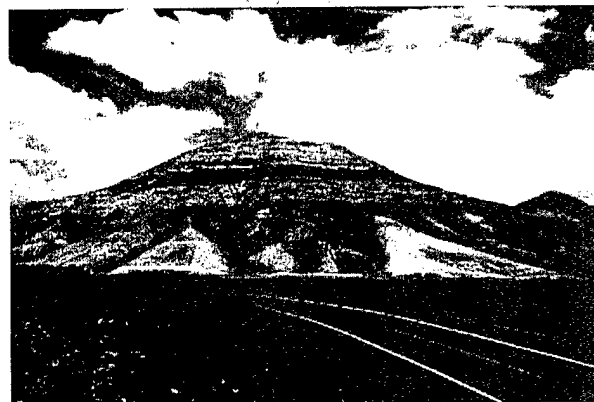


Figure 8. Large-scale first-order catchments in an arid climate (Lanzarote, Canary Islands) illustrating the geometry of Figures 6b and 6h. Note the somewhat planconvex triangular slope facets between the catchments, demonstrating the divergent flow path structure on Figure 6g.

density can be captured by equation (15). Decreasing storm duration number increases the critical contributing area and hence decreases valley density.

[35] In equation (15), A_{cr} is inversely proportional to L . When the area-length proportionality coefficient (x in equation (14)) is bigger than 1, the contributing area will exceed A_{cr} within a finite distance from the crest. For $x < 1$ and SDN sufficiently small the contributing area never exceeds A_{cr} . In other words, downstream decreasing peak discharge values (because of $x < 1$) will not be able to create enough fluvial erosion to dominate diffusion, and no valleys will be formed. To maintain equilibrium, slope-dependent creep and mass wasting processes will perform the bulk of erosion. As seen in section 4.1.3, divergent hillslopes and channels in catchment tips are the two geomorphological locations in which x is smaller than 1. Therefore in an environment dominated by short storms, long divergent hillslopes will tend to remain diffusion dominated (as concluded by Dunne [1991] for similar reasons), and sufficiently long catchments may "lose" their incised channels in the catchment tip.

5. Dynamic Equilibrium and Self-Stabilization in the Relative Storm Duration System

5.1. Slope Adjustment to Changes in Prevailing Conditions

[36] One of the key concepts in geomorphology is the notion of dynamic equilibrium [Hack, 1960]. In this section we examine how limited storm duration alters the equilibrium properties of drainage networks and slopes.

[37] Within the realm of the steady state runoff erosion law the existence of a theoretical dynamic equilibrium with respect to a uniform rate of uplift is always guaranteed because variables on the right-hand side of equation (12) are independent of the slope. On the other hand, the right-hand side of equation (13) for the nonsteady state runoff erosion law contains two variables (L , U_f) which are, in the real world, dependent on the slope. Under certain conditions this can provoke a runaway feedback in which slopes infinitely

636 steepen until other processes (e.g., mass wasting) become
637 dominant.

638 [38] To be more explicit about the relationship between
639 slope, flow path length, and runoff velocity, we can extend
640 the model by redefining two quantities:

$$L_s = L / \cos a, \quad (16)$$

642 where L_s is the "real" flow path length measured parallel to
643 the surface (as opposed to projected length, L), a is slope
644 angle, and

$$U_{fm} = \frac{D^{2/3} (\sin a)^{1/2}}{n} = \frac{Q_p^{2/5} (\sin a)^{3/10}}{n^{3/5}}, \quad (17)$$

645 where U_{fm} is flow velocity calculated by the Manning
647 equation, D is flow depth approximated by the peak
648 discharge as $D = Q_p / U_{fm}$, where Q_p is discharge per unit
649 width, and n is Manning's coefficient. Travel time can then
650 be calculated as

$$T_l = \frac{L_s}{U_{fm}} = \frac{Ln^{3/5}}{Q_p^{2/5} (\sin a)^{3/10} \cos a}. \quad (18)$$

652 [39] A number of external effects can shift the system
653 toward an increase of the slope values. This includes
654 accelerated base-level lowering, a reduction in precipitation,
655 or the appearance of bedrock layers with a high resistance to
656 erosion. A positive change in slope according to
657 equation (18) increases the flow path distance and flow
658 velocity at the same time. As long as $dU_{fm}/da > dL_s/da$,
659 travel time decreases for a given increase in slope, and
660 increased erosion rate can counterbalance the effect that is
661 responsible for the higher relief of the surface. When $dU_{fm}/$
662 $da < dL_s/da$, travel time increases for a given increase in
663 slope, and therefore erosion rate decreases. This leads to
664 further relief intensification and erosion rate reduction, until
665 the slope becomes steep enough that mass movement
666 processes become dominant. The trigonometric relationship
667 gives $a \sim 35^\circ$ to be the critical slope angle with the shortest
668 travel time, separating the stable and the nonstable zone
669 (Figure 10). In the regime above 35° an eventual slope
670 increase will not be compensated for by the intensification
671 of wash processes. In this regime, short storm duration–
672 dominated landscapes are unstable; this process alone is not
673 enough to maintain dynamic equilibrium. This effect can, in
674 short storm–dominated climatic environments, contribute to
675 the characteristic separation between fluvial and debris
676 flow–dominated channels.

677 [40] In practice, 35° slopes will almost always be dom-
678 inated by debris flows or other forms of mass wasting. We
679 therefore conclude that although a positive slope-erosion
680 feedback is possible in principle, it would only occur on
681 gradients that are too steep for normal fluvial processes to
682 operate.

683 5.2. Hydrograph Adjustment to Changes in the 684 Dominant Storm Duration

685 [41] It is possible to reveal a self-regulatory relationship
686 between hydrograph shape and long-term erosion dynamics
687 if we consider flow path (drainage network) reorganization

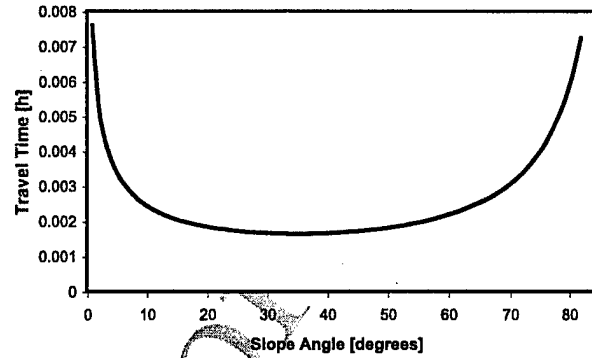


Figure 10. Slope-angle–travel time relationship in the limited storm duration environment. The critical slope value at about 35° separates stable slopes with lower values and the unstable steeper slopes (equation (18)). See text for explanation.

during landscape adaptation to new external conditions. 688 This section focuses on a potential stabilizing effect that 689 exists between the planform change of a catchment and the 690 change in the dominant storm duration. 691

[42] In the model runs, as the dominant storm duration 692 decreases, the valley network reorganizes itself toward a 693 lower valley density (Figures 4a–4c). Flow path reorgani- 694 zation also widens the basins relative to their length, 695 increasing the average area-length proportion. Peak dis- 696 charge values decrease because of decreased storm duration 697 numbers, but this decrease is counterbalanced, to some 698 extent, by the increase in peak discharge related to increased 699 area-length proportion: wider basins generate a higher peak 700 discharge at a given basin size. 701

[43] To illustrate the above feedback between morphology 702 and hydrograph shape, we generated synthetic hydrographs 703 with a rainfall-runoff simulator that uses a constant routing 704 velocity. Synthetic hydrographs were generated from two 705 simulated surfaces: one created by steady state runoff and 706 one simulated using a finite storm duration (SDN at window 707 length 1/21). Figure 11 shows unit hydrographs [Gupta et 708 al., 1986; Kirkby, 1976], and Figure 12 shows hydrographs 709 with a duration of 40 units corresponding to SDN = 1/25 at 710 the outlet. Both figures show similar tendencies. Hydro- 711 graphs generated on the surface created by nonsteady state 712 runoff (thin lines in both figures) have shorter duration, 713 show higher peak discharge values, and are slightly thinner 714 in their shape (lower F_{hs}) than hydrographs generated on the 715 surface formed by steady state runoff (bold lines in both 716 graphs). The explanation for this shift in hydrograph shape 717 lies in the morphologic differences between the two equi- 718 librium surfaces: maximal flow path length is smaller on the 719 nonsteady state surface, which leads to decreased hydro- 720 graph duration and increased peak discharge. The short- 721 storm surface has a lower degree of dissection, which 722 affects the overall length-area relationships within the basin, 723 with broader valleys having higher contributing area values 724 for a given flow path length, and this enhances runoff 725 concentration and peak discharge. Thus it appears that the 726 short-storm surface has generated a flow path structure that 727 yields more focused runoff concentration relative to the 728 perpetual storm surface. 729

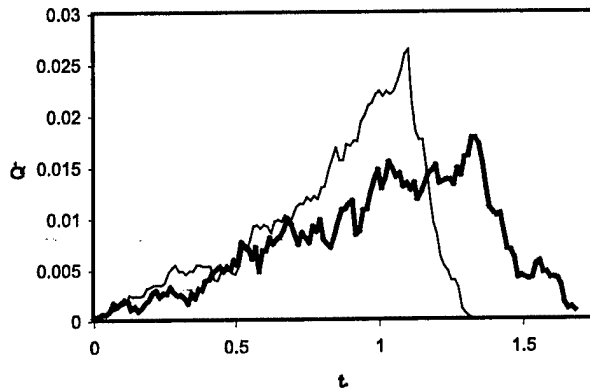


Figure 11. Unit hydrographs for two simulated surfaces. The dimensionless time $t^* = t^* U_f / A_{\max}^{0.5}$ gives the proportion of time it takes for flow to travel across one side of the simulation domain. The dimensionless discharge $Q^* = Q / (A_{\max}^* R)$ gives the proportion of total incoming rainfall over the whole domain (A_{\max}). The surface generated via nonsteady state runoff simulation (thin line) shows a higher peak discharge for the same precipitation input than the steady state runoff surface (bold line). See text for explanation.

[44] Putting these observations into the framework of landscape self-organization, we can identify a negative feedback between externally (e.g., climate change) determined discharge changes and internal (morphology determined) discharge generation. For example, as the climate shifts toward shorter storms, peak discharge decreases, but this tendency is, to some extent and with a considerable time gap, counterbalanced by the adjustment of the relief because the new equilibrium relief enhances peak discharge values again. The system tries to keep equilibrium via adjustment in network shape. On the other hand, if storms get longer or travel time decreases (e.g., as a consequence of reduced vegetation and increased routing velocity), peak discharges tend to get higher. In this case the response of the relief is to increase valley density and thereby reduce, to some extent, peak discharge values. Both field evidence and simulation experiments show that drainage density often increases in a highly sudden and rapid manner, on a much faster scale than it is decreasing [Tucker and Slingerland, 1997; Montgomery and Dietrich, 1992, 1994; Rinaldo et al., 1995a].

[45] Valley density reduction as an adjustment to decreased storm duration is a finite process. Once the storm duration number drops below a critical value, runoff will not be sufficient to maintain a valley network, valleys will tend to become infilled and unchannelled, and diffusion-denuded hillslopes will dominate the landscape. At this point the catchment shape–peak discharge compensatory relationship breaks down as well.

6. Conclusions

[46] In this paper we have presented a model that captures an important hydrogeomorphic property of catchments, in which dominant storm duration is short relative to the longest travel time within the catchment. Figure 13 demon-

strates that the “short storm phenomenon” is sufficient to explain the observed nonlinear Q_p - A relation. However, several other effects, such as limited storm cell size, can also presumably result in similar nonlinearity between contributing area and peak discharge values. Further research is needed to derive a discharge approximation for environments with limited storm size relative to catchment size and to clarify characteristic mechanisms manifested in that environment.

[47] It has been shown that a change in the dominant storm duration can, if prolonged, alter the valley density and the profile curvature of the landscape. This observation might be important when interpreting morphometric landscape statistics of forecasting landscape adaptation to new external conditions. It is important to remember, however, that the present results are based on an analysis within the detachment-limited framework, assuming that soil particles once detached remain in the fluid due to the high energy of runoff. Profile convexity within this framework has been shown to be the outcome of the manifestation of nonsteady state hydrology on the flow path geometry of the terrain. We expect that transport-limited models [e.g., Willgoose et al., 1991a, 1991b, 1991c] would display a similar geometric sensitivity, though transport-limited models can produce convex equilibrium profiles already under steady state runoff conditions if the runoff exponent (m in equation (9)) is below unity. This convexity, however, here termed the runoff exponent induced convexity, differs markedly from the flow path geometry–induced convexity described in this paper. The runoff exponent–induced convexity stretches over the entire wash processes–dominated profile length, while the flow path geometry–induced convexity appears only in positions where the area-length exponent x is below unity and where $T_r^* U_f < L$ (according to equation (14)). Slope profile convexities described by Dunne [1991] in Kenya can be interpreted in either way, but if the convex

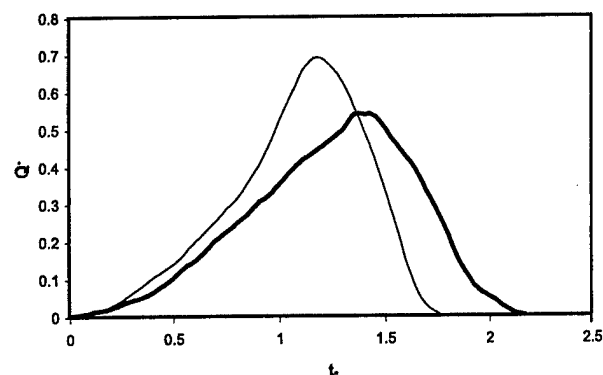


Figure 12. Forty unit duration hydrographs for two simulated surfaces (the same surfaces as in Figure 11). The dimensionless time $t^* = t^* U_f / A_{\max}^{0.5}$ gives the proportion of time it takes for flow to travel across one side of the simulation domain. The dimensionless discharge $Q^* = Q / (A_{\max}^* R)$ gives the proportion of total incoming rainfall over the whole domain (A_{\max}). Again, the nonsteady state runoff surface (thin line) shows a higher peak discharge for the same precipitation input than the steady state runoff surface (bold line).

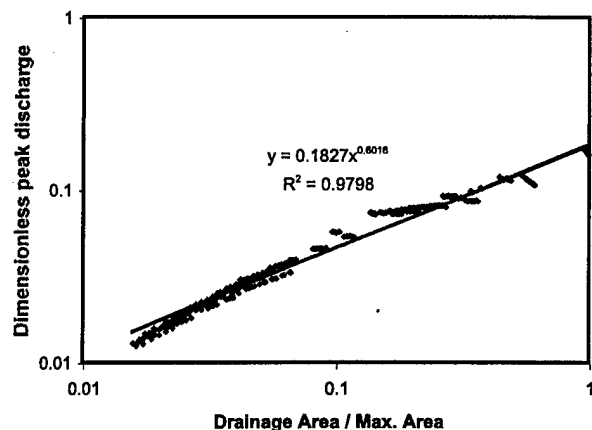


Figure 13. Simulated dimensionless peak discharge–dimensionless contributing area relationship (using equation (6)) for channel points of a simulated surface. SDN is 0.4 at window length.

portions of the slopes follow morphological characteristics of the flow path geometry–induced convexity, then the interpretation has to include the effect of flow path structure geometry on governing nonsteady state runoff production. [48] Finally, the model predicts that a negative feedback exists between storm duration, basin shape, and peak discharge. This result suggests that over the long term, a basin's shape and its hydrologic response coevolve to sculpt river basin topography and network geometry.

[49] **Acknowledgments.** This research has been supported by the Research Office of the U.S. Army, grant DAAD19-01-1-0615. We are also grateful for two anonymous reviewers for their useful comments.

References

- Ahnert, F. (1976), Brief description of a comprehensive three-dimensional process-response model of landform development, *Z. Geomorphol.*, 25, 29–49.
- Ahnert, F. (1987), Process-response models of denudation at different spatial scales, *Catena*, 10, 31–50.
- Allen, P. A., and A. L. Densmore (2000), Sediment flux from an uplifting fault block, in *Processes and Controls in the Stratigraphic Development of Extensional Basins*, pp. 367–380, Blackwell Sci., Malden, Mass.
- Bras, R. L. (1990), *Hydrology: An Introduction to Hydrologic Science*, Addison-Wesley-Longman, Reading, Mass.
- Coulthard, T. J., M. J. Kirkby, and M. G. Macklin (2000), Modelling morphic response to environmental change in an upland catchment, in *Geocomputation in Hydrology and Geomorphology*, pp. 2031–2045, John Wiley, Hoboken, N. J.
- Dick, G. S., R. S. Anderson, and D. E. Sampson (1997), Controls on flash flood magnitude and hydrograph shape, upper Blue Hills badlands, Utah, *Geology*, 25(1), 45–48.
- Dunne, T. (1991), Stochastic aspects of the relations between climates, hydrology and landform evolution, *Trans. Jpn. Geomorphol. Union*, 12(1), 1–24.
- Graf, W. L. (1988), *Fluvial Processes in Dryland Rivers*, 346 pp., Blackburn Press, Caldwell, N. J.
- Gupta, V. K., E. Waymire, and I. Rodriguez-Iturbe (1986), On scales, gravity and network structure in basin runoff, in *Scale Problems in Hydrology*, edited by V. K. Gupta, I. Rodriguez-Iturbe, and E. F. Wood, pp. 159–184, D. Reidel, Norwell, Mass.
- Hack, J. T. (1957), Studies of longitudinal stream profiles in Virginia and Maryland, *U.S. Geol. Surv. Prof. Pap.*, 294-B, 97 pp.
- Hack, J. T. (1960), Interpretation of erosional topography in humid temperate regions, *Am. J. Sci.*, 258A, 80–97.
- Howard, A. D. (1994a), Badlands, in *Geomorphology of Desert Environments*, edited by A. D. Abrahams and A. J. Parsons, pp. 213–242, Chapman and Hall, New York.
- Howard, A. D. (1994b), A detachment-limited model of drainage basin evolution, *Water Resour. Res.*, 30, 2261–2285.
- Howard, A. D. (1997), Badland morphology and evolution: Interpretation using a simulation model, *Earth Surf. Processes Landforms*, 22, 211–227.
- Howard, A. D., and G. Kerby (1983), Channel changes in badlands, *Geol. Soc. Am. Bull.*, 94(6), 739–752.
- Howard, A. D., W. E. Dietrich, and M. A. Seidl (1994), Modeling fluvial erosion on regional to continental scales, *J. Geophys. Res.*, 99, 13,971–13,986.
- Kirkby, M. J. (1971), Hillslope process-response models based on the continuity equation, in *Slopes: Form and Process, Spec. Publ. 3*, pp. 15–30, Inst. of Br. Geogr., London.
- Kirkby, M. J. (1976), Tests of the random model and its applications to basin hydrology, *Earth Surf. Processes Landforms*, 1, 197–212.
- Kirkby, M. J. (1986), A two-dimensional simulation model for slope and stream evolution, in *Hillslope Processes*, edited by A. D. Abrahams, pp. 203–222, Allen and Unwin, Concord, Mass.
- Kirkby, M. J. (1993), Long-term interactions between networks and hillslopes, in *Channel Network Hydrology*, edited by K. Beven and M. J. Kirkby, pp. 255–293, John Wiley, Hoboken, N. J.
- Kirkby, M. J. (1994), Thresholds and instability in stream head hollows: A model of magnitude and frequency for wash processes, in *Process Models and Theoretical Geomorphology*, edited by M. J. Kirkby, pp. 295–314, John Wiley, Hoboken, N. J.
- Kooi, H., and C. Beaumont (1996), Large-scale geomorphology: Classical concepts reconciled and integrated with contemporary ideas via a surface processes model, *J. Geophys. Res.*, 101, 3361–3386.
- Leopold, L. B., and T. Maddock (1953), The hydraulic geometry of stream channels and some physiographic implications, *U.S. Geol. Surv. Prof. Pap.*, 252.
- Leopold, L. B., and J. P. Miller (1956), Ephemeral streams: Hydraulic factors and their relation to the drainage net, *U.S. Geol. Surv. Prof. Pap.*, 0282-A.
- Moglen, G. E., and R. L. Bras (1995), The effect of spatial heterogeneities on geomorphic expression in a model of basin evolution, *Water Resour. Res.*, 31, 2613–2623.
- Moglen, G. E., E. A. B. Eltahir, and R. L. Bras (1998), On the sensitivity of drainage density to climate change, *Water Resour. Res.*, 34, 855–862.
- Montgomery, D. R., and W. E. Dietrich (1988), Where do channels begin?, *Nature*, 336, 232–234.
- Montgomery, D. R., and W. E. Dietrich (1992), Channel initiation and the problem of landscape scale, *Science*, 255, 826–830.
- Montgomery, D. R., and W. E. Dietrich (1994), Landscape dissection and drainage area-slope thresholds, in *Process Models and Theoretical Geomorphology*, edited by M. J. Kirkby, pp. 221–246, John Wiley, Hoboken, N. J.
- Montgomery, D. R., and E. Foufoula-Georgiou (1993), Channel network source representation using digital elevation models, *Water Resour. Res.*, 29, 3925–3934.
- Niemann, J. D., R. L. Bras, and D. Veneziano (1997), Channel network growth and river basin morphology, *Hydrol. Water Resour. Syst. Tech. Rep. 343*, Ralph M. Parsons Lab. Mass. Inst. of Technol., Cambridge.
- Rigon, R., I. Rodriguez-Iturbe, A. Maritan, A. Giacometti, D. G. Tarboton, and A. Rinaldo (1996), On Hack's law, *Water Resour. Res.*, 32, 3367–3374.
- Rinaldo, A., I. Rodriguez-Iturbe, R. Rigon, E. Ijjasz-Vasquez, and R. L. Bras (1993), Self-organized fractal river networks, *Phys. Rev. Lett.*, 70, 822–826.
- Rinaldo, A., W. E. Dietrich, R. Rigon, G. K. Vogel, and I. Rodriguez-Iturbe (1995a), Geomorphological signatures of varying climate, *Nature*, 374, 632–635.
- Rinaldo, A., G. K. Vogel, R. Rigon, and I. Rodriguez-Iturbe (1995b), Can one gauge the shape of a basin?, *Water Resour. Res.*, 31, 1119–1127.
- Rodriguez-Iturbe, I., and A. Rinaldo (1997), *Fractal River Basins: Chance and Self-Organisation*, 564 pp., Cambridge Univ. Press, New York.
- Rodriguez-Iturbe, I., and J. B. Valdes (1979), The geomorphologic structure of hydrologic response, *Water Resour. Res.*, 15, 1409–1420.
- Rodriguez-Iturbe, I., S. M. Gonzalez, and R. L. Bras (1982), A geomorphoclimatic theory of the instantaneous unit hydrograph, *Water Resour. Res.*, 18, 877–886.
- Slingerland, R., K. Furlong, and J. W. Harbaugh (1994), *Simulating Clastic Sedimentary Basins*, 220 pp., Prentice-Hall, Old Tappan, N. J.
- Strahler, A. N. (1964), Quantitative geomorphology of drainage basins and channel networks, in *Handbook of Applied Hydrology*, edited by V. T. Chow, pp. 4–39, McGraw-Hill, New York.
- Tarboton, D. G., and R. L. Bras (1992), A physical basis for drainage density, *Geomorphology*, 5, 59–76.

- 927 Tucker, G. E., and R. L. Bras (1998), Hillslope processes, drainage density,
928 and landscape morphology, *Water Resour. Res.*, 34, 2751–2764. 947
- 929 Tucker, G. E., and R. L. Bras (2000), A stochastic approach to modeling the
930 role of rainfall variability in drainage basin evolution, *Water Resour. Res.*,
931 36, 1953–1964. 948
- 932 Tucker, G. E., and R. L. Slingerland (1997), Drainage basin responses to
933 climate change, *Water Resour. Res.*, 33, 2031–2047. 949
- 934 Tucker, G. E., S. T. Lancaster, N. M. Gasparini, R. L. Bras, and S. M.
935 Rybarczyk (2001), An object-oriented framework for hydrologic and
936 geomorphic modeling using triangulated irregular networks, *Comput.*
937 *Geosci.*, 27(8), 959–973. 950
- 938 Veneziano, D., G. E. Moglen, P. Furcolo, and V. Iacobellis (2000), Stochas-
939 tic model of the width function, *Water Resour. Res.*, 36, 1143–1157. 951
- 940 Whipple, K. X., and G. E. Tucker (1999), Dynamics of the stream-power
941 river incision model: Implications for height limits of mountain ranges,
942 landscape response timescales, and research needs, *J. Geophys. Res.*, 104,
943 17,661–17,674. 952
- 944 Willgoose, G. R. (1989), A physically based channel network and catch-
945 ment evolution model, Ph.D. thesis, Ralph M. Parsons Lab. Dep. of Civil
946 Eng., Mass. Inst. of Technol., Cambridge. 953
- Willgoose, G. R., R. L. Bras, and I. Rodriguez-Iturbe (1991a), Results from
a new model of river basin evolution, *Earth Surf. Processes Landforms*,
16, 237–254. 954
- Willgoose, G. R., R. L. Bras, and I. Rodriguez-Iturbe (1991b), The relation-
ship between catchment and hillslope properties: Implications of a catch-
ment evolution model, *Geomorphology*, 5(1/2), 21–38. 955
- Willgoose, G. R., R. L. Bras, and I. Rodriguez-Iturbe (1991c), A coupled
network growth and hillslope evolution model: 1. Theory, *Water Resour.*
Res., 27, 1671–1684. 956
- Wolman, M. G., and J. P. Miller (1960), Magnitude and frequency of forces
in geomorphic processes, *J. Geol.*, 68(1), 54–74. 957
- P. B. Solyom and G. E. Tucker, School of Geography and the
Environment, Oxford University, Mansfield Road, Oxford OX1 3TB,
UK. (peter.solyom@geog.ox.ac.uk; greg.tucker@geog.ox.ac.uk) 959
960
961

Appendix D

Tucker, G.E. (2004) Drainage basin sensitivity to tectonic and climatic forcing: implications of a stochastic model for the role of entrainment and erosion thresholds. *Earth Surface Processes and Landforms*, 29, 185-205.

DRAINAGE BASIN SENSITIVITY TO TECTONIC AND CLIMATIC FORCING: IMPLICATIONS OF A STOCHASTIC MODEL FOR THE ROLE OF ENTRAINMENT AND EROSION THRESHOLDS

GREGORY E. TUCKER*

School of Geography and the Environment, University of Oxford, Oxford, UK

Received 5 September 2002; Revised 27 March 2003; Accepted 7 April 2003

ABSTRACT

Long-term average rates of channel erosion and sediment transport depend on the frequency–magnitude characteristics of flood flows that exceed an erosion threshold. Using a Poisson model for rainfall and runoff, analytical solutions are developed for average rates of stream incision and sediment transport in the presence of such a threshold. Solutions are derived and numerically tested for three erosion/transport formulas: the Howard–Kerby shear-stress incision model, the Bridge–Dominic sediment transport model, and a generic shear-stress sediment transport model. Results imply that non-linearity resulting from threshold effects can have a first-order impact on topography and patterns of dynamic response to tectonic and climate forcing. This non-linearity becomes significant when fewer than about half of flood events are capable of detaching rock or sediment. Predicted morphology and uplift-gradient scaling is more closely consistent with observations and laboratory experiments than conventional slope-linear or shear-linear erosion laws. These results imply that particle detachment thresholds are not details that can be conveniently ignored in long-term landscape evolution models. Copyright © 2004 John Wiley & Sons, Ltd.

KEY WORDS: landscape evolution; model; threshold; stochastic; rainfall

INTRODUCTION

One of the challenges in modelling long-term landscape evolution lies in correctly capturing the stochastic nature of geomorphic processes (e.g. Willgoose *et al.*, 1991; Kirkby, 1994; Densmore *et al.*, 1998; Benda and Dunne, 1997a,b; Tucker and Bras, 2000; Molnar, 2001). Natural variability in the occurrence of floods, landslides, and other forms of sediment transport must be considered as an integral part of the physics behind any ‘geomorphic time’ transport law, and likewise must be considered in evaluating present-day geomorphic systems such as gravel-bed rivers (e.g. Benda and Dunne, 1997b), and in making predictions about future impacts. Indeed, only by quantifying the stochastic nature of sediment transport can we hope to extrapolate the physics of individual processes over time scales relevant to most geomorphic systems.

Some efforts have been made to incorporate stochastic flow variability into models of overland flow erosion (e.g. Kirkby, 1994), bedload transport (e.g. Benda and Dunne, 1997b; Molnar, 2001; Fuller *et al.*, 2003), and long-term drainage basin evolution (Willgoose *et al.*, 1991; Tucker and Bras, 2000). In the latter case, analytical solutions for long-term fluvial transport and/or incision rate were obtained by integrating an instantaneous transport (incision) law over a spectrum of flood (Willgoose *et al.*, 1991) or storm events (Tucker and Bras, 2000). A significant limitation of both models, however, was the neglect of thresholds for soil or rock detachment and sediment entrainment.

Thresholds for erosion are often neglected in studies of long-term erosion rates. Such thresholds, however, introduce a source of non-linearity that can have a tremendous influence on the sensitivity of erosion rates to variations in climate (e.g. Tucker and Slingerland, 1997). Dietrich *et al.* (1993) showed, for example, that the predicted extent of potential overland flow erosion in a small watershed depended critically on the magnitude of a threshold for erosional penetration of a resistant grass mat. Field experiments (Abrahams *et al.*, 1994;

* Correspondence to: G. E. Tucker, School of Geography and the Environment, Oxford University, Mansfield Road, Oxford, OX1 3TB UK.
E-mail: greg.tucker@geog.ox.ac.uk

Prosser and Slade, 1994; Prosser and Dietrich, 1995) have demonstrated that similar vegetation–erosion thresholds play an important role in grassland and shrubland environments around the world.

Erosion thresholds are of course not limited to vegetated hillslopes and unchannelled valleys but are a potentially critical component in the erosion mechanics of gravel-bed and bedrock rivers. In the case of bedrock rivers, it is reasonable to assume that significant rates of incision can only occur during flood events that are large enough to mobilize a coarse sediment veneer. Thus, any change in the frequency of floods capable of exceeding this threshold can be expected to produce a corresponding change in average incision rates, even though the mean flow may show very little variation (e.g. Knox, 1983). Similarly, tectonically driven changes in channel gradient can potentially alter the proportion of flood events capable of significant work. It is critical to understand such non-linear behaviour at a quantitative level if we are to assess properly the influence of tectonic forcing and climate changes on large-scale erosion rates (e.g. Molnar and England, 1990; Tucker and Slingerland, 1997; Tucker and Bras, 2000; Molnar, 2001).

Even at the largest scales, recent work suggests that fluvial erosion thresholds may exert a surprising influence on both the height and longevity of mountain ranges. Snyder *et al.* (2000) found that the conventional 'stream power' channel erosion theory (lacking a threshold) was unable to explain the surprisingly low relief contrast between two regions of similar lithology and climate but varying uplift rates. However, the same model can easily explain the observed relief contrast when stochastic forcing is accounted for and the threshold term is retained (Snyder *et al.*, 2003). This result, though not necessarily a unique validation of the underlying theory, does imply that the non-linearity imparted by fluvial erosion thresholds can significantly impact the scaling of relief with tectonic input (Whipple and Tucker, 1999; Tucker and Whipple, 2002). Similarly, Baldwin *et al.* (2003) recently showed that a finite erosion threshold can significantly prolong the lifespan of a decaying orogen, thus providing one possible answer to the riddle of why ancient mountain ranges such as the Appalachians and the Urals still survive.

In this paper, I describe a stochastic method for modelling long-term sediment transport and erosion rates that (a) incorporates an erosion threshold, and (b) captures the integrated effects of a spectrum of runoff events. The model is an extension to that of Tucker and Bras (2000) and yields analytical solutions for long-term transport and erosion rates without the need to ignore entrainment thresholds, which are shown to introduce a non-linear effect that has significant implications for large-scale relief and morphology. In particular, the modified model implies that the existence of a threshold in an erosional system can have a first-order impact on the scaling relationship between tectonic uplift rate and drainage network relief, on the sensitivity of erosion rates to climate variability, and in many cases on the shape of terrain itself. The stochastic-threshold theory can be used to investigate a range of different types of geomorphic problem, including the topographic expression of active mountain belts (e.g. Whipple and Tucker, 1999, 2002; Snyder *et al.*, 2000; Tucker and Whipple, 2002), the long-term persistence of topography in ancient orogens (Baldwin *et al.*, 2003), and long-term rates of soil loss as a function of rainfall frequency–magnitude characteristics (Boardman and Favis-Mortlock, 1999).

POISSON RAINFALL MODEL

The Poisson rectangular pulse rainfall model of Eagleson (1978) represents rainstorms as random pulses with independent, exponentially distributed intensity, duration, and spacing (Figure 1). The probability density functions for intensity, p (L/T), duration, t_r (T), and interstorm interval, t_b (T), are

$$\text{Rainfall intensity} \quad f(p) = \frac{1}{P} \exp\left(-\frac{p}{P}\right) \quad (1)$$

$$\text{Storm duration} \quad f(t_r) = \frac{1}{T_r} \exp\left(-\frac{t_r}{T_r}\right) \quad (2)$$

$$\text{Interstorm period} \quad f(t_b) = \frac{1}{T_b} \exp\left(-\frac{t_b}{T_b}\right) \quad (3)$$

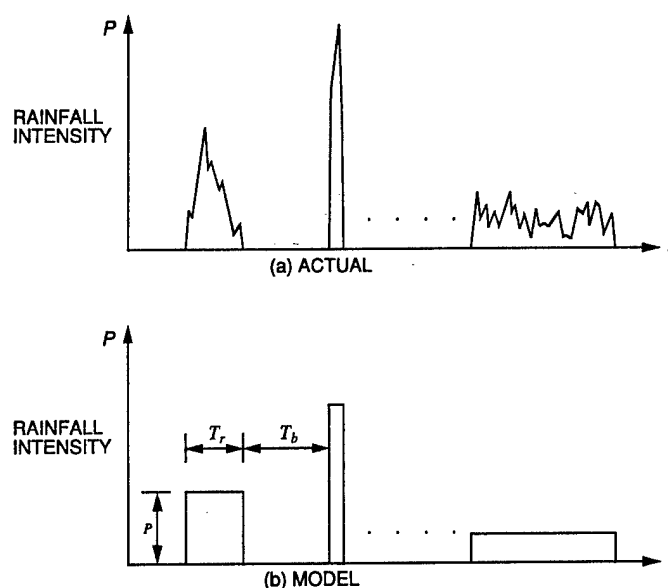


Figure 1. Schematic illustration of the Poisson rainfall model (from Tucker and Bras (2000), after Eagleson (1978)). Copyright 2000 American Geophysical Union, reproduced by permission of American Geophysical Union

where the three parameters, P , T_r , and T_b , are the mean intensity, duration, and interstorm period, respectively (note the difference in notation from Tucker and Bras, 2000). Infiltration and interception losses are here parameterized in terms of an infiltration capacity, I (L/T), so that storm runoff rate is defined as

$$R = p - I, \quad p > I \quad (4)$$

and the probability density function for runoff rates is given by

$$f(R) = \frac{1}{P} \exp\left(-\frac{(R + I)}{P}\right) \quad (5)$$

By assuming a spatially uniform infiltration capacity the model obviously leaves out some of the richness of real catchment hydrology. In effect, I is a scale-dependent lumped parameter which is independent of P , T_r , and T_b . Treating infiltration this way can be justified on two grounds: first, that hillslope-scale (i.e. short-range) soil variability will tend to be averaged out within a channel network, and second, that including variability in soil properties would simply tend to smooth the otherwise sharp transition implied by Equation 4. The implied independence between I and the other variables would be most applicable to an arid or semi-arid landscape with low soil moisture. In more humid environments, the sequence of storm events could be expected to play a greater role in controlling runoff rates. This would presumably lead to greater variability, and possibly also to an increase in the time scale of variability.

THEORY FOR PARTICLE DETACHMENT

Excess shear stress theory

One of the most common formulas for detachment of resistant bedrock or cohesive soil is

$$E = k_c(\tau - \tau_c)^a \quad (6)$$

where E is the detachment rate (dimensions of L/T), τ is bed shear stress, τ_c is threshold shear stress below which the detachment rate is insignificant, and k_c and a are parameters (e.g. Foster and Meyer, 1972; Howard and Kerby, 1983; Howard, 1994). The exponent a is not arbitrary, but rather reflects the physics of particle detachment (Whipple and Tucker, 1999; Whipple *et al.*, 2000). Given the large uncertainty regarding the mechanics of bedrock channel incision, there is no compelling reason to favour Equation 6 over the following alternative form, which is both dimensionally consistent and easier to solve:

$$E = k_c(\tau^a - \tau_c^a) \quad (7)$$

In this form, the τ^a term can be interpreted either in terms of shear stress (in which case $a = 1$) or in terms of unit stream power (in which case $a = 3/2$, τ_c^a is proportional to a critical unit stream power required for entrainment, and the coefficient terms relating velocity and shear stress are subsumed into k_c).

By applying a force balance for steady, uniform flow in a wide channel, and using either the Manning or Darcy–Weisbach flow resistance equation to describe friction, bed shear stress can be written in terms of channel gradient, S , and specific water discharge, q (L^2/T):

$$\tau = k_i q^\alpha (\sin \theta)^\beta \approx k_i q^\alpha S^\beta \quad (8)$$

where θ is the channel-bed gradient expressed as an angle (e.g. Howard, 1994; Tucker and Slingerland, 1997). If the Manning equation is used, $\alpha = 3/5$, $\beta = 7/10$, and $k_i = \rho g n^{3/5}$, where ρ is fluid density, g is gravitational acceleration, and n is roughness. If the Darcy–Weisbach equation is used, $\alpha = 2/3$, $\beta = 2/3$, and $k_i = (\rho g^{2/3} f^{1/3})/2$, with f being a dimensionless roughness parameter.

To represent channel width, the usual approach is to substitute the following empirical hydraulic geometry relations:

$$W_b = k_w Q_b^{\omega_b} \quad (9a)$$

$$\frac{W}{W_b} = \left(\frac{Q}{Q_b} \right)^{\omega_s} \quad (9b)$$

where Q is total discharge ($= qW$), W_b is a characteristic channel width (such as bankfull width, hence the 'b') and Q_b is a characteristic discharge (usually either bankfull or mean annual). Exponents ω_b and ω_s refer to downstream and at-a-station variations, respectively (Leopold and Maddock, 1953). For sheetflow, channel width is irrelevant. For rill erosion, an alternative approach based on rill geometry could be adopted, while for self-formed alluvial channels the shear-stress ratio approach of Parker (1978) could be substituted for Equation 9.

Combining Equations 7–9, the instantaneous rate of detachment in terms of channel slope and total discharge is

$$E = k_c (k_i^a k_w^{-\alpha a} Q^{\alpha a(1-\omega_b)} Q_b^{\alpha a(\omega_b-\omega_s)} S^{\beta a} - \tau_c^a) \quad (10)$$

The connection with rainfall comes via the two discharge factors. To express discharge as a function of rainfall intensity, Tucker and Bras (2000) used the simple approach of assuming steady and spatially uniform runoff, such that total discharge in a channel is equal to the rainfall input without attenuation

$$Q = (P - I)A = RA, \quad P > I \quad (11)$$

To maintain consistency with this approach, the bankfull discharge Q_b is defined as a function of a bankfull-equivalent runoff rate, R_b , such that

$$Q_b = R_b A \quad (12)$$

Equations 11 and 12 represent the simplest basin-response function one could reasonably use. It is appropriate for relatively small basins (in which storm duration is typically longer than the basin's concentration time) dominated by infiltration-excess runoff. In fact, a more realistic response function could be substituted, though this would also require including event duration as an additional random variable in Equation 11.

Long-term average detachment rates

Combining Equations 10–12 gives an expression for instantaneous bed scour rate as a function of the topographic variables A and S

$$E = k_c(k_t^a k_w^{-a\alpha} R^{a\alpha(1-\omega_b)} A^{a\alpha(1-\omega_b)} R_b^{-a\alpha(\omega_b-\omega_t)} S^{a\beta} - \tau_c^a) \quad (13)$$

Averaging Equation 13 over many storm events:

$$\begin{aligned} \bar{E} &= \int_{R_c}^{\infty} f(R) E(R) dR \\ &= \frac{1}{P} \int_{R_c}^{\infty} \exp\left(\frac{R+1}{P}\right) k_c [k_t^a k_w^{-a\alpha} R_b^{-a\alpha(\omega_b-\omega_t)} A^{a\alpha(1-\omega_b)} R^{a\alpha(1-\omega_b)} S^{a\beta} - \tau_c^a] dR \end{aligned} \quad (14)$$

Note the lower bound on the integration. R_c is a 'critical runoff intensity' at which, for given slope, area, and other parameters, $\tau = \tau_c$. We can find R_c from Equation 13 by setting $E = 0$ (corresponding to $\tau = \tau_c$) and solving for R :

$$R_c = (\tau_c k_t^{-1} k_w^{\alpha} R_b^{\alpha(\omega_b-\omega_t)} A^{-\alpha(1-\omega_b)} S^{-\beta})^{\left[\frac{1}{\alpha(1-\omega_t)}\right]} \quad (15)$$

Note that R_c depends on area and slope: the larger these are, the smaller a given runoff event needs to be to exceed the threshold. Substituting Equation 15 in 14:

$$\bar{E} = k_c k_t^a k_w^{-a\alpha} P^{-1} R_b^{-\varepsilon_b} A^{m_b} S^{n_b} \exp\left(-\frac{I}{P}\right) \int_{R_c}^{\infty} \exp\left(-\frac{R}{P}\right) (R^{\gamma_b} - R_c^{\gamma_b}) dR \quad (16)$$

where $\varepsilon_b = a\alpha(\omega_b - \omega_t)$, $\gamma_b = a\alpha(1 - \omega_t)$, $m_b = a\alpha(1 - \omega_b)$, and $n_b = a\beta$. For notational convenience the variables to the left of the integral are called C , and the two terms inside the integral are labelled X and Y , respectively, so that Equation 16 becomes:

$$\bar{E} = C(X - Y) \quad (17)$$

Solving for X :

$$X = \int_{R_c}^{\infty} \exp\left(-\frac{R}{P}\right) R^{\gamma_b} dR \quad (18)$$

The solution to this is the incomplete gamma function, $\Gamma(a, x)$ (Press *et al.*, 1988)

$$X = P^{(\gamma_b+1)} \Gamma(\gamma_b + 1, R_c/P) \quad (19)$$

Solving for Y :

$$Y = R_c^{\gamma_b} P \exp\left(-\frac{R_c}{P}\right) \quad (20)$$

Reassembling the pieces, we have:

$$\bar{E} = \left[P^{\gamma_b} R_b^{-\epsilon_b} \exp\left(-\frac{I}{P}\right) k_e k_t^a k_w^{-\alpha} \Gamma(\gamma_b + 1) \right] [A^{m_b} S^{n_b}] \left[\frac{\Gamma(\gamma_b + 1, R_c/P) - \left(\frac{R_c}{P}\right)^{\gamma_b} \exp\left(-\frac{R_c}{P}\right)}{\Gamma(\gamma_b + 1)} \right] \quad (21)$$

$$= K_i A^{m_b} S^{n_b} \Phi \quad (22)$$

The average detachment rate can be seen as the product of three factors: (i) an erosion coefficient that depends on soil/rock properties, rainfall frequency and magnitude, channel geometry and roughness, and soil permeability; (ii) topography (drainage area and gradient); and (iii) a threshold factor Φ that ranges from 0 to 1. The threshold factor decreases monotonically as R_c/P grows (Figure 2). For values of γ_b in the range 0.5–2, it shrinks to zero when the critical runoff rate is several times larger than the mean rainfall intensity. Note that when $R_c = 0$, the equation reduces to the zero-threshold case in Tucker and Bras (2000, Equation 26).

Finally, to write Equation 21 in terms of a long-term average erosion rate, we multiply by the fraction of time storms are occurring

$$\langle E \rangle = \left(\frac{T_r}{T_r + T_b} \right) \bar{E} = K A^{m_b} S^{n_b} \Phi \quad (23)$$

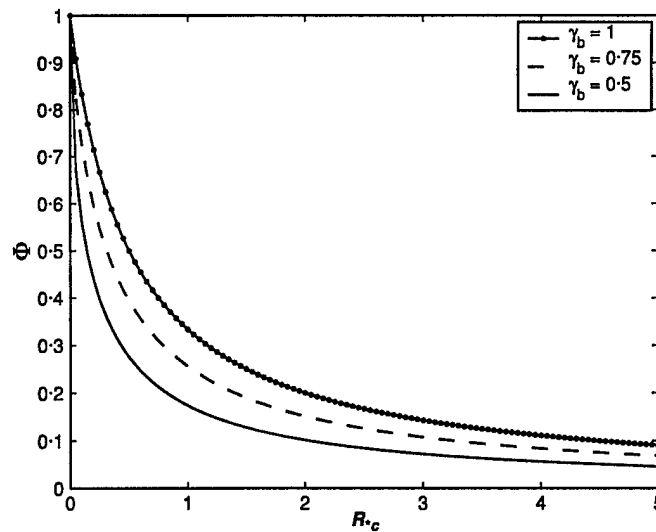


Figure 2. Threshold factor Φ in Equation 22 plotted as a function of dimensionless critical runoff rate $R_c = R_c/P$, for $\gamma_b = 0.5, 0.75$, and 1

$$\text{where } K = K_i \left(\frac{T_r}{T_r + T_b} \right) \quad (24)$$

Thus, the long-term average erosion rate can still be expressed as a function of area and slope, but with modifying pieces that describe the role of flow variability and an erosion threshold (which itself depends on A and S , thus introducing a non-linear component).

Non-dimensionalization

To simplify the analysis, dimensionless quantities are defined as follows. Runoff, threshold runoff and infiltration capacity are normalized by mean storm intensity, while drainage area is normalized by a characteristic length scale L^2 (mainstream length is a natural choice for L ; Whipple and Tucker, 1999), and mean storm duration is normalized by mean recurrence interval:

$$R_* = R/P \quad (25)$$

$$R_{*c} = R_c/P \quad (26)$$

$$A_* = A/L^2 \quad (27)$$

$$T_{*r} = \left(\frac{T_r}{T_r + T_b} \right) \quad (28)$$

$$I_* = \frac{I}{P} \quad (29)$$

Using these dimensionless quantities, it is possible to express shear stress as the product of the three dimensionless variables R_* , A_* and S multiplied by a lumped parameter that includes all the remaining parameters. Substituting Equations 25–27, 9, 11 and 12 into Equation 8, shear stress can be written

$$\tau = [k_r k_w^{-\alpha} P^{\delta_s} R_b^{-\varepsilon} L^{2\delta_b}] R_*^{\delta_s} A_*^{\delta_b} S^{\beta} = \tau_r (R_*^{\delta_s} A_*^{\delta_b} S^{\beta}) \quad (30)$$

where $\delta_s = \alpha(1 - \omega_s)$, $\delta_b = \alpha(1 - \omega_b)$, and $\varepsilon = \alpha(\omega_b - \omega_s)$. The quantity

$$\tau_r \equiv k_r k_w^{-\alpha} P^{\delta_s} R_b^{-\varepsilon} L^{2\delta_b} \quad (31)$$

has dimensions of force per unit area and is used as a reference shear stress. It is equal to the shear stress produced when $R = P$, $A = L^2$, and $S = 1$. Using τ_r as a scaling factor, dimensionless shear stress and critical shear stress are defined as

$$\tau_* \equiv \tau/\tau_r, \quad \tau_{*c} \equiv \tau_c/\tau_r \quad (32)$$

Substituting these dimensionless variables (Equations 25–32) into Equation 23 gives a dimensionless form of the detachment capacity equation:

$$\langle E \rangle_* \equiv \frac{\langle E \rangle}{k_c \tau_r^a T_{*r} \exp(-I_*)} = A_*^{m_b} S^{n_b} \Gamma(\gamma_b + 1) \left[\frac{\Gamma(\gamma_b + 1, R_{*c}) - R_{*c}^{\gamma_b} \exp(-R_{*c})}{\Gamma(\gamma_b + 1)} \right] \quad (33)$$

The dimensionless form highlights relationships between parameters and the relative sensitivities among them. It is used below to analyse the implications of an erosion threshold for drainage basin dynamics.

THEORY FOR SEDIMENT TRANSPORT

Numerous formulas have been developed to model bedload, suspended load, and total-load transport (e.g. Yang, 1996; Prosser and Rustomji, 2000). These formulas typically differ in their applicability in terms of grain-size ranges and transport stages. Rather than attempt a comprehensive treatment of all of these, I focus on two examples. The first is a modified form of the Bagnold bedload equation (Bridge and Dominic, 1984; Slingerland *et al.*, 1994), and its use here is motivated by three considerations. First, the use of a bedload rather than total-load formula is motivated by the expectation that the coarse bedload fraction, though typically only a small volumetric proportion of the total load, will tend to control the stream gradient because of its larger entrainment threshold (e.g. Howard, 1980). Second, the Bridge-Dominic form of the Bagnold formula uses a simple polynomial form from which an analytical solution can be directly obtained. Third, in a comparative study by Gomez and Church (1989), the related (original) Bagnold stream-power approach performed better than other approaches as a predictor of bedload transport rates given limited hydraulic information.

The second transport formula considered here is a generic formula based on excess shear stress. It is chosen for its generality. By examining both of these types of formula, it becomes easier to judge which aspects of the analysis are specific to individual formulas and which are general and robust outcomes.

Bridge-Dominic transport formula

For sediment of a given (uniform) size and density, the volumetric specific bedload transport rate [L^2T^{-1}] is

$$q_s = K_{bd} \sqrt{\rho} (U_* - U_{*c}) (\tau - \tau_c) \quad (34)$$

where U_* is shear velocity ($= \sqrt{\tau/\rho}$) and K_{bd} is a transport coefficient with an experimentally determined value of $K_{bd} \approx 10/[(\sigma - \rho)g\rho^{1/2}]$, where σ is sediment particle density (Slingerland *et al.*, 1994). Note that Equation 34 predicts the same scaling with shear stress ($q_s \sim \tau^{1.5}$) as in the well known formula of Meyer-Peter and Müller (1948).

By writing shear stress in terms of slope, discharge, and width (i.e. combining Equations 8, 9, 11, and 12 and substituting into Equation 34), applying the non-dimensionalization discussed above, and integrating over the full spectrum of storm events, we can write the long-term average transport capacity in dimensionless form as

$$\begin{aligned} \langle Q_s \rangle = A_* \left(\frac{3}{2} \gamma_s + \omega_s \right) S \left(\frac{3}{2} \beta \right) & [\Gamma(\gamma_1 + 1, R_{*c}) \\ & - R_{*c}^{\delta/2} \Gamma(\gamma_2 + 1, R_{*c}) - R_{*c}^{\delta} \Gamma(\gamma_3 + 1, R_{*c}) + R_{*c}^{3\delta/2} \Gamma(\gamma_4 + 1, R_{*c})] \end{aligned} \quad (35)$$

where dimensionless transport capacity is defined as

$$\langle Q_s \rangle \equiv \frac{\langle Q_s \rangle}{\rho^{-1/2} K_{bd} W_r \tau_r^{3/2} \exp(-I_*) T_r} \quad (36)$$

The parameter W_r is a reference channel width defined as

$$W_r \equiv k_n P^\omega R_b^{(\omega_s - \omega_s)} L^{2\omega_s} \quad (37)$$

and

$$\gamma_i \equiv \left\{ \frac{3}{2} \alpha(1 - \omega_s) + \omega_s, \alpha(1 - \omega_s) + \omega_s, \frac{1}{2} \alpha(1 - \omega_s) + \omega_s, \omega_s \right\}, \quad \text{for } i = 1, 2, 3, 4 \quad (38)$$

Note the area and slope variables in Equation 35; these also appear inside R_{*c} . The four terms in square brackets in Equation 35 reflect the polynomial form of the Bridge-Dominic transport formula. As with the average

detachment-rate expression, the average transport-rate equation predicts a rapid decline in mean transport rate as the threshold (represented here by R_{*c}) grows large in a relative sense.

Generic shear-stress transport capacity formula

The Bridge–Dominic transport formula is only one of many that have been used in studies of long-term drainage basin evolution. In many cases, the simpler shear-stress formula

$$Q_s = Wk_f(\tau - \tau_c)^p \quad (39)$$

has been used (e.g. Densmore *et al.*, 1998; Tucker and Bras, 1998). For the Meyer–Peter and Müller (1948) formula, $p = 3/2$; for high-discharge sand-bed streams, Howard (1994) notes that many total-load formulas give p on the order of 3. The form of Equation 39 makes stochastic analytical solutions intractable for $p \neq 1$. However, an analytical solution can be obtained when Equation 39 is approximated using the alternative form

$$Q_s = Wk_f(\tau^p - \tau_c^p) \quad (40)$$

Clearly, there are differences between Equations 39 and 40, particularly when τ is near τ_c . These differences, however, are arguably much less significant than the differences between alternative sediment transport formulas for which there is a similar degree of empirical support. In other words, uncertainty regarding sediment transport relations is larger than the potential inaccuracy introduced by using Equation 40 in place of 39. Furthermore, as shown below, the conclusions drawn in this study are quite robust with regard to the form of transport formula employed.

Using the same approach that was applied to the detachment law and Bridge–Dominic transport law, Equation 40 has the following solution for long-term average transport rate:

$$\langle Q_s \rangle = A_s^{\delta_s} S^{\beta} [\Gamma(p\delta_s + \omega_s + 1, R_{*c}) - R_{*c}^{\delta_s} \Gamma(\omega_s + 1, R_{*c})] \quad (41)$$

where

$$\langle Q_s \rangle \equiv \frac{\langle Q_s \rangle}{k_f W_r \tau_r^p \exp(-I_* T_r)} \quad (42)$$

The similarity to the Bridge–Dominic formula can be appreciated by comparing Equations 41 and 35. As with the detachment-rate expression, the long-term average transport equations provide a means of modelling average sediment transport rates over long time spans while retaining both the threshold and factors that describe the inherent variability of rainfall and flooding.

NUMERICAL SOLUTIONS

In order to explore the implications for topographic form, the three erosion/transport laws are solved numerically using the CHILD landscape evolution model. The numerical model is discussed in detail by Tucker *et al.* (2001a,b) and will be reviewed only briefly here. The model domain consists of a triangulated matrix of nodes representing a topographic surface. The surface area associated with each node i is the region lying closer to that node than to any other; this is the Voronoi cell about node i (Figure 3). Detachment and sediment transport are driven by a series of storms generated at random from the probability distributions (1–3) (Figure 1).

The model runs are summarized in Table I, and default parameter values are listed in Table II. The domain of each simulation consists of a square mesh containing 2601 nodes, with an open, fixed-elevation boundary along the lower edge (see Figure 8). Twelve model calculations were run with constant, spatially uniform uplift (relative to the fixed lower boundary) until the mean elevation reached a quasi-steady state. In each of these runs, about 3×10^5 random storms were sampled over the duration of the run. Four additional runs were computed using a scarp-bounded plateau as an initial condition, and no uplift.

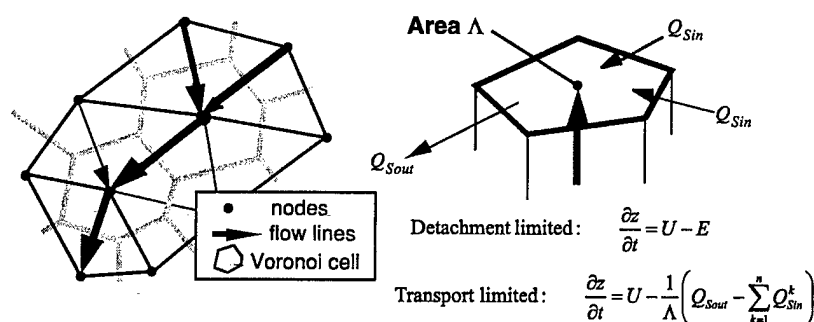


Figure 3. Illustration of numerical solution to erosion and transport equations in CHILD. (Left) Relationship between nodes, triangles, and Voronoi cells, showing steepest-descent flow routing method. (Right) Schematic illustration of solution scheme based on continuity of mass within a Voronoi cell. Q_{Sin}^k refers to instantaneous sediment flux from the k th upstream neighbour, and n is the total number of upstream neighbours. In each numerical simulation, one of the two equations is solved by a Monte Carlo method in which a sequence of random storm events is generated from exponential probability distributions. During each event, one of the two continuity equations shown in the figure is solved for each node using an explicit forward-difference method with variable time steps

Table I. Summary of numerical models runs

Detachment / transport law	Test condition	τ_c	Figure
Slope-area detachment law (4 runs)	Equilibrium	0, 0.001, 0.01, 0.1	4
Generic shear-stress transport law (4 runs)	Equilibrium	0, 0.001, 0.01, 0.1	5
Bridge-Dominic transport law (4 runs)	Equilibrium	0, 0.001, 0.01, 0.1	6
Slope-area detachment law	Transient relaxation	0	8A
Slope-area detachment law	Transient relaxation	0.1	8B
Bridge-Dominic transport law	Transient relaxation	0	8C
Bridge-Dominic transport law	Transient relaxation	0.1	8D

Table II. Default model parameter values

Parameter	Value
Mesh dimensions	10 km by 10 km
Average point spacing	200 m
No. points/no. interior points	2601/2401
Run duration	(varies)
P	1 m/year
T_r	(varies)
T_b	0
k_s^*	$0.002 \text{ m}^{5/2} \text{ s}^2 \text{ kg}^{-3/2}$
$f(\text{in } k_i = 1/2 \rho g^{2/3} f^{1/3})$	0.08
α	$2/3$
β	$2/3$
a^*	$3/2$
τ_c	0, 31.24, or 62.48 Pa
$K_{bd}(= 10/[(\sigma/\rho - 1) g \rho^{3/2}])^\dagger$	$1.95 \times 10^{-5} \text{ m}^{7/2} \text{ s}^2 \text{ kg}^{-3/2}$
$k_f(= 8/[(\sigma/\rho - 1) g \rho^{3/2}])^\ddagger$	$1.56 \times 10^{-5} \text{ m}^{7/2} \text{ s}^2 \text{ kg}^{-3/2}$
p^\ddagger	$3/2$
U	0.001 m/year
ω_b	0.5
ω_s	0.5
R_b	§

* Detachment law only.

† Bridge-Dominic transport law only.

‡ Generic shear-stress transport law only.

§ Not applicable, because $\omega_s = \omega_b$.

IMPLICATIONS FOR EQUILIBRIUM TOPOGRAPHY

Equilibrium topography is defined as topography in which the denudation rate equals the rate of baselevel lowering at a given boundary location (e.g. a fixed shoreline or active fault), so that the height at any point is constant in time. The extent to which equilibrium topography exists in nature is uncertain (e.g. Whipple, 2001; Hasbargen and Paola, 2002; Willett and Brandon, 2002). Nonetheless, the equilibrium state makes a convenient starting point for comparative analysis, and it is a special case of the more general (and probably more common) case of approximately spatially uniform rates of erosion and sediment yield over a catchment.

The equilibrium gradient of a mountain stream may be controlled by either (a) its capacity to detach bedrock (e.g. Howard, 1994), (b) its capacity to transport sediment (e.g. Howard, 1980; Molnar, 2001), or (c) a combination of the two, in the sense that rock abrasion requires a certain sediment transport capacity to provide abrasive tools (Sklar and Dietrich, 2001; Whipple and Tucker, 2002). At present, we lack any compelling evidence to distinguish among these possibilities in most mountain rivers, so it is prudent to consider all three as working hypotheses and to explore whether there are diagnostic differences among these different models.

A sensitive measure of drainage basin topography is the slope–area relationship (Willgoose *et al.*, 1991; Howard, 1994; Tucker and Bras, 1998; Tucker and Whipple, 2002), which describes the concavity of longitudinal stream profiles and is closely linked to three-dimensional morphology. Models like Equation 6, in the absence of threshold effects, predict a power-law slope–area relationship under conditions of uniform climate, lithology, and erosion rate. The fact that slope–area data often show a reasonably linear trend in log–log space is often taken as evidence in support of such models. The predicted slope–area relationship remains unaltered by threshold effects for the stochastic form of the simple detachment model (Equation 23). In general, Φ (Equation 23) is a function of slope and drainage area, which implies that detachment rate cannot be modelled as a simple power function of these two variables. However, in the special case of spatially uniform erosion rate, R_c becomes independent of S and A . To prove this, one can postulate the existence of an equilibrium relationship of the form $S = cA^{-m/n}$, where c is independent of area and slope. When this is substituted into R_c (Equation 15), the slope and area variables cancel, thus demonstrating the existence of a solution for which the above is true. This means that the existence of an erosion threshold does not alter the predicted slope–area relationship under uniform K and erosion rate. This result is confirmed by numerical solutions (Figure 4). Note, however, that slope–area scaling will deviate from the zero-threshold case when erosion rate (or uplift rate) varies systematically in space.

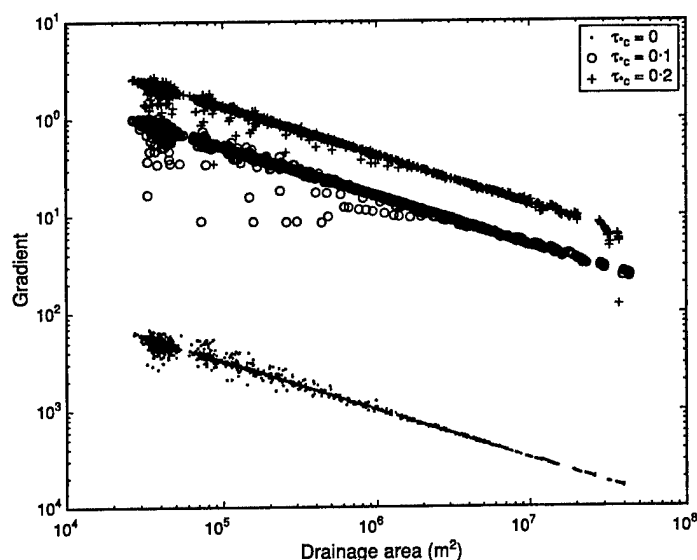


Figure 4. Gradient versus drainage area for three runs using the shear-stress detachment formula, with $\tau_c = 0, 0.1$, and 0.2 . Each point represents one node (least squares regression yields a slope of -0.50 for each run)

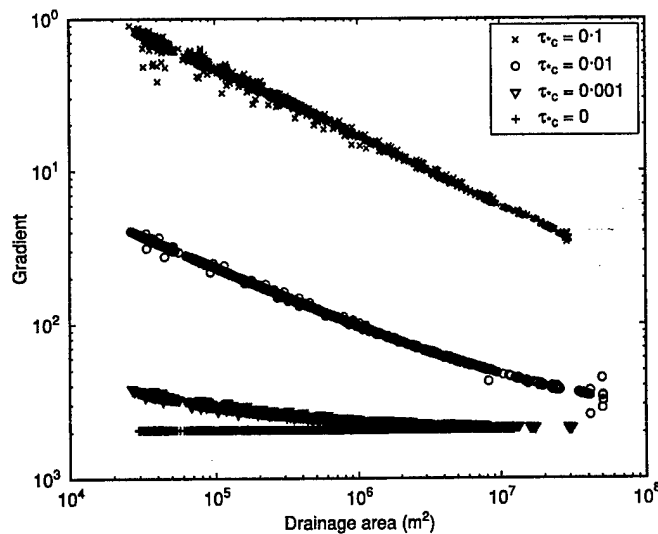


Figure 5. Gradient versus drainage area for three transport-limited runs using the generic shear-stress transport capacity formula, with $p = 3/2$ and $\tau_c = 0, 0.001, 0.01$, and 0.1 . (Trend slopes obtained from least-squares regression are, in order of increasing τ_c , 0.00 , -0.10 , -0.36 , and -0.45 , respectively.) Values of N_{ST} near the outlet (drainage area $3 \times 10^7 \text{ m}^2$) are, in order of increasing τ_c , 0 , 0.028 , 0.88 , and 28 , respectively

For transport-limited models, threshold effects substantially increase predicted concavity, bringing it much closer to generally observed values. Consider the case of an equilibrium drainage basin in which the transport capacity (Equation 35 or 41) is just equal to the sediment supply at each point in a drainage network. Where entrainment thresholds are negligible, Howard (1994) showed that the resulting stream profiles tend to have relatively low concavities and therefore tend to produce rather gentle terrain (Tucker and Whipple, 2002). However, for gravel-bed rivers that are typical of mountain regions, we know that entrainment thresholds are not small. For example, in gravel-bed streams with mobile bed and banks, theory and observations indicate that the cross-section averaged bankfull shear stress is often a relatively constant fraction (1.2–1.4) of threshold shear stress for the section-averaged median grain size (Parker, 1978; Paola and Seal, 1995; Talling, 2000).

Equations 35 and 41 yield no obvious analytical solutions for equilibrium gradient when $\tau_c > 0$. However, numerical simulations (Figures 5 and 6) show that slope–area scaling is significantly altered by a finite threshold. In both of these examples, transport capacity scales as the $3/2$ power of bed shear stress (equivalently, it scales linearly with unit stream power), in which case the zero-threshold equilibrium solution gives spatially uniform stream gradients. However, if there is an appreciable entrainment threshold, channels become concave (approaching $S \sim A^{-0.5}$). This is so because the minimum gradient required to exceed the shear stress for entrainment becomes smaller with increasing discharge (and hence with drainage area).

Further insight into slope–area scaling can be gained from an analytical solution to the constant-discharge (i.e. non-stochastic) form of Equation 40 (the generic excess-shear formula; Tucker and Bras, 1998, Equation 24). Equilibrium occurs when the bed sediment influx due to base-level lowering (here assumed uniform in space) equals the transport rate at any given point in the drainage network, that is, $Q_s = \phi AU$, where ϕ represents the fraction of eroded material that is incorporated into the bed sediment load rather than wash or dissolved load. Rewritten to include at-a-station channel-width variation (Equation 9b), this turns out to contain two dimensionless terms (square brackets) that describe, respectively, capacity and competence:

$$S = \frac{1}{A_*^{\delta_s/\beta} R_*^{\delta_r/\beta}} \left[\frac{\phi L^2 U}{k_f W_r \tau_r^p R_*^{\omega_r} \zeta} A_*^{1-\omega_b} + \tau_c^p \right]^{\frac{1}{n}} \quad (43)$$

Capacity (transport-limited) Competence (supply-limited)

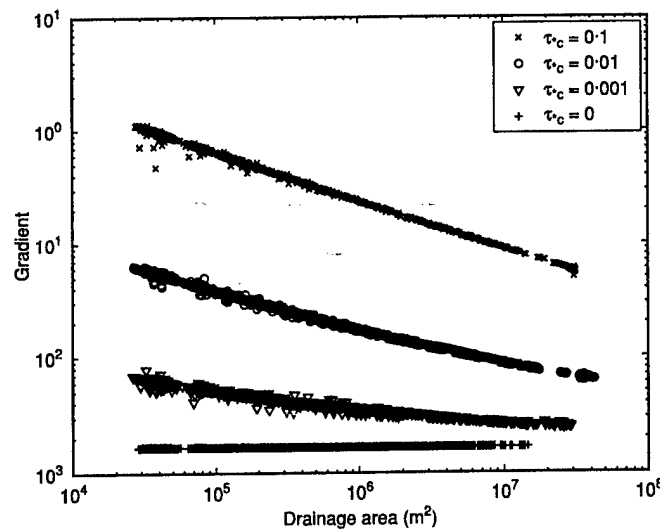


Figure 6. Gradient versus drainage area for three transport-limited runs using the modified Bagnold bedload transport formula, with $\tau_c = 0, 0.001, 0.01$, and 0.1 . (Trend slopes obtained from least-squares regression are, in order of increasing τ_c , $0.00, -0.16, -0.33$, and -0.43 , respectively). Values of N_{ST} near the outlet (drainage area $3 \times 10^7 \text{ m}^2$) are, in order of increasing τ_c , $0, 0.035, 1.1$, and 35 , respectively (calculation of N_{ST} from Equation 44 using K_{bd} in place of k_f)

where ζ stands for $T_s \exp(-I_s)$. In this case, R_s should be interpreted as a characteristic runoff rate that approximates the full spectrum of events. The second dimensionless term on the right-hand side represents the threshold contribution. When it is large, transport rate is limited by competence and concavity tends to be large (for typical α , β , and p), and conversely. A useful way to represent the relative degree of supply (competence) versus capacity limitation is by taking the ratio of the second term to the first to form a dimensionless 'supply-transport' number:

$$N_{ST} = \frac{k_f W \tau_c^p \zeta}{\phi A U} \quad (44)$$

Note that both numerator and denominator have dimensions of volume flux. In Figures 5 and 6, the transition from low to high concavity occurs when N_{ST} is near unity. The supply-transport number can, in principle, be applied in a straightforward way to river data. One of the more difficult variables to estimate is ϕ . This variable depends in part on the grain size composition of sediment flux from hillslopes, and would presumably be larger where landsliding is a dominant transport mechanism, and where bedrock is only weakly fractured. One could estimate ϕ using a typical frequency distribution for particle sizes resulting from fragmentation phenomena (e.g. a Rosin distribution) with an upper cutoff based on a hydraulic criterion for particle suspension. Predicting the parameters of such a distribution on the basis of process mechanics and parent rock is an important topic for future research.

IMPLICATIONS FOR SENSITIVITY TO TECTONIC FORCING: GRADIENT-UPLIFT RELATIONSHIP

The foregoing slope-area analysis implies a strongly non-linear relationship between uplift rate and equilibrium stream gradient for τ_c . This is quite important because it has clear implications for the question of how steep a mountain range must grow in order to reach erosional equilibrium (Whipple and Tucker, 1999; Tucker and Whipple, 2002; Willett *et al.*, 2002). Figure 7 illustrates the relationship between required (equilibrium) gradient and either incision rate (Equation 33) or transport rate (Equations 35 and 41). Curves show the impact of increasingly large thresholds. Each curve consists of two parts: a highly curved non-linear portion in which the mean dimensionless shear stress is relatively close to the threshold value, and, at higher gradients, a linear trend

in which $\tau_*/\tau_{*c} \gg 1$ (the linear trend for detachment and generic-transport laws reflects the choice of parameters; see caption to Figure 7). The relationships in Figure 7 represent a significant departure from the (linear, in these examples) scaling that would exist under $\tau_{*c} = 0$. They are consistent with both laboratory and field experiments, as discussed below.

IMPLICATIONS FOR LANDSCAPE RELAXATION

Patterns of river profile and drainage basin relaxation following an episode of rapid base-level lowering can provide information about the dynamics involved (Rosenbloom and Anderson, 1994; Weissel and Seidl, 1998; Whipple and Tucker, 1999; Tucker and Whipple, 2002). To explore the implications of the above theory for landscape relaxation, a set of simulations were run in which the initial condition consisted of a c. 1000 m high plateau with a gradient of 0.001 toward the scarp edge, bounded on one end by an escarpment (a drop of 1000 m over a distance of about 200 m along one boundary). Experiments were run for each of the three models discussed above, and for values of τ_{*c} of 0 and 0.1. Figure 8 compares the resulting topography for two of these models and for $\tau_{*c} = 0$ and 0.1 (results for the generic bedload transport model are similar to those for the modified Bagnold model, and are not shown). The figure shows topography at the point at which 40 per cent of the initial mass has been removed.

Without a threshold, the detachment-limited model predicts wave-like recession of a series of valleys (Figure 8A). The rate of retreat of each valley head depends on the drainage area at the valley head. The longitudinal profiles have a sigmoidal shape, with an abrupt downstream transition from an actively retreating steep reach to an essentially flat profile (Figures 8A and 9A). (Note that the flat portion is simply an artifact of the assumption that sediment is essentially infinitely transportable; in reality one would expect a minimum gradient to be sustained in order to transport incoming sediment; cf. Howard, 1994; Tucker and Slingerland, 1994.) This morphology reflects the fact that the erosion law used is a linear kinematic wave equation (note that $n_b = 1$ here), so that the steep stream gradients at the initial scarp face are preserved as the gorge heads retreat. However, when a finite threshold is present, the stream profiles below the gorge heads become smooth and concave upward (Figures 8B and 9B). This shape reflects the rapid decline in erosion capacity with decreasing gradient.

Figures 8C and 9C show the topography predicted by a transport-limited model for $\tau_{*c} = 0$. The terrain is very smooth and the profiles are convex upward. This reflects both the initial condition (also concave upward) and the strong diffusive component in Equation 41 which is particularly significant when R_{*c} is small. However, when a threshold is required to mobilize bed sediment, the model terrain becomes much rougher (Figure 8D). Stream profiles are again concave upward (Figure 9). The physical explanation is that transport capacity grows rapidly (i.e. more than linearly) with catchment area when a threshold is present. All else equal, the larger the catchment, the greater the fraction of runoff events that can mobilize sediment. A larger basin provides more sediment that must be carried, but this is more than made up for by the increased frequency and magnitude of threshold-exceeding discharges that a larger catchment can produce.

DISCUSSION

The theory developed in this paper predicts that the dual effects of competence and capacity introduce a form of non-linearity that influences large-scale morphologic behaviour. These non-linear effects are most pronounced when fewer than about half of all events are capable of entraining bed material. This is illustrated by the example in Figure 10, which shows the gradient-erosion curves (solid) predicted by the detachment model (under $n_b = 1$). The dashed curves are contours showing the proportion of flood events that are effective (i.e. threshold-crossing). The intersection of the solid curves with the dashed curves represents the point at which, for a given slope and τ_{*c} , a certain proportion of events exceeds τ_{*c} . For example, the intersection of the bottom gradient-erosion curve (representing $\tau_{*c} = 0.1$) with the dashed line marked 50 per cent indicates that at this combination of slope and τ_{*c} , only half of all events exceed the erosion threshold. The area below this dashed line represents the region in which fewer than half of all flood events are capable of causing erosion. This region coincides with the more highly curved portion of the gradient-erosion relationship: in other words, the smaller the proportion of effective events, the more non-linear the relationship between gradient and erosion.

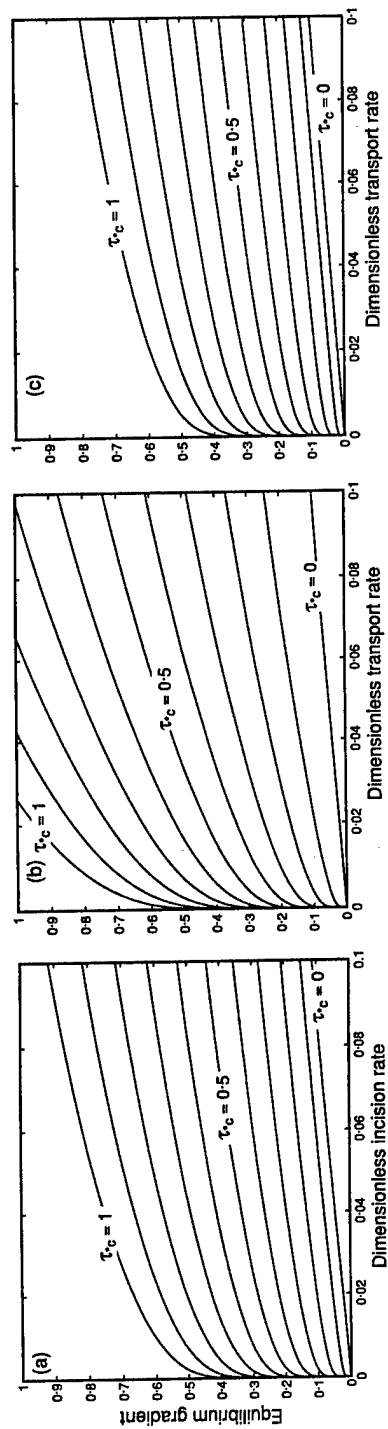


Figure 7. Equilibrium channel gradient as a function of incision rate or transport rate, for unit drainage area. (a) Excess-shear detachment model with $a = 3/2$. (b) Modified Bagnold transport model. (c) Generic excess-shear transport model with $p = 3/2$.

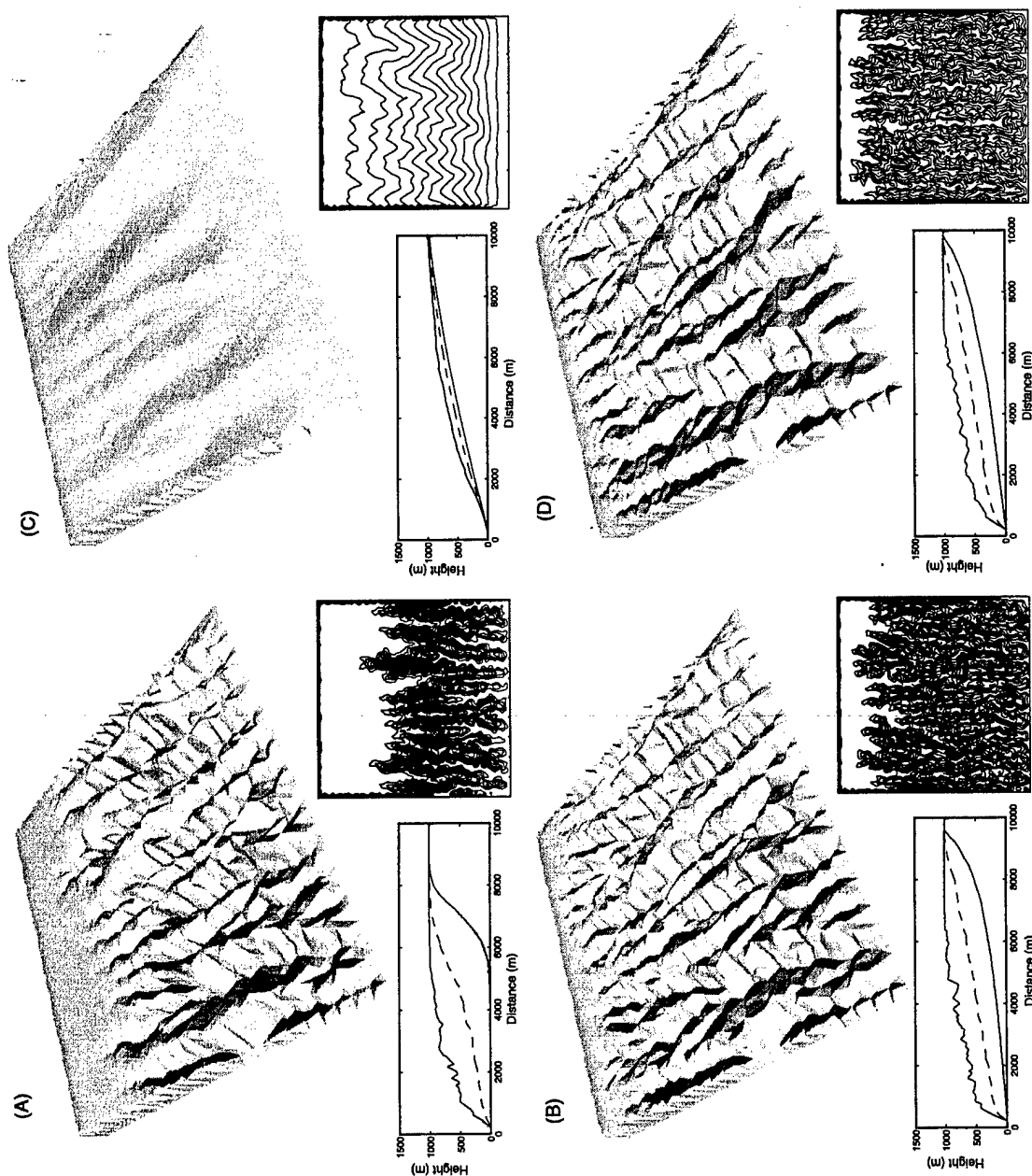


Figure 8. Images of four numerical simulations with plateau as initial condition. Each is shown at time of 40 per cent removal of initial mass. Insets in lower left of each simulation show profiles of maximum (upper), minimum (lower), and mean (dashed) topography. Insets in lower right show elevation contours. (A) Detachment model, $\tau_c = 0$. (B) Detachment model, $\tau_c = 0.1$. (C) Modified Bagnold transport model, $\tau_c = 0$. (D) Modified Bagnold model, $\tau_c = 0.1$

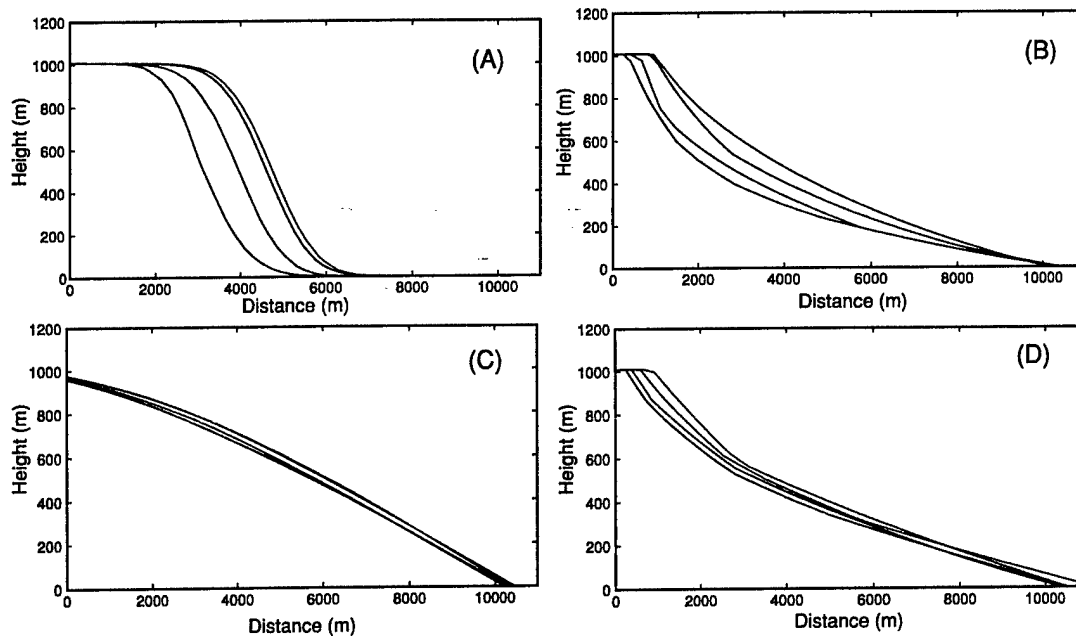


Figure 9. Representative longitudinal stream profiles from the four simulations pictured in Figure 8. X-axis is along-channel distance

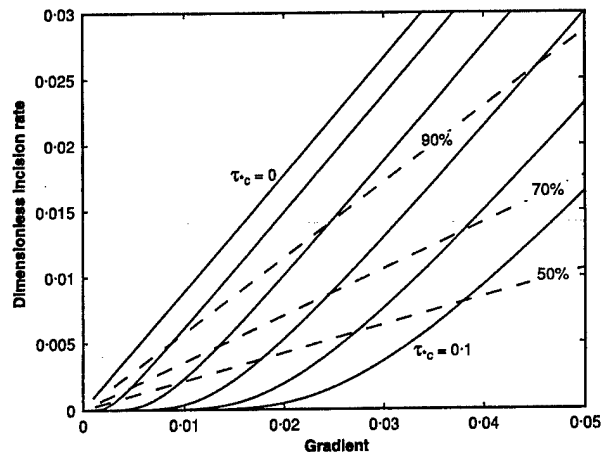


Figure 10. Predicted dimensionless incision rates (solid curves) and fraction of effective events ($R_e > R_{e,c}$; dashed curves) for $\tau_c = 0, 0.025, 0.05, 0.075$, and 0.1 . The plot region below the 50 per cent curve represents the regime in which fewer than 50 per cent of events contribute to erosion, and similarly for the 70 per cent and 90 per cent curves

Figure 10 illustrates that when the fraction of effective events is small, a given relative change in gradient will have a proportionately larger impact on long-term average transport and/or erosion rates because both competence and capacity will be affected. For example, if tectonic tilting were to double the gradient of two gravel streams with different mean sizes of bed material, the stream with the coarser bed would be expected to show a larger relative change in average bedload transport rate. A similar difference in sensitivity should exist with respect to changes in discharge frequency and magnitude (Tucker and Bras, 2000). This simple view of course neglects any potential adjustments in hydraulic geometry or bed-sediment texture; such adjustments could be expected to play an additional role, and that role remains to be teased out. Nonetheless, the predicted contrast in sensitivity between high-threshold and low-threshold systems can be expected to have an important impact on fluvial system responses to both tectonic and climatic forcing.

There are several indirect lines of evidence to suggest that these predicted threshold effects are an important aspect of many natural fluvial systems. First, in bedload-dominated streams, bankfull shear stress is typically close to the entrainment threshold for bed sediment (Parker, 1978; Dade and Friend, 1998). For such streams, significant transport will occur in perhaps only one flood per year on average. Based on the data of Hawk (1992) for the continental USA, typical storm (and therefore presumably peak discharge) frequencies range from a few tens of events per year in arid regions to a few hundred in humid settings. Thus, flood events close to or above bankfull represent only a small fraction (certainly well below 50 per cent) of all storm events and, presumably, hydrograph peaks. Bedload-dominated streams should therefore typically fall well within the non-linear range on Figure 10, all else being equal. This conclusion may not apply, however, to unconfined channels with loose, mobile banks. In such systems, adjustments in channel geometry can potentially offset the non-linear effects of changes in gradient or flood frequency (Parker, 1978). This case may be atypical for steep mountain channels.

A second line of argument for the significance of erosion thresholds comes from experimental and empirical evidence. Lague *et al.* (2003) developed a laboratory simulation of drainage basin formation on an actively uplifting block of cohesive sediment. Their results showed a threshold-linear relationship between gradient and uplift rate (i.e. a linear relation with a positive intercept). This is consistent with an erosion law that is linear in gradient above a certain threshold for particle detachment.

Topographic data from two regions of known uplift, the Mendocino triple junction area (Snyder *et al.*, 2000, 2003) and the Siwalik Hills (Lague and Davy, 2003), provide further evidence. Both data sets are consistent with a threshold-linear erosion law in the sense that linear regression of valley gradient against uplift rate is both statistically significant and yields a large positive intercept (Lague and Davy, 2003). A further line of evidence comes from an analysis of stream profiles along the eastern Australian escarpment by Weissel and Seidl (1998), which showed concave-upward profile forms with a distinct slope break at the plateau. These forms are consistent with any of the threshold models (and also with a non-linear stream-power law; Weissel and Seidl, 1998; Tucker and Whipple, 2002), but inconsistent with their (linear) threshold-free equivalents (Figure 9). In each of these field cases, threshold-induced non-linearity is not the only explanation that could account for the data. However, the fact that such non-linearity is to be expected simply from considerations of basic sediment transport mechanics suggests that it is at least a likely culprit.

The differences between purely linear erosion-transport theory (that is, linear in gradient; Figures 8A,C and 9A,C) and threshold-linear theory (Figures 8B,D and 9B,D) are quite striking. Non-linear behaviour arising from a detachment threshold also impacts the time scale of landscape response to perturbations. For example, Baldwin *et al.* (2003) showed that a rapid decline in erosion rate with decreasing gradient implies that topography can survive much longer than conventional erosion theory (such as the famous 'stream power' law) implies. In other words, a threshold-linear erosion law provides a plausible explanation for long-lived topography in ancient orogens such as the Urals and Appalachians.

The strong non-linearity introduced by detachment thresholds has important implications for drainage basin responses to climate change. It has been hypothesized that the worldwide acceleration in erosion rates during the past 2–4 Ma is a direct result of late Cenozoic climate deterioration (Molnar and England, 1990; Zhang *et al.*, 2001). At first glance, this seems paradoxical because global cooling would presumably have been accompanied by a reduction in the intensity of the hydrologic cycle. Even if this were not the case, there are clearly some regions of the world, such as eastern Africa, that (for a variety of reasons) have undergone regional aridification in the late Cenozoic. Two related solutions to the paradox have been suggested. The first is that increased long-term (e.g. glacial–interglacial scale) climate variability during the late Cenozoic led to accelerated denudation because of non-linearities in geomorphic response (Zhang *et al.*, 2001). This hypothesis is supported by numerical landscape evolution modelling (Tucker and Slingerland, 1997). The second, related, explanation is based on the hypothesis that, due to non-linear effects, a more variable short-term rainfall regime can drive greater fluvial transport and erosion rates, all else being equal (Leopold, 1951; Tucker and Bras, 2000; Molnar, 2001). Because more arid climates are typically associated with greater short-term discharge variability, climatic drying could, paradoxically, lead to increased fluvial transport rates (Molnar, 2001). Rainfall statistics based on the Poisson model, like the power-law stream discharge statistics cited by Molnar (2001), show increased variability under more arid climates. For example, data compiled by Hawk (1992) from rainfall

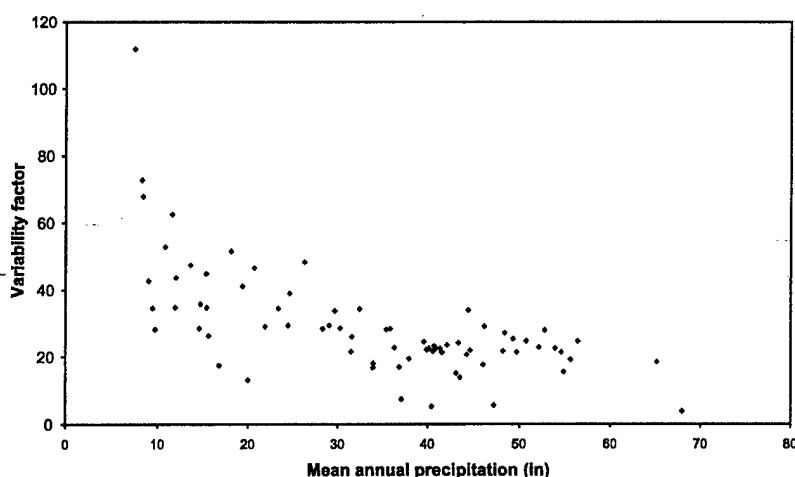


Figure 11. Relationship between precipitation variability and mean annual precipitation, derived from hourly precipitation data for 75 stations in the United States. Variability factor is defined as maximum monthly average storm intensity (that is, mean storm intensity for the month with the greatest mean intensity) divided by mean annual precipitation. Monthly mean rainfall intensities were obtained from hourly precipitation data by Hawk (1992). The highest monthly intensity is from Phoenix, Arizona; the greatest mean annual precipitation is from Astoria, Oregon

stations in the United States show that the greatest rainfall variability, defined as the ratio of maximum monthly average rainfall intensity to mean annual precipitation (a measure of variability similar to that used by Tucker and Bras (2000)), occurs under arid and semi-arid climates (Figure 11). Thus, although the approach used in the present study differs from that of Molnar (2001) in its use of a Poisson rainfall model rather than a power-law distribution of stream discharges, the implications are the same.

Although there is some evidence in support of the stochastic-threshold theory developed in this paper, there remains a need for more direct tests, and for extending the model to incorporate factors such as variable grain sizes, sediment-supply effects, and dynamic adjustments in channel geometry. Direct tests are difficult because we cannot carry out full-scale experiments. However, the predicted morphologic differences among the different models considered here (Figures 8, 9) are distinctive enough that it should be possible in principle to discriminate between them given the right 'natural experiments'. The ideal case would be that of a channel network incising a low-relief surface in response to a rapid but short-lived episode of base-level lowering. Examples might include uplifted marine terraces, or rapid stream incision into low-relief terrain during the last glacial maximum. If the threshold-linear theory is applicable, then channel networks on detachment-resistant material and/or bedload-dominated networks should show concave-upward profiles with a sharp break at the plateau. Suspended-load-dominated channel networks developed on easily detached sediment might show longitudinal profiles more like those of Figure 9C.

CONCLUSIONS

Models of long-term landscape denudation must encapsulate the average effects of a spectrum of essentially random driving forces. This is true whether the target problem is decadal-average soil loss rates on agricultural land or average incision rates in a mountain river system over millions of years. Probabilistic modelling of storm and flood occurrence provides a natural way to incorporate such variability. The extended theory described in this paper makes it possible to calculate the integrated effect of a spectrum of storm events in the presence of an erosion threshold.

Application of stochastic-threshold theory to two bedload transport models (modified Bagnold and a generic excess-shear model) and one detachment model (excess shear stress) implies that threshold effects can induce strongly non-linear behaviour when the threshold is large enough that fewer than about half of flood events are capable of entraining or detaching sediment. These non-linear effects can have a significant impact on

morphology and on landscape sensitivity to tectonic and climatic forcing. The bedload transport theory predicts that equilibrium stream profiles will be straight or have low concavity when a dimensionless supply-transport number is below unity (representing capacity-limited behaviour), and will be more strongly concave upward when this number is above unity (representing competence-limited behaviour). This difference in concavity is mirrored by a strong difference in landscape texture. The detachment theory predicts that equilibrium concavity will be unaltered by threshold effects. In all three cases, stochastic-threshold theory implies a non-linear relationship between mean erosion rate and average valley gradient (or relief). The predicted erosion-gradient relationship is consistent with data from experimental work (Lague *et al.*, 2003) and DEM analyses in two field settings (Snyder *et al.*, 2000, 2003; Lague and Davy, 2003). Finally, threshold-induced non-linearity is shown to have a strong impact on the dynamics and morphology of an eroding plateau. In particular, although the details vary, each of the three threshold erosion-transport models predicts concave-upward profiles terminating in a sharp slope break at the plateau surface.

Because the predicted morphology is distinctive at least in certain respects, the theory can in principle be tested by analyses of field case studies in which initial and boundary conditions are reasonably well known. Regardless of whether stochastic-threshold theory provides a more correct model of actual river basin dynamics, the fact that the morphologic outcomes are so distinctly different from conventional erosion laws means that there is a need for caution in applying these simpler erosion laws.

ACKNOWLEDGEMENTS

This paper was inspired by conversations with Peter Molnar on erosion and flood frequency; it was he who suggested the alternative form of the erosion and transport laws. I am indebted to Rafael Bras, Daniel Collins, Nicole Gasparini, Peter Solyom, Noah Snyder, and Kelin Whipple for valuable comments and numerous discussions of these issues. The CHLD model was originally developed at MIT by S. Lancaster, N. Gasparini, R. Bras, and G. Tucker. I am grateful to Chris Paola and an anonymous reviewer for very helpful reviews. Financial support for this research was provided by the US Army Research Office (DAAD19-01-1-0615).

REFERENCES

- Abrahams AD, Parsons AJ, Wainwright J. 1994. Resistance to overland flow on semiarid grassland and shrubland hillslopes, Walnut Gulch, southern Arizona. *Journal of Hydrology* **156**: 431–446.
- Baldwin JA, Whipple KX, Tucker GE. 2003. Implications of the stream-power river incision model for the post-orogenic decay of topography. *Journal of Geophysical Research* **108**: doi 10.1029/2001JB000550.
- Benda L, Dunne T. 1997a. Stochastic forcing of sediment supply to channel networks from landsliding and debris flow. *Water Resources Research* **33**: 2849–2863.
- Benda L, Dunne T. 1997b. Stochastic forcing of sediment routing and storage in channel networks. *Water Resources Research* **33**: 2865–2880.
- Boardman J, Favis-Mortlock D. 1999. Frequency-magnitude distributions for soil erosion, runoff and rainfall – a comparative analysis. *Zeitschrift für Geomorphologie, Supplement Band* **115**: 51–70.
- Bridge JS, Dominic DD. 1984. Bed load grain velocities and sediment transport rates. *Water Resources Research* **20**: 476–490.
- Dade WB, Friend PF. 1998. Grain-size, sediment transport regime and channel slope of alluvial rivers. *Journal of Geology* **106**: 661–675.
- Densmore AL, Ellis MA, Anderson RS. 1998. Landsliding and the evolution of normal-fault-bounded mountains. *Journal of Geophysical Research* **103**: 15 203–15 219.
- Dietrich WE, Wilson CJ, Montgomery DR, McKean J. 1993. Analysis of erosion thresholds, channel networks, and landscape morphology using a digital terrain model. *Journal of Geology* **101**: 259–278.
- Eagleson PS. 1978. Climate, soil, and vegetation: 2. the distribution of annual precipitation derived from observed storm sequences. *Water Resources Research* **14**: 713–721.
- Foster GR, Meyer LD. 1972. A closed-form erosion equation for upland areas. In *Sedimentation: Symposium to Honor Professor H. A. Einstein*, Shen HW (ed.). Colorado State University: Fort Collins, CO; 12.1–12.19.
- Fuller C, Willett SD, Slingerland R, Hovius N. 2003. A stochastic model of sediment supply, transport and storage in a Taiwan mountain drainage basin. *Journal of Geology* **111**(1): 71–88.
- Gomez B, Church M. 1989. An assessment of bed load sediment transport formulae for gravel bed rivers. *Water Resources Research* **25**(6): 1161–1186.
- Hasbargen LE, Paola C. 2000. Landscape instability in an experimental drainage basin. *Geology (Boulder)* **28**(12): 1067–1070.
- Hawk KL. 1992. *Climatology of station storm rainfall in the continental United States: parameters of the Bartlett-Lewis and Poisson rectangular pulses models*. MS thesis, Department of Civil and Environmental Engineering, Massachusetts Institute of Technology.
- Howard AD. 1980. Thresholds in river regimes. In *Thresholds in Geomorphology*; Coates DR, Vitek JD (eds). Allen and Unwin: Boston; 227–258.

- Howard AD. 1994. A detachment-limited model of drainage basin evolution. *Water Resources Research* **30**: 2261–2285.
- Howard AD, Kerby G. 1983. Channel changes in badlands. *Geological Society of America Bulletin* **94**: 739–752.
- Kirkby MJ. 1994. Thresholds and instability in stream head hollows: a model of magnitude and frequency for wash processes. In *Process Models and Theoretical Geomorphology*, Kirkby MJ (ed.). John Wiley: New York; 295–314.
- Knox JC. 1983. Responses of river systems to Holocene climates. In *Late Quaternary environments of the United States: volume 2, The Holocene*; Wright HE, Porter SC (eds). University of Minnesota Press: Minneapolis; 26–41.
- Lague D, Davy P. 2003. Constraints on the long-term colluvial erosion law by analyzing slope-area relationships at various tectonic uplift rates in the Siwaliks Hills (Nepal). *Journal of Geophysical Research* **108**(B2): doi:10.1029/2002JB001893.
- Lague D, Crave A, Davy P. 2003. Laboratory experiments simulating the geomorphic response to tectonic uplift. *Journal of Geophysical Research* **108**(B1): doi:10.1029/2002JB001785.
- Leopold LB. 1951. Rainfall frequency: an aspect of climatic variation. *Transactions of the American Geophysical Union* **32**: 347–357.
- Leopold L, Maddock T. 1953. *The hydraulic geometry of stream channels and some physiographic implications*. Professional Paper 252, United States Geological Survey.
- Meyer-Peter E, Müller R. 1948. Formulas for bed-load transport, Proc. Second Congress: Stockholm. *International Association of Hydraulic Structures Research* **30**: 3203–3212.
- Molnar P. 2001. Climate change, flooding in arid environments, and erosion rates. *Geology* (Boulder) **29**(12): 1071–1074.
- Molnar P, England P. 1990. Late Cenozoic uplift of mountain ranges and global climate change: chicken or egg? *Nature* **346**: 29–34.
- Paola C, Seal R. 1995. Grain size patchiness as a cause of selective deposition and down-stream fining. *Water Resources Research* **31**(5): 1395–1407.
- Parker G. 1978. Self-formed straight rivers with equilibrium banks and mobile bed. Part 2. The gravel river. *Journal of Fluid Mechanics* **89**: 127–148.
- Press WH, Flannery BP, Teukolsky SA, Vetterling WT. 1988. *Numerical Recipes in C: The Art of Scientific Computing*. Cambridge University Press: Cambridge.
- Prosser IP, Dietrich WE. 1995. Field experiments on erosion by overland flow and their implication for a digital terrain model of channel initiation. *Water Resources Research* **31**(11): 2867–2876.
- Prosser IP, Rustomji P. 2000. Sediment transport capacity relations for overland flow. *Progress in Physical Geography* **24**: 179–193.
- Prosser IP, Slade CJ. 1994. Gully formation and the role of valley-floor vegetation, south-eastern Australia. *Geology* **22**: 1127–1130.
- Rosenbloom NA, Anderson RS. 1994. Hillslope and channel evolution in a marine terraced landscape, Santa Cruz, California. *Journal of Geophysical Research, B, Solid Earth and Planets* **99**(7): 14 013–14 029.
- Sklar LS, Dietrich WE. 2001. Sediment and rock strength controls on river incision into bedrock. *Geology* (Boulder) **29**(12): 1087–1090.
- Slingerland RL, Harbaugh JW, Furlong KP. 1994. *Simulating Clastic Sedimentary Basins*. Prentice-Hall: New York.
- Snyder NP, Whipple KX, Tucker GE, Merritts DJ. 2000. Landscape response to tectonic forcing: DEM analysis of stream profiles in the Mendocino triple junction region, northern California. *Geological Society of America Bulletin* **112**: 1250–1263.
- Snyder NP, Whipple KX, Tucker GE. 2003. The importance of a stochastic distribution of floods and erosion thresholds in the bedrock river incision problem. *Journal of Geophysical Research* **108**(B2): doi:10.1029/2001JB001655.
- Talling PJ. 2000. Self-organization of river networks to threshold states. *Water Resources Research* **36**(4): 1119–1128.
- Tucker GE, Bras RL. 1998. Hillslope processes, drainage density, and landscape morphology. *Water Resources Research* **34**: 2751–2764.
- Tucker GE, Bras RL. 2000. A stochastic approach to modeling the role of rainfall variability in drainage basin evolution. *Water Resources Research* **36**(7): 1953–1964.
- Tucker GE, Slingerland RL. 1994. Erosional dynamics, flexural isotasy, and long-lived escarpments; a numerical modeling study. *Journal of Geophysical Research, B, Solid Earth and Planets* **99**(6): 12 229–12 243.
- Tucker GE, Slingerland RL. 1997. Drainage basin response to climate change. *Water Resources Research* **33**(8): 2031–2047.
- Tucker GE, Whipple KX. 2002. Topographic outcomes predicted by stream erosion models: sensitivity analysis and intermodel comparison. *Journal of Geophysical Research* **107**(B9): doi:10.1029/2001JB000162.
- Tucker G, Lancaster S, Gasparini N, Bras R. 2001a. *The Channel-Hillslope Integrated Landscape Development model (CHILD)*, *Landscape erosion and evolution modeling*. Kluwer Academic/Plenum Publishers: New York.
- Tucker GE, Lancaster ST, Gasparini NM, Bras RL, Rybarczyk SM. 2001b. An object-oriented framework for distributed hydrologic and geomorphic modeling using triangulated irregular networks. In *GeoComp 99: GeoComputation and the geosciences*. Pergamon: New York; 959–973.
- Weissel JK, Seidl MA. 1998. Inland propagation of erosional escarpments and river profile evolution across the Southeast Australian passive continental margin. In *Rivers over Rock: Fluvial Processes in Bedrock Channels*. American Geophysical Union: Washington, DC; 189–206.
- Whipple KX. 2001. Fluvial landscape response time; how plausible is steady-state denudation? In *The steady-state orogen; concepts, field observations, and models*. Yale University Kline Geology Laboratory: New Haven, CT; 313–325.
- Whipple KX, Tucker GE. 1999. Dynamics of the stream power river incision model: implications for height limits of mountain ranges, landscape response timescales and research needs. *Journal of Geophysical Research* **104**: 17 661–17 674.
- Whipple KX, Tucker GE. 2002. Implications of sediment-flux-dependent river incision models for landscape evolution. *Journal of Geophysical Research, B, Solid Earth* **107**(2): doi:10.1029/2000JB000044.
- Whipple KX, Hancock GS, Anderson RS. 2000. River incision into bedrock; mechanics and relative efficacy of plucking, abrasion, and cavitation. In *Special focus on the Himalaya*, Geissman J-W, Glazner AF (eds). *Geological Society of America Bulletin* **112**(3): 490–503.
- Willett SD, Brandon MT. 2002. On steady states in mountain belts. *Geology* (Boulder) **30**(2): 175–178.
- Willgoose G, Bras RL, Rodriguez II. 1991. A coupled channel network growth and hills-lope evolution model; 1, Theory. *Water Resources Research* **27**(7): 1671–1684.
- Yang CT. 1996. *Sediment Transport: Theory and Practice*. McGraw Hill: New York.
- Zhang P, Molnar P, Downs WR. 2001. Increased sedimentation rates and grain sizes 2–4 Myr ago due to the influence of climate change on erosion rates. *Nature* (London) **410**(6831): 891–897.

Appendix E

Collins, D., Bras, R., and Tucker, G.E. (2004) Modeling the effects of vegetation-erosion coupling on landscape evolution: *Journal of Geophysical Research - Earth Surface*, v. 109, no. F3, F03004, doi:10.1029/2003JF000028.

Modeling the effects of vegetation-erosion coupling on landscape evolution

D. B. G. Collins and R. L. Bras

Department of Civil and Environmental Engineering, Massachusetts Institute of Technology, Cambridge, Massachusetts, USA

G. E. Tucker¹

School of Geography and the Environment, Oxford University, Oxford, UK

Received 10 February 2003; revised 25 May 2004; accepted 3 June 2004; published 3 August 2004.

[1] From rainfall interception at the canopy to added soil cohesion within the root zone, plants play a significant role in directing local geomorphic dynamics, and vice versa. The consequences at the regional scale, however, are known in less quantitative terms. In light of this, the numerical Channel-Hillslope Integrated Landscape Development model is equipped with coupled vegetation-erosion dynamics, allowing for sensitivity analysis on the various aspects of vegetation behavior. The processes considered are plant growth, plant death, and the additional resistance imparted by plants against erosion. With each process is associated a single parameter, whose effects on the spatiotemporal nature of a 1 km² basin is studied. Through their inhibition of erosion, plants steepened the topography and reduced drainage density, yet, in doing so, made erosive events more extreme. Plants more susceptible to erosion act to decouple neighboring cells and cause extensive and perennial network and channel adjustments. **INDEX TERMS:** 1824 Hydrology: Geomorphology (1625); 1851 Hydrology: Plant ecology; 3210 Mathematical Geophysics: Modeling; 1815 Hydrology: Erosion and sedimentation; **KEYWORDS:** ecogeomorphology, fluvial, erosion, landscape, modeling

Citation: Collins, D. B. G., R. L. Bras, and G. E. Tucker (2004), Modeling the effects of vegetation-erosion coupling on landscape evolution, *J. Geophys. Res.*, 109, F03004, doi:10.1029/2003JF000028.

1. Introduction

[2] Vegetation has been long considered an important ingredient of geomorphic processes. *Lyell* [1834, p. 113] remarks that

It is well known that a cover of herbages and shrubs may protect a loose soil from being carried away by rain, or even by the ordinary action of a river, and may prevent hills of loose sand from being blown away by the wind; for the roots bind together the separate particles into a firm mass and the leaves intercept the rainwater, so that it dries up gradually, instead of flowing off in a mass and with great velocity.

Root cohesion and diminished runoff are identified here as contributors to reduced erosion. These themes are echoed in *Viles's* [1990] synopsis of biogeomorphology and in many accounts of geomorphic response to land use change.

[3] The expansion of pinyon-juniper woodlands in the western United States in the last 100 years has led to accelerated erosion, threatening long-term ecosystem stability and productivity [*Wilcox et al.*, 1996]. The cause is competition-induced loss of the subcanopy and subsequent weakening of the protective vegetative soil cover. The

combined effect of agriculture following logging in North Fish Creek, Wisconsin, from the late 1880s resulted in threefold increases in flood peaks and fivefold increases in sediment loads [*Fitzpatrick and Knox*, 2000]. Further examples are provided by *Clark and Wilcock* [2000], *DeRose et al.* [1998], and *Nortcliff et al.* [1990], illustrating the diversity and complexity of vegetation-erosion interactions.

[4] The impacts of geomorphology on ecology have also been studied, most notably by *Hack and Goodlett* [1960] in the central Appalachians of the United States: forest form changes with topography. *Thom* [1967], *Pickup and Chewings* [1996], *Florinsky and Kuryakova* [1996], and *Nichols et al.* [1998] reiterate this observation in a diverse array of ecosystems, highlighting issues of erosion and sedimentation, slope aspect, and soil moisture accumulation.

[5] These regional effects result from plant-scale changes in geomorphic processes, of which *Lyell* [1834] mentioned but a few. They may be hydrologic, hydraulic, chemical, or geotechnical in nature.

[6] Plant canopies intercept rainfall, changing its volume, pathway (stemflow versus throughfall), and erosivity, all of which are species-dependent [*Aldridge and Jackson*, 1968; *Gregory and Walling*, 1973; *Lee*, 1980; *Mosley*, 1982; *Woo et al.*, 1997; *Wainwright et al.*, 2000]. Surface litter provides further protection against raindrop impact [*Geddes and Dunkerley*, 1999] and also acts to

¹Now at Cooperative Institute for Research in Environmental Sciences and Department of Geological Sciences, University of Colorado, Boulder, Colorado, USA.

store water [Sala and Calvo, 1990]. The soil's infiltration capacity and hydraulic conductivity are generally increased by the presence of roots and vacant macropores [Whipkey, 1966; Nassif and Wilson, 1975; Greenway, 1987; Newman et al., 1998], while transpiration reduces the soil moisture and pore pressures [Brenner, 1973; Federer, 1973; Biddle, 1983].

[7] Flow resistance may increase or decrease, depending on the distribution of surface plants and debris [Chow, 1959; Reid, 1989; Smock et al., 1989; Prosser and Slade, 1994; Abrahams et al., 1995; Prosser et al., 1995]. These hydraulic effects, in conjunction with the additional cohesion offered by roots, are considered responsible for elevated thresholds for sediment entrainment [Graf, 1979; Reid, 1989; Prosser and Slade, 1994; Prosser et al., 1995]. In studying a montane area of Colorado, Graf [1979] identified a biomass-dependent critical tractive force of channel flow separating cut from uncut channels. Similarly, Reid [1989] and Prosser and Slade [1994] have determined a range of critical shear stresses corresponding to various vegetation states.

[8] Slope stability may also increase or decrease in response to plant roots. In addition to subsurface hydrologic changes, plants may anchor regolith to itself or to bedrock and transmit wind and surcharge forces [Greenway, 1987; Preston and Crozier, 1999]. Much work has been conducted on root strength [O'Loughlin, 1974; Ziemer, 1981; Terwilliger and Waldron, 1991; Schmidt et al., 2001]. Changes in landslide occurrence are often associated with changes in land use, particularly logging, in microclimate and in climate [Glade, 2003; Jakob, 2000; Johnson and Wilcock, 2002; Trauth et al., 2000].

[9] The most notable process affected by vegetation on which Gilbert [1877] commented was the heightened rate of chemical weathering associated with plant growth and decay. More quantitative assessments of the role of biologically associated chemicals and the mechanical stress of plant roots have been made since [Yatsu, 1988; Viles, 1990; Lucas, 2001].

[10] An ideal testing ground and nursery for hypotheses of regional ecogeomorphology is numerical simulation. Numerical modeling of abiotic landscape evolution has progressed extensively since Culling's [1960] seminal work. In addition to the standard fluvial component [Willgoose et al., 1991; Howard, 1994; Tucker and Slingerland, 1996; Tucker and Bras, 2000], the register of simulated processes includes tectonics [Koons, 1989; Beaumont et al., 1992; Tucker and Slingerland, 1994], mass wasting [Densmore et al., 1997; Howard, 1997; Densmore et al., 1998], and seepage erosion [Howard, 1995; Luo, 2001]. Often, consideration will be made of the biotic environment, such as the effects vegetation has on flow hydraulics and sediment transport [Mitas and Mitasova, 1998; Coulthard et al., 2000; Evans and Willgoose, 2000], but these are generally static, exogenous factors.

[11] Of the models that address the dynamic behavior of vegetation, and its effect on erosion, most notable are the agricultural Water Erosion Prediction Project (WEPP) [Flanagan and Nearing, 1995] and the geomorphic models of Kirkby [1995], Benda and Dunne [1997], Howard [1999], Lancaster et al. [2001], and Gabet and Dunne [2003]. Foci of the latter set include mass wasting and root

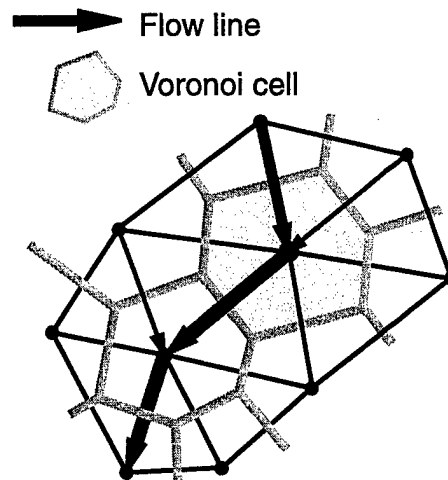


Figure 1. A set of nodes and their corresponding Voronoi cells. Surface discharge passes from node to node across cell edges.

cohesion, fire, disturbance and fluvial erosion thresholds, and hydrologic and climatologic processes. A report by Tucker and Bras [1999] is the source of the vegetation model explored here and will be detailed in section 2.1.

2. Model Formulation

[12] The numerical model used in this research is the Channel-Hillslope Integrated Landscape Development (CHILD) model [Lancaster, 1998; Tucker and Bras, 1999, 2000; Tucker et al., 2001a, 2001b]. The more relevant features of the model are presented here; highlighted are the vegetation-related modifications of Tucker and Bras [1999].

[13] CHILD imitates landscape evolution by simulating discrete rainfall events, routing the runoff through an elevation field, and deforming this field according to an interplay of various geomorphic processes. This field is represented by a triangular irregular network of nodes defining a mesh of Voronoi polygons (Figure 1). In these simulations the distribution of polygon geometries is essentially uniform. Channel width is determined from hydraulic geometry relationships [Leopold and Maddock, 1953] and is embedded within a cell, over which channel changes are averaged. The geomorphic processes considered here are fluvial erosion, hillslope diffusion, and tectonic uplift or base-level lowering. Sequential change in the elevation field is represented by

$$\frac{\partial z}{\partial t} = U - \epsilon + \frac{\partial z}{\partial t} \Big|_{\text{creep}}, \quad (1)$$

where U is the rate of uniform and steady tectonic uplift or base-level lowering, ϵ is the fluvial erosion rate, and $(\partial z / \partial t)_{\text{creep}}$ is the diffusional flux.

[14] Each iteration comprises a storm event, uniform in space and time, and an interstorm period. Storm and interstorm durations are independent exponential random variables, as is the storm intensity. The distributions have

means of \bar{T}_r , \bar{T}_b , and \bar{P} , respectively [Eagleson, 1978]:

Rainfall intensity

$$f(P) = \frac{1}{\bar{P}} \exp(-P/\bar{P}) \quad (2)$$

Storm duration

$$f(T_r) = \frac{1}{\bar{T}_r} \exp(-T_r/\bar{T}_r) \quad (3)$$

Interstorm duration

$$f(T_b) = \frac{1}{\bar{T}_b} \exp(-T_b/\bar{T}_b) \quad (4)$$

[15] CHILD permits the use of a number of runoff production schemes. In this study, Horton (infiltration-excess) runoff is assumed, in which the precipitation rate, P , less the infiltration rate, I_c , amounts to the rate of runoff, q , yielded by each Voronoi cell:

$$q = \begin{cases} a(P - I_c) & : P > I_c \\ 0 & : P \leq I_c \end{cases} \quad (5)$$

where a is the Voronoi cell area. Surface runoff at a point becomes the sum of the contributions of the upstream and local sources.

[16] A Hortonian model is adopted for simplicity's sake, reducing the direct applicability to fewer environments. Compared with saturation excess generation, the only tangible difference will likely lie in shorter hillslope lengths. Thus the dynamics of fluvial erosion-vegetation coupling would likely be comparable.

[17] Sediment transport processes on hillslopes, soil creep, and rain splash are modeled as a linear diffusion process [e.g., Culling, 1960]:

$$\frac{\partial z}{\partial t} \Big|_{\text{creep}} = k_d \nabla^2 z, \quad (6)$$

where k_d is a diffusion transport coefficient. Other forms of mass wasting (landslides, debris flows) are not considered, again for simplicity's sake. This limits the applicability of the model to low-relief regions and justifies the linear diffusion model.

[18] Fluvial erosion and sediment transport is based on an excess stream power, or excess shear stress, model [Tucker and Bras, 2000]:

$$\epsilon = \begin{cases} k_b(\tau - \tau_c)^p & : \tau > \tau_c \\ 0 & : \tau \leq \tau_c \end{cases} \quad (7)$$

$$\tau = k_t Q^{mb} A^{ma} S^{nb}, \quad (8)$$

where ϵ is the sediment detachment rate, k_b is an erodibility parameter, τ is the applied local shear stress, τ_c is the critical shear stress, a threshold for sediment entrainment, p is a parameter that depends on the mode of sediment transport, k_t is a hydraulic roughness coefficient, Q is the volumetric discharge, A is the drainage area, and mb , ma , and nb are exponents that depend on the nature of the detachment process. Values for the coefficients used are in Table 1.

Table 1. Fixed Model Parameter Values

Parameter	Value
U , mm yr ⁻¹	0.1
I_c , mm h ⁻¹	0
\bar{P} , mm h ⁻¹	1.6
\bar{T}_r , days	0.5
\bar{T}_b , days	6.5
k_d m yr ⁻¹	0.01
k_b , kg ^{-1.5} m ^{1.5} s ²	0.1
p	1.5
k_t , kg m ^{-0.05} yr ^{0.55}	1.5
mb	0.45
ma	-0.15
nb	0.7

[19] For the purposes of this work the entire catchment is considered detachment limited, akin to a number of other studies [Seidl and Dietrich, 1992; Anderson, 1994; Howard et al., 1994; Tucker and Slingerland, 1994, 1996, 1997; Moglen and Bras, 1995]. This is somewhat justified by the caprock effect cohesive vegetation plays in protecting the soil. All runoff erosion is thus sediment flux from the basin.

[20] One underlying assumption of the model is that regolith is sufficiently thick not to alter the erosional processes. Weathering rate, buffered by regolith thickness, is implicitly assumed to keep pace with surficial erosion. As a by-product, the strong association between vegetation and weathering becomes redundant.

2.1. Dynamic Vegetation Modeling

[21] As discussed in section 1, vegetation affects landscape evolution in a multitude of ways. However, this model is not an attempt to reproduce a landscape per se but rather to better understand the mechanisms by which the landscape operates. This cannot be accomplished without an isolated sensitivity analysis of such mechanisms. A bare ecogeomorphic minimum is to include both vegetation dynamics and a coupling with the erosion, as set forward by Tucker and Bras [1999].

[22] The state variable used to describe vegetation is the channel and riparian vegetation density, V . The variable V ranges from 0 to 1 and represents the proportional coverage at or near ground level. It can be taken to represent either a single plant species or a community. As these channels may be ephemeral in both hydrologic and erosional senses, what channel vegetation exists need not be aquatic.

2.1.1. Vegetation Growth

[23] Following disturbance, vegetation will begin to regrow and colonize newly cleared land. Growth is often modeled with a logistic equation, in which growth rates are small both at low density (reproduction limited) and at high density (resource limited) [e.g., Thornes, 1990]. However, as the present focus is on channel and riparian vegetation only and given the proximity of both nonchannel and uneroded channel plants as well as the fecundity of plants in general, the reproduction limitation on growth rate is less consequential. This yields the following mathematical relation:

$$\frac{dV}{dt} = \frac{1}{T_v} (1 - V), \quad (9)$$

where T_v is a growth timescale of the particular vegetation communities. Therefore, simulated here, the only resource

for which plants compete is space, a proxy for photosynthetically active radiation. This is not to disregard the importance of soil moisture, nutrients, and other factors controlling growth: These are considered to play secondary roles.

[24] T_v represents the time taken for a plant to grow to a stage where it can noticeably limit erosion. This is distinct from the time until maturity or average height. Three years has been considered the length of uninterrupted time required for blue gramma (*Bouteloua gracilis*), a tufted perennial grass, to establish to a point where it can withstand large erosion events in gully rehabilitation efforts in Colorado (J. Kulbeth, personal communication, 2000). For attributes of the plant functional types being considered, grasses and smaller shrubs as well as climate, a useful range of experimental values is thus T_v (years) $\in \{1, 2, 3, 5, 10\}$. The growth time constant will vary among species, but here we adopt a single value to represent the plant community as a whole.

2.1.2. Vegetation Loss

[25] In nature, plants die and are removed by a wide variety of processes, such as fire, herbivory, and resource stress. Here only loss due to fluvial erosion is considered as it is the fluvial properties of vegetation that are being explored. Thus as regolith is removed at the channel head, bottom, or bank, so too is the vegetation rooted into that substrate. This necessarily depends upon the tendency of basal erosion to undermine or stress plants. Undermining of plants would depend on the vertical root distribution for each plant within the community, the soil cohesion, and nominal plant surcharge and wind loading. Stress, which may be seen as starving a plant of water and nutrients by dislocating its reservoir, in turn depends on plant physiology and root distribution. It is thus not a trivial matter to relate soil loss to vegetation loss. The simplest of models, a linear dependence on excess shear stress, is therefore used:

$$\frac{dV}{dt} = \begin{cases} -K_v V (\tau - \tau_c) & : \tau > \tau_c \\ 0 & : \tau \leq \tau_c \end{cases} \quad (10)$$

in which K_v is a species-dependent vegetation erodibility parameter.

[26] Equation (10) has no quantitative basis as of yet, making K_v the parameter about which the least is known. For this reason the initial stage of the study simulated landscapes with expected values of the different parameters in an attempt to identify the range of values of K_v that yielded realistic landforms. The criterion for an acceptable value was a satisfactory slope for a given drainage area; the value of K_v obtained was $1 \text{ Pa}^{-1} \text{ yr}^{-1}$. To study the effect of this parameter on the landscape, it was varied over two orders of magnitude: $K_v (\text{Pa}^{-1} \text{ yr}^{-1}) \in \{0.1, 0.5, 1, 5, 10\}$.

2.1.3. Erosion Reduction by Plants

[27] Vegetation would modify many of the process models within CHILD: the precipitation volume, infiltration capacity, hydraulic roughness, detachment coefficient, detachment threshold, and diffusion coefficient. Yet for the purpose of a focused study, only one is selected. Arguably, the most important process to consider is the governing regolith erodibility. In an excess shear stress model this is described by three parameters, k_b , τ_c , and p , and experiments on τ_c have been the most rigorous [Reid, 1989; Prosser

and Slade, 1994; Prosser et al., 1995]. From these data, conservative thresholds for sediment detachment and entrainment for a range of conditions and species, generally herbaceous, may be extracted. The effective critical shear stress, τ_c , is thus modeled as the sum of resistances imparted by the soil's cohesion, $\tau_{c,s}$, and the addition due to the protective vegetation, $\tau_{c,v}$, factored by local vegetation density,

$$\tau_c = \tau_{c,s} + V\tau_{c,v} \quad (11)$$

The critical shear stress due to the soil alone is assumed constant, while that due to a plant community is dynamic and species-, or community-, dependent. This permits spatially and temporally variable critical shear stresses.

[28] A range of total critical shear stresses of 20–200 Pa appears to represent a wide range of vegetation states from bare ground to a secure, resistant vegetation cover of herbs and shrubs. Taking a mean value to be 100 Pa and the contribution from soil alone, $\tau_{c,s}$, to be 20 Pa, the mean contribution from plants is considered 80 Pa. A range of useful values, to cover a wide range of plant conditions or species, is therefore $\tau_{c,v} (\text{Pa}) \in \{20, 50, 80, 130, 180\}$.

2.2. Simulation Procedure

[29] Numerical simulations of landscape evolution are performed, in which each parameter of the vegetation model is varied to ascertain its effect on the nature of a generalized low-relief landscape with semiarid grassland and Hortonian overland flow. No attempt is made to validate the model as it is intended solely as a framework to explore potential impacts of vegetation-erosion coupling in long-term landscape evolution.

[30] The initial topography for each simulation was a $1 \times 1 \text{ km}$ plateau, with an elevation of 300 m and with an average node spacing of 50 m. Drainage is only permitted through a single corner of the domain. Simulations, thus started, are left to evolve until some long-term equilibrium condition is reached. This was a subjective decision based on consistency of the mean elevation time series over a suitably long simulation time. Since the nature of the equilibrium dynamics were unknown before simulating, no quantitative measure was used to identify its onset. After each simulation had reached equilibrium the areal mean elevation and vegetation density were recorded each year for 500,000 years. During this time the complete spatial description (elevation and vegetation cover) of the landscape was recorded at most every 20,000 years.

[31] There are 14 simulations in total, covering 14 sets of parameter values. Since essentially two questions are asked, two control runs are developed. The first control case does not incorporate the effects of vegetation and is denoted "Bare." The second incorporates median values of each vegetation parameter, allowing a base for sensitivity analyses, and is denoted "Basic." For each of the three vegetation parameters, four additional simulations were run, with the parameters and nomenclature as in Table 2.

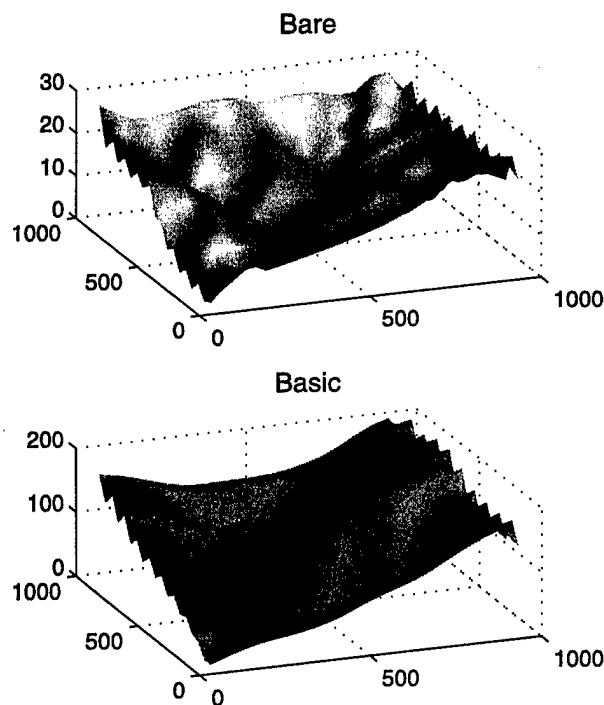
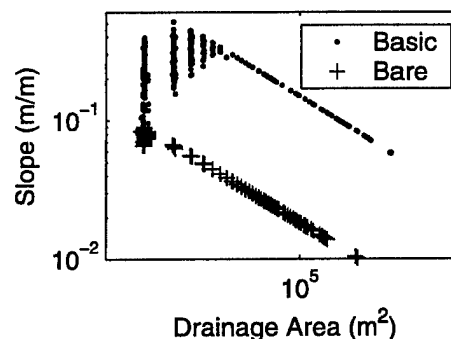
3. Topography

[32] The most striking evidence of vegetation-dominated erosion is in the topographies of the Bare and Basic

Table 2. The 14 Simulations With Their Set of Vegetation Parameter Values

Simulation	$\tau_{c,v}$, Pa	T_v , years	K_v , $\text{Pa}^{-1} \text{y}^{-1}$
Bare	0
Basic	80	3	1
Tau1	20	3	1
Tau2	50	3	1
Tau4	130	3	1
Tau5	180	3	1
Tv1	80	1	1
Tv2	80	2	1
Tv4	80	5	1
Tv5	80	10	1
Kv1	80	3	0.1
Kv2	80	3	0.5
Kv4	80	3	5
Kv5	80	3	10

simulations (Figure 2). The vegetated landscape has greater relief and is dissected less than its barren counterpart. This is likewise apparent in their slope-area relationships (Figure 3), which show a greater intercept of the fluvial slope-area (S-A) portion and a greater hillslope length for the vegetated simulation. These results are simply the projection of a higher critical shear stress, dynamic or not, on fluvial incision. While concavity remains constant, the greater threshold increases slopes and requires a greater drainage area to be exceeded before the onset of channelization, with the concomitant reduction in drainage density. Our analysis of the S-A relationships indicates that higher and steeper slopes result from higher $\tau_{c,v}$ and lower K_v , respectively; no discernible difference arises from variation of T_v .

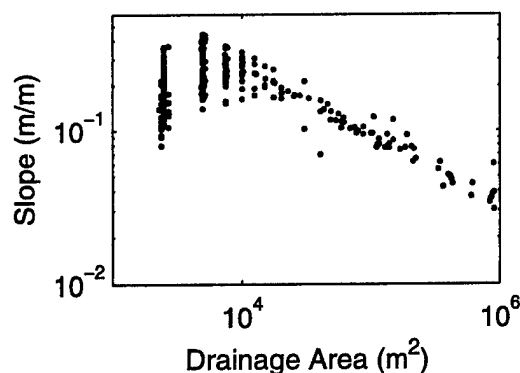
**Figure 2.** Equilibrium basins of the unvegetated Bare and vegetated Basic simulations. The barren landscape has lower relief and is more dissected.**Figure 3.** Slope-area (S-A) relationships for the equilibrium Bare and Basic landscapes of Figure 2, again showing the difference in slopes and hillslope lengths.

[33] While the fluvial portions of the S-A relations presented thus far are exceedingly straight, two simulations, Kv4 and Kv5, produced more scattered data (Figure 4). These simulations dealt with vegetation that is particularly susceptible to loss from erosion. The scatter is a result of over an order of magnitude greater number of cells whose flow direction changes during 500,000 years of equilibrium simulation compared with other simulations. These changes occurred predominantly in the hillslopes and lower-order channels but caused large downstream variations in drainage area, continually perturbing the channel and preventing attainment of a consistent grade.

[34] Differences in shear stress between neighboring cells, which inevitably arise, allow for a longitudinal variation in erosion rate. One cell may be eroding, while its neighbor is not. With a rapid loss of vegetation in the eroding cell, erosion is accentuated. The high K_v therefore acts to decouple spatially distributed cells, in turn instigating flow direction changes.

4. Time Series

[35] To assess the actual dynamics of an equilibrium landscape, time series of spatial mean elevation, z , erosion rate, E , and vegetation density, V , are considered. Elevation

**Figure 4.** Landscapes with highly erodible vegetation, Kv5, exhibiting scattered S-A data in the fluvial domain, a result of numerous changes in flow direction upstream and subsequent fluctuations in fluvial drainage area.

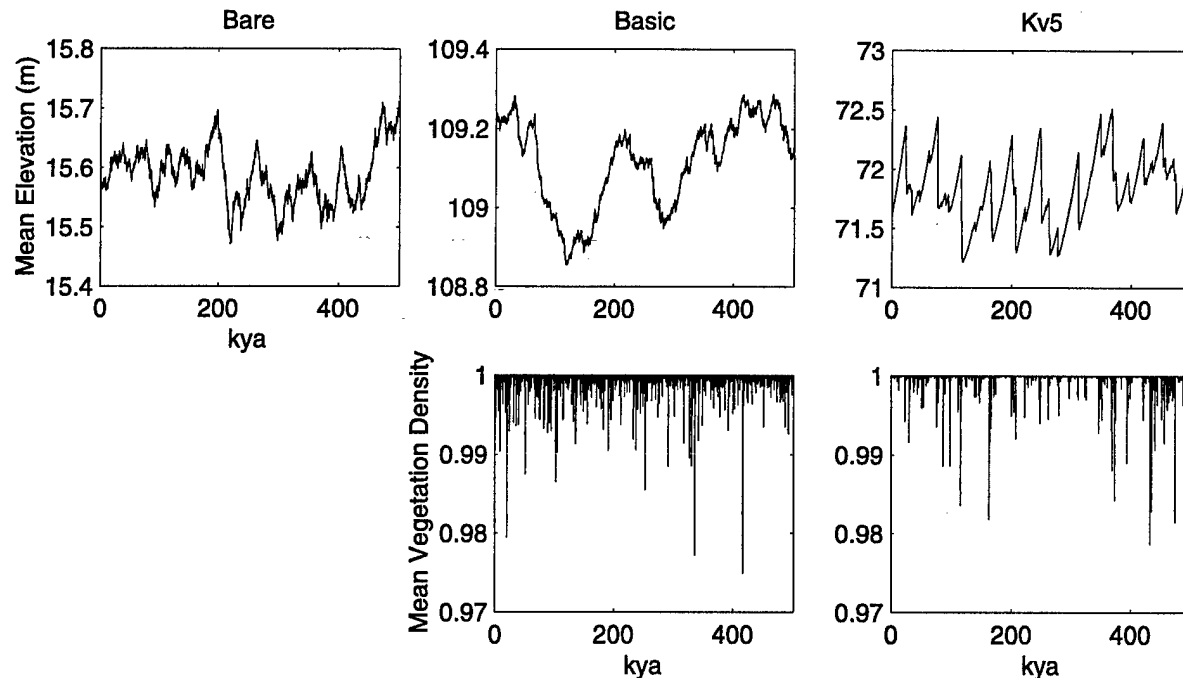


Figure 5. Mean elevation and vegetation cover 500,000 year time series for Bare, Basic, and Kv5.

and vegetation density are those values at the beginning of a time step of Δt . The mean erosion rate over this time is obtained as

$$E = U - \frac{\bar{z}_{t+\Delta t} - \bar{z}_t}{\Delta t}, \quad (12)$$

which, in the detachment limited system, equals sediment flux.

[36] Figure 5 illustrates mean elevation and vegetation dynamics of Bare, Basic, and Kv5 at the centennial resolution for 500,000 years. Bare and Kv5 represent two extremes, unvegetated and easily destroyed vegetation; Basic represents average vegetation conditions. The Bare and Basic elevation series are both rough, although the latter is slightly less so. All other simulations, save Kv4 and Kv5, resemble the Bare and Basic time series in this regard, as do their vegetation time series. There are subtle differences, however: Our analysis indicates that the variance of the mean elevation increases steadily with greater $\tau_{c,v}$ and that a similar trend is observed for K_v , while no such trend is evident for T_v . This increased variability derives from the destabilizing effect of temporarily increased slopes, which, once devegetated, find themselves oversteepened. Much larger erosive events are thus outcomes of more erosion-retardant vegetation. This highlights an issue of timescales: On the short term, strong vegetation may reduce erosion, yet after equilibrium is attained, net erosion is the same as without vegetation.

[37] Closer inspection of the Basic and Kv5 elevation time series spanning the first 50,000 years of the equilibrium series accentuates the differences between the two simulations (Figure 6). Kv5 is more continuous, with fewer abrupt, yet consequentially larger, erosive events. These events

follow long periods of steady net uplift. It is not these calm periods that cause such variation but rather the extensive loss of highly erodible vegetation during erosive storms. The increased variability in erosion as K_v increases implies that the dynamic vegetation provides inertia to a changing landscape.

[38] Spectral analysis of the time series (Figure 7) shows that the elevation series of Basic is a random walk process with uncorrelated white noise: the erosion. Vegetation density similarly shows no dominant frequency, a reasonable outcome given the strong coupling with erosion. These observations are essentially identical for all simulations except Kv4 and Kv5, and only in the erosion series power spectrum do they differ. For landscapes with highly erodible vegetation the erosion events are not uncorrelated. Instead, they also resemble a random walk, a further indication that the landscape characteristic possesses momentum. The breaking of symmetry between the vegetation and erosion spectra supports the spatial decoupling of erosion and vegetation to which the flow direction changes have been attributed, modulating the climate's stochastic signal.

5. Biogeography

[39] The time series show a landscape covered almost perennially with vegetation, interrupted intermittently by erosive events. Figure 8 depicts the probability distribution of vegetation states drawn from the entire set of Basic spatial data. It shows that the number of fully vegetated cells exceeds the others by two orders of magnitude and that no cells have cover $<99.7\%$. Since nonunity cover equates to active erosion, this provides an indication of the drainage density but also shows that despite a

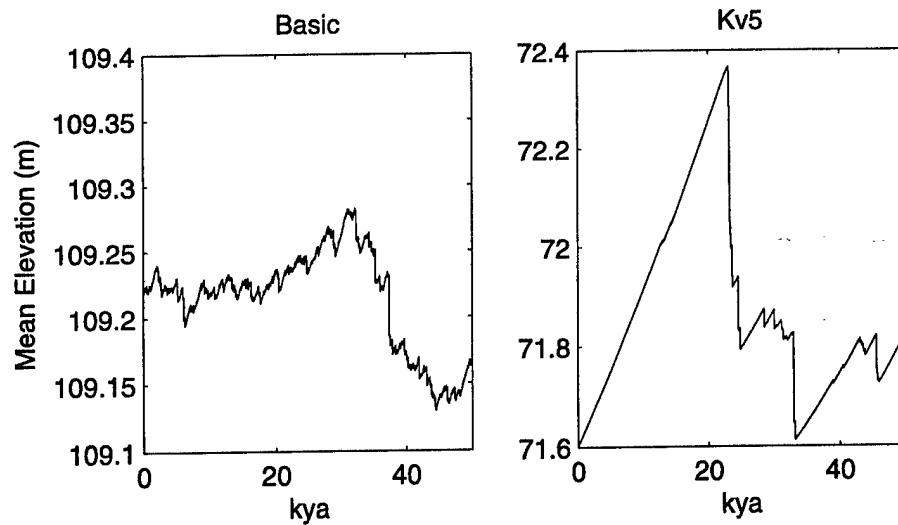


Figure 6. Mean elevation 50,000 year time series for Basic and Kv5.

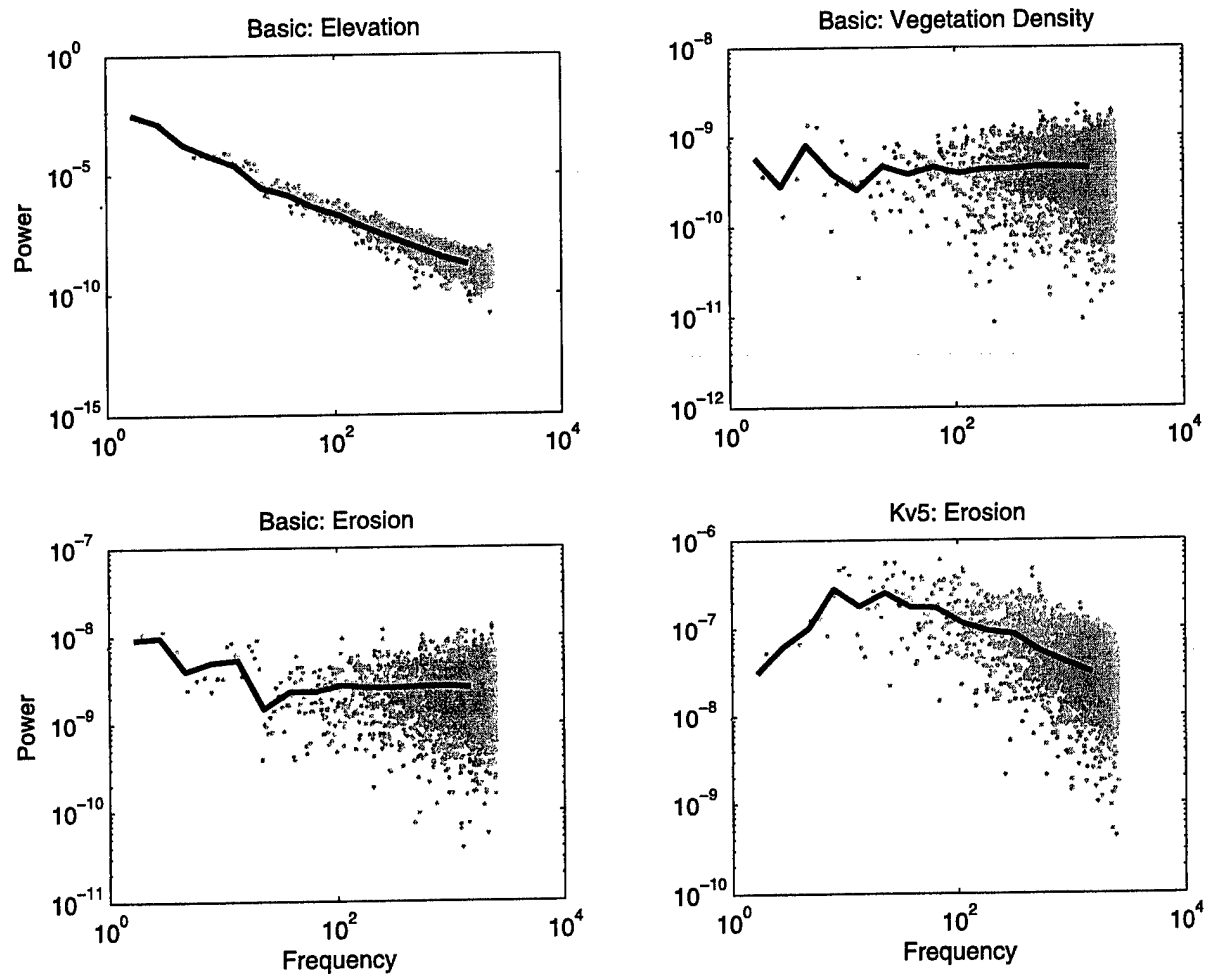


Figure 7. Power spectra of mean elevation, vegetation cover, and erosion rate for Basic and erosion rate for Kv5. Basic's elevation resembles an AR(1) process with uncorrelated white noise (erosion). All simulations resemble this, except for Kv4 and Kv5, and these differ only in their erosion spectra (also correlated).

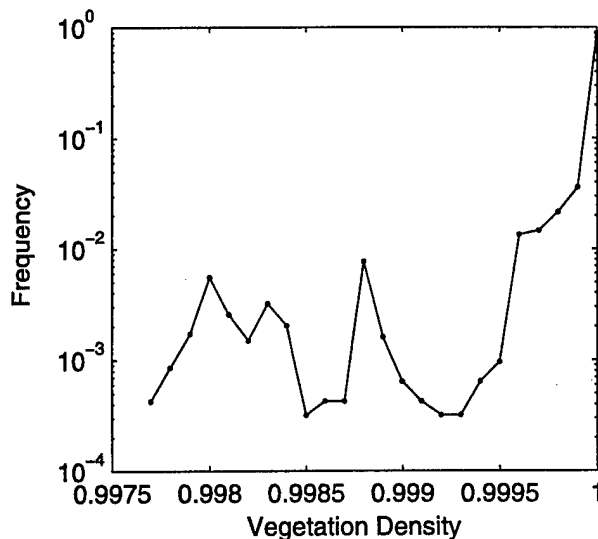


Figure 8. Distribution of spatial vegetation density of Basic over 500,000 years. The majority of states are fully vegetated, while the remainder are minimally unvegetated.

distinctly fluvial signature in the S-A data, channels are almost entirely vegetated.

[40] Dense cover is depicted in two consecutive vegetation maps of Basic (Figure 9). The sparser cells trace the drainage network, which is essentially constant. There are marginally fewer cells with subunity density in Figure 9b, indicating a reduction in active erosion and thus of instantaneous drainage density. Additionally, it is not the outlet that is more sparsely covered but rather the tributary nearest the outlet. This nonmonotonic variation of vegetation density along channels reflects the nonmonotonic nature of incision and excess shear stress.

[41] To explore the variability of vegetation states, and their correlation with drainage area, consider the proportion

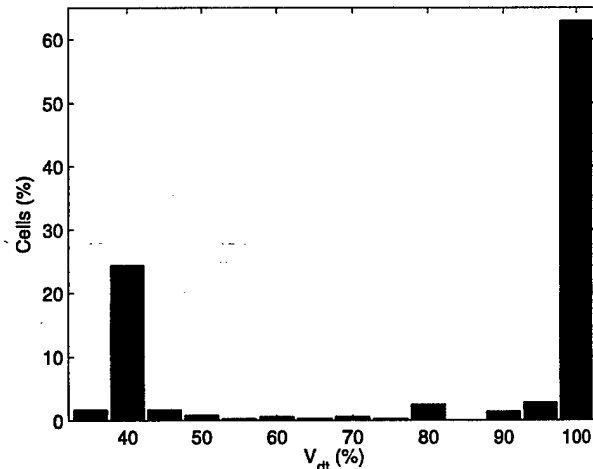


Figure 10. Distribution of V_{dt} , the duration a cell is fully vegetated over the entire Basic simulation. Cells with full time coverage are perennial hillslopes. The lower mode corresponds to the fluvial reaches.

of time a cell is fully vegetated, V_{dt} . As erosion necessarily causes a loss of vegetation, perpetual full cover ($V_{dt} = 100\%$) implies a perennial absence of fluvial erosion; Figure 10 shows that 63% of the domain are these pure hillslopes. The distribution is bimodal, however, with the lower mode corresponding to the more fluvial reaches. Mapped onto an averaged S-A diagram of Basic (Figure 11), one sees a separation in data based on V_{dt} . These contours obey the same scaling as the fluvial regime and indicate two important issues: (1) delineation of a specific drainage area as the divide between hillslope and channel is invalid and (2) inside the cloud of data points within the traditional hillslope region lie cells that are ephemeral channels in an erosional sense; the dominance of either erosion or diffusion fluctuates over time. These channels no longer have

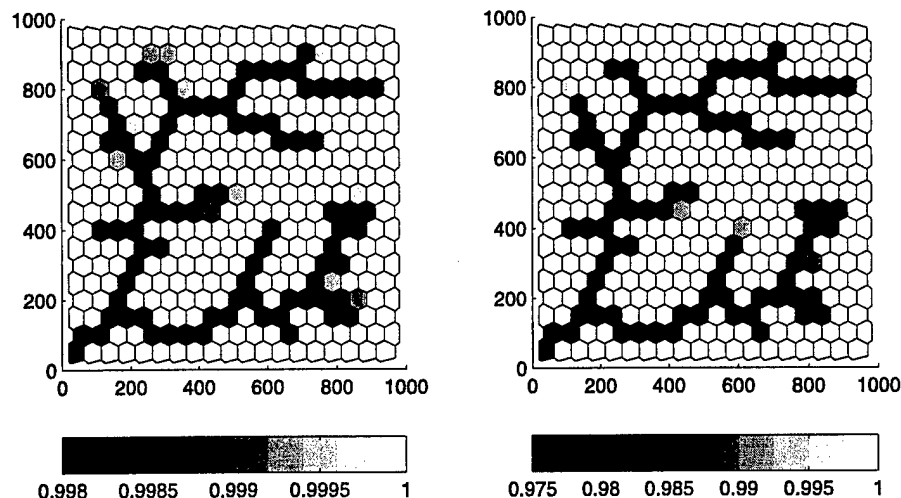


Figure 9. Two vegetation maps for Basic (with different scales) show the spatial and temporal variability of vegetation cover. With vegetation density related to erosion intensity, there is evidence of discontinuous incision.

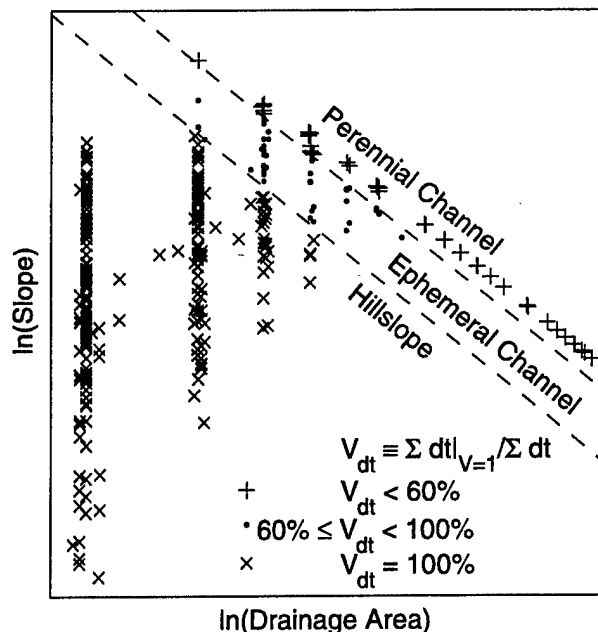


Figure 11. V_{dt} used to discriminate regions based on the varying dominance of diffusive and fluvial processes. The perennial channel is essentially purely fluvial, and the hillslope is purely diffusional. The ephemeral channel, in an erosional sense, is governed at times by fluvial erosion and at other times by diffusion.

a distinct head in time, nor is this channel head uniformly definable in S-A terms across the landscape. While these results are highlighted with the inclusion of vegetation, this is a purely abiotic phenomenon as it is the variation of applied shear stress derived from the stochastic climate that causes fluctuations in channel head location, and it is the network geometry that is likely the cause of the spatially variable nature of these channel heads. Both of these phenomena deserve more attention outside the context of a vegetation mantle.

[42] Since there are no tangible differences arising from variations in T_v , and since mean vegetation density was always near unity, it follows that these timescales of regrowth were always much faster than the timescale of erosion, a product of the storm arrival and intensity distribution. Two possible alternatives to this exist: growth and colonization rates should be slower and hence timescales longer; and the recurrence interval of erosion should be shorter. The former may be addressed by controlling plant mortality in more ways than one, such as through drought or grazing. When there is a drought, there would be no erosion, and no loss due to erosion, but there would likely be loss due to water stress; thus storms following a drought would have more potential to erode. This, in effect, equates to the second alternative, of more frequent erosion.

6. Conclusions

[43] This preliminary work was an attempt not just to study the geomorphic outcomes of dynamic vegetation but also to study the ecologic outcomes of erosion. In this sense,

it may be termed ecogeomorphology for its attempt to couple the abiotic and biotic aspects of a landscape into one. As such, the model formulation may act as a springboard for more research bridging the two composite sciences.

[44] Variations in K_v , on the other hand, produced both static and dynamic changes. Plants that are less easily removed with their substrate allow for a steeper landscape, but by restraining change, erosion variability is less. Plants lost at even a hint of erosion perpetuate said erosion, with dynamics notably divergent from the other simulations, modulating the climate's stochastic signal.

[45] Adding to work of numerous previous authors, these model results illustrate some intricacies of dynamic vegetation in the context of erosion and solidify long-standing observations. Vegetation makes landscapes steeper but sometimes at the expense of making erosion events more variable. In an engineering context, such variability translates to greater hazard or management cost. Vegetation imparts inertia to a landscape by resisting both the inception and cessation of erosion, modulating the dynamics of the exogenous forcings. Vegetation also reduces drainage density and highlights the transient and variable nature of erosionally active channel extent.

[46] Despite having varied the three vegetation parameters independently, it is likely that there are physiological correlations between each one. The strategy of early successional plants, for example, is to establish and grow quickly as they are out-competed by other species in the face of disturbances. Rapid growth necessitates an absence of sturdy construction. Additionally, roots that bind the soil better, limiting erosion, are also likely to keep a plant intact should erosion indeed occur. Exceptions to these rules include a plant's litter production and low-lying foliage, both of which would retard sediment detachment but may not prevent a plant from being loosed itself.

[47] Channels filled with vegetation pose no dilemma at the 1 km² scale, but for larger basins, should this phenomenon persist, model reality breaks down. Extending the basin scale accordingly would be a method of testing this hypothesis, and should vegetation remain, the model must be modified. Accounting for soil moisture or distinguishing between soil and debris are reasonable solutions as plants are less likely to grow where there is no soil, or where they are forever inundated.

[48] The model requires further development, in validation and in extension of the biological and physical processes discussed earlier. This will be duly pursued in subsequent work.

[49] **Acknowledgments.** This work was supported financially by NASA Headquarters under the Earth System Science Fellowship Grant NGT5-ESS/00-0000-0085. We also wish to thank the Army Research Office (DAAD19-01-1-0513) and the National Research Council of Italy. Discussions with Nicole Gasparini, Vanessa Teles, and Erkan Istanbuloglu were of particular help in this research as were the comments of the editors and three anonymous reviewers.

References

- Abrahams, A. D., A. J. Parsons, and J. Wainwright (1995), Effects of vegetation change on inter-rill runoff and erosion, Walnut Gulch, southern Arizona, *Geomorphology*, 13, 37–48.
- Aldridge, R., and R. J. Jackson (1968), Interception of rainfall by manuka (*Leptospermum scoparium*) at Taita, New Zealand, *N. Z. J. Sci.*, 11, 301–317.

- Anderson, R. S. (1994), Evolution of the Santa Cruz Mountains, California, through tectonic growth and geomorphic decay, *J. Geophys. Res.*, 99, 20,161–20,179.
- Beaumont, C., P. Fullsack, and J. Hamilton (1992), Erosional control of active compressional orogens, in *Thrust Tectonics*, edited by K. R. McClay, pp. 1–18, Chapman Hall, New York.
- Benda, L., and T. Dunne (1997), Stochastic forcing of sediment supply to channel networks from landsliding and debris flow, *Water Resour. Res.*, 33, 2849–2863.
- Biddle, P. G. (1983), Patterns of soil drying and moisture deficit in the vicinity of trees on clay soils, *Geotechnique*, 33(2), 107–126.
- Brenner, R. P. (1973), A hydrological model study of a forested and a cutover slope, *Hydrol. Sci. Bull.*, 18(26), 124–144.
- Chow, V. T. (1959), *Open Channel Hydraulics*, McGraw-Hill, New York.
- Clark, J. J., and P. R. Wilcock (2000), Effects of land-use change on channel morphology in northeastern Puerto Rico, *Geol. Soc. Am. Bull.*, 112(12), 1763–1777.
- Coulthard, T. J., M. J. Kirkby, and M. G. Macklin (2000), Modelling geomorphic response to environmental change in an upland catchment, *Hydrol. Proc.*, 14, 2031–2045.
- Culling, W. E. H. (1960), Analytical theory of erosion, *J. Geol.*, 68, 336–344.
- Densmore, A. L., R. S. Anderson, B. G. McAdoo, and M. A. Ellis (1997), Hillslope evolution by bedrock landslides, *Science*, 275, 369–372.
- Densmore, A. L., M. A. Ellis, and R. S. Anderson (1998), Landsliding and the evolution of normal-fault-bounded mountains, *J. Geophys. Res.*, 103, 15,203–15,219.
- DeRose, R. C., B. Gomez, M. Marden, and N. A. Trustrum (1998), Gully erosion in Mangatu Forest, New Zealand, estimated from digital elevation models, *Earth Surf. Processes Landforms*, 23, 1045–1053.
- Eagleson, P. S. (1978), Climate, soil, and vegetation: 2. The distribution of annual precipitation derived from observed storm sequences, *Water Resour. Res.*, 14, 713–721.
- Evans, K. G., and G. R. Willgoose (2000), Post-mining landform evolution modelling: 2. Effects of vegetation and surface ripping, *Earth Surf. Processes Landforms*, 25, 803–823.
- Federer, C. A. (1973), Forest transpiration greatly speeds streamflow recession, *Water Resour. Res.*, 9, 1599–1604.
- Fitzpatrick, F. A., and J. C. Knox (2000), Spatial and temporal sensitivity of hydrogeomorphic response and recovery to deforestation, agriculture, and floods, *Phys. Geogr.*, 21(2), 89–108.
- Flanagan, D. C., and M. A. Nearing (1995), USDA-Water Erosion Prediction Project (WEPP), *Lab. Rep. 10*, Natl. Soil Erosion Res. Lab., West Lafayette, Ind.
- Florinsky, I. V., and G. A. Kuryakova (1996), Influence of topography on some vegetation cover properties, *Catena*, 27, 123–141.
- Gabet, E. J., and T. Dunne (2003), A stochastic sediment delivery model for a steep Mediterranean landscape, *Water Resour. Res.*, 39(9), 1237, doi:10.1029/2003WR002341.
- Geddes, N., and D. Dunkerley (1999), The influence of organic litter in the erosive effects of raindrops and of gravity drops released from desert shrubs, *Catena*, 36, 303–313.
- Gilbert, G. K. (1877), Report on the geology of the Henry Mountains, U.S. Geogr. and Geol. Surv. of the Rocky Mt. Reg., Washington, D. C.
- Glade, T. (2003), Landslide occurrence as a response to land use change: A review of evidence from New Zealand, *Catena*, 51, 297–314.
- Graf, W. L. (1979), The development of montane arroyos and gullies, *Earth Surf. Processes*, 4, 1–14.
- Greenway, D. R. (1987), Vegetation and slope stability, in *Slope Stability*, edited by M. G. Anderson and K. S. Richards, pp. 187–230, John Wiley, Hoboken, N. J.
- Gregory, K. J., and D. E. Walling (1973), *Drainage Basin Form and Process: Geomorphological Approach*, John Wiley, Hoboken, N. J.
- Hack, J. T., and J. C. Goodlett (1960), Geomorphology and forest ecology of a mountain region in the central Appalachians, *U.S. Geol. Surv. Prof. Pap.*, 347.
- Howard, A. D. (1994), A detachment-limited model of drainage basin evolution, *Water Resour. Res.*, 30, 2261–2285.
- Howard, A. D. (1995), Simulation modeling and statistical classification of escarpment planforms, *Geomorphology*, 12, 187–214.
- Howard, A. D. (1997), Badland morphology and evolution: Interpretation using a simulation model, *Earth Surf. Processes Landforms*, 22, 211–227.
- Howard, A. D. (1999), Simulation of gully erosion and bistable landforms, in *Incised River Channels*, edited by S. Darby and A. Simon, pp. 277–300, John Wiley, Hoboken, N. J.
- Howard, A. D., W. E. Dietrich, and M. A. Seidl (1994), Modeling fluvial erosion on regional to continental scales, *J. Geophys. Res.*, 99, 13,971–13,986.
- Jakob, M. (2000), The impacts of logging on landslide activity at Clayoquot Sound, British Columbia, *Catena*, 38, 279–300.
- Johnson, A. C., and P. Wilcock (2002), Association between cedar decline and hillslope stability in mountainous regions of southeast Alaska, *Geomorphology*, 46, 129–142.
- Kirkby, M. (1995), Modelling the links between vegetation and landforms, *Geomorphology*, 13, 319–335.
- Koons, P. O. (1989), The topographic evolution of collisional mountain belts: A numerical look at the Southern Alps, New Zealand, *Am. J. Sci.*, 289, 1041–1069.
- Lancaster, S. T. (1998), A nonlinear river meandering model and its incorporation in a landscape evolution model, Ph.D. thesis, Mass. Inst. of Technol., Cambridge.
- Lancaster, S. T., S. K. Hayes, and G. E. Grant (2001), Modeling sediment and wood storage and dynamics in small mountainous watersheds, in *Geomorphic Processes and Riverine Habitat*, *Water Sci. Appl.*, vol. 4, edited by J. M. Dorava et al., pp. 85–102, AGU, Washington, D. C.
- Lee, R. (1980), *Forest Hydrology*, 349 pp., Cambridge Univ. Press, New York.
- Leopold, L., and T. Maddock (1953), The hydraulic geometry of stream channels and some physiographic implications, *U.S. Geol. Surv. Prof.*, 252.
- Lucas, Y. (2001), The role of plants in controlling rates and products of weathering: Importance of biological pumping, *Annu. Rev. Earth Planet. Sci.*, 29, 135–163.
- Luo, W. (2001), LANDSAP: A coupled surface and subsurface cellular automata model for landform simulation, *Comput. Geosci.*, 27, 363–367.
- Lyell, C. H. (1834), *Principles of Geology: Being an Attempt to Explain the Former Changes of the Earth's Surface by References to Causes Now in Operation*, vol. 3, John Murray, London.
- Mitas, L., and H. Mitasova (1998), Distributed soil erosion simulation for effective erosion prevention, *Water Resour. Res.*, 34, 505–516.
- Moglen, G. E., and R. L. Bras (1995), The effect of spatial heterogeneities on geomorphic expression in a model of basin evolution, *Water Resour. Res.*, 31, 2613–2623.
- Mosley, M. P. (1982), The effect of a New Zealand beech forest canopy on the kinetic energy of water drops and on surface erosion, *Earth Surf. Processes Landforms*, 7, 103–107.
- Nassif, S. H., and E. M. Wilson (1975), The influence of slope and rain intensity on runoff and infiltration, *Hydrol. Sci. Bull.*, 20, 539–553.
- Newman, B. D., A. R. Campbell, and B. P. Wilcox (1998), Lateral subsurface flow pathways in a semiarid ponderosa pine hillslope, *Water Resour. Res.*, 34, 3485–3496.
- Nichols, W. F., K. T. Killingbeck, and P. V. August (1998), The influence of geomorphological heterogeneity on biodiversity II. A landscape perspective, *Consult. Bio.*, 12, 370–379.
- Nortcliff, S., S. M. Ross, and J. B. Thornes (1990), Soil moisture, runoff and sediment yield from differentially cleared tropical rainforest plots, in *Vegetation and Erosion*, edited by J. B. Thornes, pp. 37–450, John Wiley, Hoboken, N. J.
- O'Loughlin, C. L. (1974), A study of tree root strength deterioration following clearfelling, *Can. J. For. Res.*, 4(1), 107–113.
- Pickup, G., and V. H. Chewings (1996), Correlations between DEM-derived topographic indices and remotely-sensed vegetation cover in rangelands, *Earth Surf. Processes Landforms*, 21(6), 517–529.
- Preston, N. J., and M. J. Crozier (1999), Resistance to shallow landslide failure through root-derived cohesion in east coast hill country soils, North Island, New Zealand, *Earth Surf. Processes Landforms*, 24, 665–675.
- Prosser, I. P., and C. J. Slade (1994), Gully formation and the role of valley-floor vegetation, southeastern Australia, *Geology*, 22, 1127–1130.
- Prosser, I. P., W. E. Dietrich, and J. Stevenson (1995), Flow resistance and sediment transport by concentrated overland flow in a grassland valley, *Geomorphology*, 13, 71–86.
- Reid, L. M. (1989), Channel incision by surface runoff in grassland catchments, Ph.D. thesis, Univ. of Wash., Seattle.
- Sala, M., and A. Calvo (1990), Response of four different Mediterranean vegetation types to runoff and erosion, in *Vegetation and Erosion*, edited by J. B. Thornes, pp. 347–362, John Wiley, Hoboken, N. J.
- Schmidt, K. M., J. J. Roering, J. D. Stock, W. E. Dietrich, D. R. Montgomery, and T. Schaub (2001), The variability of root cohesion as an influence on shallow landslide susceptibility in the Oregon Coast Range, *Can. Geotech. J.*, 38, 995–1024.
- Seidl, M. A., and W. E. Dietrich (1992), The problem of channel erosion into bedrock, *Catena*, 23, suppl., 101–124.
- Smock, L. A., G. M. Metzler, and J. E. Gladden (1989), Role of debris dams in the structure and functioning of low-gradient headwater streams, *Ecology*, 70(3), 764–775.
- Terwilliger, V. J., and L. J. Waldron (1991), Effects of root reinforcement on soil-slip patterns in the Transverse Ranges of southern California, *Geol. Soc. Am. Bull.*, 103, 775–785.

- Thom, B. G. (1967), Mangrove ecology and deltaic geomorphology: Tabasco, Mexico, *J. Ecol.*, 55, 301–343.
- Thornes, J. B. (1990), The interaction of erosional and vegetational dynamics in land degradation: Spatial outcomes, in *Vegetation and Erosion*, edited by J. B. Thornes, pp. 41–53, John Wiley, Hoboken, N. J.
- Trauth, M. H., R. A. Alonso, K. R. Haselton, R. L. Hermanns, and M. R. Strecker (2000), Climate change and mass movements in the northwest Argentine Andes, *Earth Planet. Sci. Lett.*, 179(2), 243–256.
- Tucker, G. E., and R. L. Bras (1999), Dynamics of vegetation and runoff erosion, in *A 3D Computer Simulation Model of Drainage Basin and Floodplain Evolution: Theory and Applications*, technical report, U.S. Army Corps of Eng. Construct. Eng. Res. Lab., Champaign, Ill.
- Tucker, G. E., and R. L. Bras (2000), A stochastic approach to modeling the role of rainfall variability in drainage basin evolution, *Water Resour. Res.*, 36, 1953–1964.
- Tucker, G. E., and R. L. Slingerland (1994), Erosional dynamics, flexural isostasy, and long-lived escarpments: A numerical modeling study, *J. Geophys. Res.*, 99, 12,229–12,243.
- Tucker, G. E., and R. Slingerland (1996), Predicting sediment flux from fold and thrust belts, *Basin Res.*, 8, 329–349.
- Tucker, G. E., and R. L. Slingerland (1997), Drainage basin responses to climate change, *Water Resour. Res.*, 33, 2031–2047.
- Tucker, G. E., S. T. Lancaster, N. M. Gasparini, R. L. Bras, and S. M. Rybarczyk (2001a), An object-oriented framework for distributed hydrologic and geomorphic modeling using triangular irregular networks, *Comput. Geosci.*, 27, 959–973.
- Tucker, G., S. Lancaster, N. Gasparini, and R. Bras (2001b), The Channel-Hillslope Integrated Landscape Development Model (CHILD), in *Land-scape Erosion and Evolution Modeling*, edited by R. S. Harmon and W. W. Dow III, pp. 349–384, Kluwer Acad., Norwell, Mass.
- Viles, H. A. (1990), The agency of organic beings: A selective review of recent work in biogeomorphology, in *Vegetation and Erosion*, edited by J. B. Thornes, pp. 5–24, John Wiley, Hoboken, N. J.
- Wainwright, J., A. J. Parsons, and A. D. Abrahams (2000), Plot-scale studies of vegetation, overland flow and erosion interactions: Case studies from Arizona and New Mexico, *Hydrol. Processes*, 14, 2921–2943.
- Whipkey, R. Z. (1966), Subsurface stormflow from forested slopes, *Bull. Int. Assoc. Sci. Hydrol.*, 10(2), 74–85.
- Wilcox, B. P., J. Pitlick, C. D. Allen, and D. W. Davenport (1996), Runoff and erosion from a rapidly eroding pinyon-juniper hillslope, in *Advances in Hillslope Processes*, vol. 1, edited by M. G. Anderson and S. M. Brooks, pp. 61–78, John Wiley, Hoboken, N. J.
- Willgoose, G., R. L. Bras, and I. Rodriguez-Iturbe (1991), A coupled channel network growth and hillslope evolution model: 1. Theory, *Water Resour. Res.*, 27, 1671–1684.
- Woo, M. K., G. Fang, and P. D. diCenzo (1997), The role of vegetation in the retardation of hill erosion, *Catena*, 29, 145–159.
- Yatsu, E. (1988), *The Nature of Weathering*, Sozisha, Tokyo.
- Ziemer, R. R. (1981), Roots and the stability of forested slopes, *Publ. Int. Assoc. Hydrol. Sci.*, 132, 343–361.

R. L. Bras and D. B. G. Collins, Department of Civil and Environmental Engineering, Massachusetts Institute of Technology, Cambridge, MA 02139, USA. (rlbras@storm.mit.edu; daniel_@mit.edu)

G. E. Tucker, Cooperative Institute for Research in Environmental Sciences, University of Colorado, Boulder, CO 80309-0399, USA. (gtucker@cires.colorado.edu)

REPORT DOCUMENTATION PAGE (SF298)
(Continuation Sheet)

Page 1 of 34 (excluding appendices)

**MODELING THE DYNAMICS OF GULLY AND ARROYO FORMATION,
FORT CARSON AND PINON CANYON MANEUVER SITE, COLORADO**

Proposal # 41586-EV

Agreement number DAAD19-01-1-0615

FINAL REPORT

Reporting Period 1 June, 2001 to 31 May, 2004

Prepared by Gregory E. Tucker

Current address:

Department of Geological Sciences

CIRES

University of Colorado

2200 Colorado Avenue

Boulder, CO 80309-0399

email: gtucker@cires.colorado.edu

August, 2004

(1) Publications during reporting period

(a) Manuscripts submitted but not yet published:

- (1) Solyom, P., and Tucker, G.E., The effect of limited storm duration on landscape evolution, drainage basin geometry and hydrograph shapes: *Journal of Geophysical Research ES*, in press 2004.
- (2) Istanbuluoglu, E., Bras, R.L., Flores, H., and Tucker, G.E., Implications of Bank Failures and Fluvial Erosion for Gully Development: Field Observations and Modeling. Submitted to *Journal of Geophysical Research - Earth Surface*, March, 2004.

(b) Papers published in peer-reviewed journals or books

- (1) Bogaart, P.W., Tucker, G.E., and de Vries, J.J. (2003) Channel network morphology and sediment dynamics under alternating periglacial and temperate regimes: A numerical simulation study: *Geomorphology*, vol. 54, no. 3/4, p. 257-277.
- (2) Collins, D., Bras, R., and Tucker, G.E. (2004) Modeling the effects of vegetation-erosion coupling on landscape evolution: *Journal of Geophysical Research - Earth Surface*, v. 109, no. F3, F03004, doi:10.1029/2003JF000028.

REPORT DOCUMENTATION PAGE (SF298)
(Continuation Sheet)

Page 1 of 34 (excluding appendices)

**MODELING THE DYNAMICS OF GULLY AND ARROYO FORMATION,
FORT CARSON AND PINON CANYON MANEUVER SITE, COLORADO**

Proposal # 41586-EV

Agreement number DAAD19-01-1-0615

FINAL REPORT

Reporting Period 1 June, 2001 to 31 May, 2004

Prepared by Gregory E. Tucker

Current address:

Department of Geological Sciences

CIRES

University of Colorado

2200 Colorado Avenue

Boulder, CO 80309-0399

email: gtucker@cires.colorado.edu

August, 2004

(1) Publications during reporting period

(a) Manuscripts submitted but not yet published:

- (1) Solyom, P., and Tucker, G.E., The effect of limited storm duration on landscape evolution, drainage basin geometry and hydrograph shapes: *Journal of Geophysical Research ES*, in press 2004.
- (2) Istanbuluoglu, E., Bras, R.L., Flores, H., and Tucker, G.E., Implications of Bank Failures and Fluvial Erosion for Gully Development: Field Observations and Modeling. Submitted to *Journal of Geophysical Research - Earth Surface*, March, 2004.

(b) Papers published in peer-reviewed journals or books

- (1) Bogaart, P.W., Tucker, G.E., and de Vries, J.J. (2003) Channel network morphology and sediment dynamics under alternating periglacial and temperate regimes: A numerical simulation study: *Geomorphology*, vol. 54, no. 3/4, p. 257-277.
- (2) Collins, D., Bras, R., and Tucker, G.E. (2004) Modeling the effects of vegetation-erosion coupling on landscape evolution: *Journal of Geophysical Research - Earth Surface*, v. 109, no. F3, F03004, doi:10.1029/2003JF000028.